UNIVERSITY OF TRENTO - Italy

International Doctoral School in Biomolecular Sciences

26th cycle

Lipidomics Investigations in Cell Biology

PhD thesis of:

Yang Yu

Centre for Integrative Biology (CIBIO)

Academic Year 2012 – 2013

Tutor: Prof. Graziano Guella

Bioorganic Chemistry Laboratory (Dept. Physics)

Advisors: Prof. Paolo Macchi (CIBIO),

Dr. Urska Vrhovsek (FEM)

'Declaration of Authorship:

I (Yang Yu) confirm that this is my own work and the use of all material from other sources has been properly and fully acknowledged.'

Tutor: Prof. Graziano Guella

PhD Candidate: Yang Yu

Abbreviations

ADMEM	Advanced-Dulbecco's Modified Essential Medium
CAD	Collision gas
CE	Collision Energy
Chol	Cholesterol
CID	Collision-Induced Dissociation
CUR	CURtain gas
CXP	Collision Cell Exit Potential
DAG	Diglycerides
DESI	Desorption Electrospray Ionization
DHAP	DiHydroxyAcetonePhosphate
DHAPAT	DiHydroxyAcetonePhosphate AcylTransferase
DLPC	1,2-Dilauroyl-*sn*-glycero-3-PhosphoCholine
DMEM	Dulbecco's Modified Essential Medium
DOPA	1,2-Dioleoyl-*sn*-glycero-3-Phosphate
DOPC	1,2-Dioleoyl-*sn*-glycero-3-PhosphoCholine
DOPS	1,2-Dioleoyl-*sn*-glycero-3-Phospho-L-Serine
DP	Declustering Potential
DSPG	1,2-Dioctadecanoyl-sn-glycero-3-Phospho-(1'-rac-Glycerol)
EI	Electron Ionization
EIC	Extracted Ion Chromatogram
EP	Entrance Potential
ePC	plasmanyl (or ether) PC
ER	Endoplasmic Reticulum
ESI	Electrospray Ionization
FBS	Fetal Bovine Serum
FP	Focusing Potential
GC-MS	Gas Chromatography–Mass Spectrometry
GL	GlycoLipids
GlcCer	GlucosylCeramide
GPL	GlyceroPhosphoLipids
GSL	GlycoSphingoLipids
^{1}H DQCOSY	Double Quantum COherence SpectroscopY
^{1}H-^{13}C HMBC	proton-carbon Multiple-Bond Correlation
^{1}H-^{13}C HSQC	proton-carbon Single Quantum Correlation
HIF 1-a	Hypoxia-Inducible Factor 1-alpha
HIF	Hypoxia-Inducible Factor
HPLC	High Performance Liquid Chromatography
IS	IonSpray

LPC	Lyso PhosphoCholines
LPE	Lyso PhosphoEthanolamines
LPL	Lyso PhosphoLipids
MALDI TOF MS	Matrix-Assisted Laser Desorption Ionization Time-Of-Flight Mass spectrometer
MS	Mass Spectrometry
MUFA	Mono-Unsaturated Fatty Acid
MVDA	MultiVariate Data Analysis
NEB	NEBulizer gas
NLS	Neutral Loss Scanning
NMR	Nuclear Magnetic Resonance
NPLC	Normal Phase Liquid Chromatography
OPLS-DA	Orthogonal Projections to Latent Structures-Discriminant Analysis
PA	Phosphatidic Acids
PAF	Platelet-Activating Factor
PC	PhosphoCholines
PC1	Principal Component 1
PC2	Principal Component 2
PCA	Principal Component Analysis
PE	PhosphoEthanolamines
PG	PhosphoGlycerols
PI	PhosphoInositols
PIS	Precursor Ion Scanning
PL	PhosphoLipids
PLS-DA	Partial Least Squares Discriminant Analysis
pPC	plasmenyl (or vinyl-ether) PC
PS	PhosphoSerines
PUFA	Poly-Unsaturated Fatty Acid
QQQ MS	Triple Quadruple Mass Spectrometer
REIMS	Rapid Evaporative Ionization Mass Spectrometry
RP-HPLC	Reversed Phase High Performance Liquid Chromatography
RTK	Receptor Tyrosine Kinases
S1P	Sphingosine-1-Phophate
SL	SphingoLipids
TAG	Triglycerides
TEM	TEMperature
TIC	Total Ion Chromatogram
TOCSY	TOtally Correlated SpectroscopY
UI	Unsaturation Index
UVDA	UniVariate Data Analysis
VIP	Variable Influence on Projection

Table of Contents

Chapter 1. Abstract

Cell membrane is the biological barrier serving as both territorial defense and the communication hinge for the interior of cell from its surroundings. As building blocks of cellular membranes and also precursor for second messengers, a variety of lipids play essential roles in cellular membrane dynamics as well as important functions such as cell proliferation, apoptosis, signal transduction and membrane trafficking modulation. Lipidomics, representing the systematic and integrative studies of diversified lipids (lipidome) in a biological system, is an emerging yet rapid developing field and hence requires advanced and complementary analytical techniques as well as multiple statistical tools. Our development of reliable analytical methodology (the advanced Mass Spectrometric and high-resolution NMR techniques) and application of multiple statitistical approaches (multivariate data analysis and univariate t-test) enable us to achieve these comprehensive understandings.

We have investigated, first of all, the effects induced by hypoxia on cervical cancer derived cells (HeLa cells) to see how and how much the changes in phospholipids profile are able to get light into the targeted biological problem (hypoxia) and provide a preliminary insight into the underlying mechanisms. We found that hypoxia stimulation dramatically reduced the total amount of cellular phosphoinositols (PI) but prominently increased the amount of lyso phosphocholines (lyso-PC) and lyso phosphoethanolamines (lyso-PE). Moreover, our studies suggested the polyunsaturated phospholipids species as stronger biomarkers upon hypoxia treatment. The evaluation of changes in the average unsaturation index (UI) of the membrane lipids acyl chains revealed that UI slightly increased in several lipid classes, thus affecting membrane fluidity and further membrane-dependent functions. The plausible mechanisms by HeLa cells to adapt to hypoxia conditions are briefly reported as well.

We have also conducted the comparative lipidomic studies of urothelial cancer cell line RT4 (a model system of a benign tumor) and T24 (a model system of a metastatic tumor) aiming to reveal probable roles and relevant differential changes of membrane lipids with respect to urinary bladder metastasis progress. Significant changes of lipids metabolism were found to correlate with urothelial nonmetastatic and metastatic cell models. The most remarkable finding was that the malignant cell type (T24) showed a strong decrease of ether PC species complemented by a sharp increase of the length and the average unsaturation number of lipids acyl chains. Ceramide-based sphinglipids also showed altered profiles in these two cell types. Such analyses suggest a certain significant re-organization of cellular membrane in malignant cell transformation, involving variations in compositional lipid structures and possible signaling transduction pathways. Observations of such reduction of the 1-alkyl PC species and the chain shortening of lipid species might serve as a tool in urinary bladder cancer intervention.

Chapter 2. Introduction

2.1 Lipids and lipidomics

Lipids are hydrophobic or amphiphilic low molecular weight substances soluble in organic solvents but with a low solubility in water. In general, based on their chemically functional backbone, lipids are prevalently classified into eight categories, namely fatty acyls, glycerolipids, glycerophospholipids, sphingolipids, sterol lipids, prenol lipids, saccharolipids, and polyketides [1]. Such primary categorization can facilitate further detailed lipid classification on the basis of enormous combination of various hydrophobic and hydrophilic elements. For example, in mammalian cells, fatty acyl chains have different carbon chain lengths and huge possibilities of double bond positions. The diverse fatty acid backbones and their combination with various functional head groups can theoretically lead to thousands of lipid species with classified characters. The cell membrane is the biological barrier which constitutes the first territorial defense as well as the communication points for the interior of cells from the outside environment. The classical model of cell membrane consists of phospholipid bilayer embedding proteins and other lipids such as sterols and glycolipids. As building blocks of cells, the structural characteristics of lipid molecules can exert critical effects on cellular membrane dynamics since membrane lipids are precursors for second messengers and play major roles in important cellular functions including cell proliferation, apoptosis, signal transduction pathways and regulation of membrane trafficking [2, 3]. For mammalian cells, the main bioactive lipid components of biological membranes are glycerophospholipids (GPL), cholesterol (Chol) and sphingolipids (SL), which will be studied and discussed within the scheme of my thesis.

Glycerophospholipids (GPL) indicate *"any derivative of the sn-glycero-3-phosphoric acid containing at least an O-acyl group (a fatty acid), O-alkyl group (a fatty alcohol), or a O-alk-1'-enyl group (a fatty aldehyde) bound in sn-1 or sn-2 of a glycerol and a polar head in sn-3 position consisting of a nitrogenous base, glycerol, or inositol group" [4]*. This lipid category has the common diacylglycerophosphate backbone attached to a highly varied polar head groups, leading to wide-ranging classes of glycerophospholipids sharing some common features but generally possessing distinct characteristics. There are six major glycerophospholipids (GPL) classes (Fig. 1), namely phosphocholines (PC), phosphoethanolamines (PE), phosphoinositols (PI), phosphoglycerols (PG), phosphoserines (PS), phosphatidic acids (PA). Replacement of the $–OCOCH_2$-moiety, usually on carbon 1 of glycerol, with an ether bond ($-OCH_2CH_2-$) or with a vinyl ether bond (-OCH=CH-) can result in different GPL classes called plasmanyl (1-alkanyl) or plasmenyl (1-alkenyl) phospholipid, respectively. The most common forms of the ether or vinyl ether PL in human body are plasmanyl (or plasmenyl) pPC and pPE. Besides, the lyso-derivatives of the diacylphosphatidylcholine (or ethanolamine) are also important participants in cellular functionality such as inflammatory responses, although present in low concentrations in mammalian cells (Fig. 1, bottom left). Besides, each GPL class can be subdivided into a range of molecular species on the basis of backbone variation in carbon chain length, position of chain attachment and double bonds as well as number of unsaturation.

Cholesterol (Fig. 2) is the main representatives of another category of important lipids, called sterols, and it is the only sterol biosynthesized by animals. Cholesterol is an important plasmic membrane lipid wherein it is associated tightly with the fatty acid chains of phospholipids (~ one molecule of cholesterol per molecule of phospholipid). Such structural features and the distribution contribute to the outer membrane leaflet rigidity and impermeability

to the water-soluble compounds [5]. Together with GPL and sphingolipids, cholesterol is important as cellular membrane building block and in particular enriched in lipid raft with SM. Besides, cholesterol is essential for viability and cell proliferation.

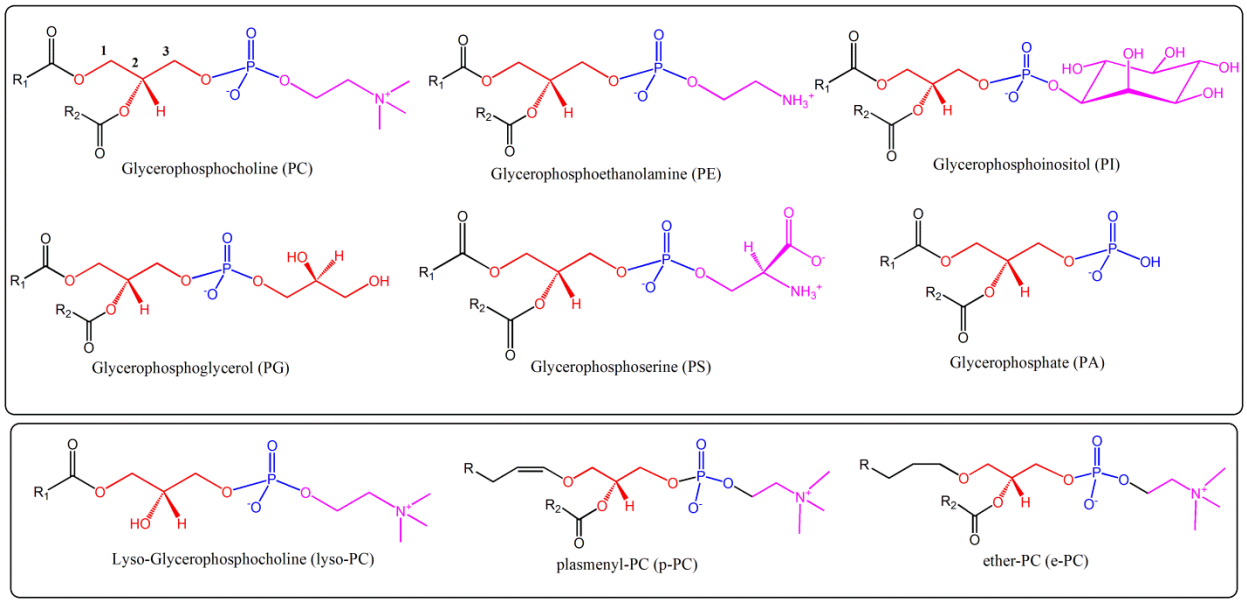

Fig. 1 Main GPL classes

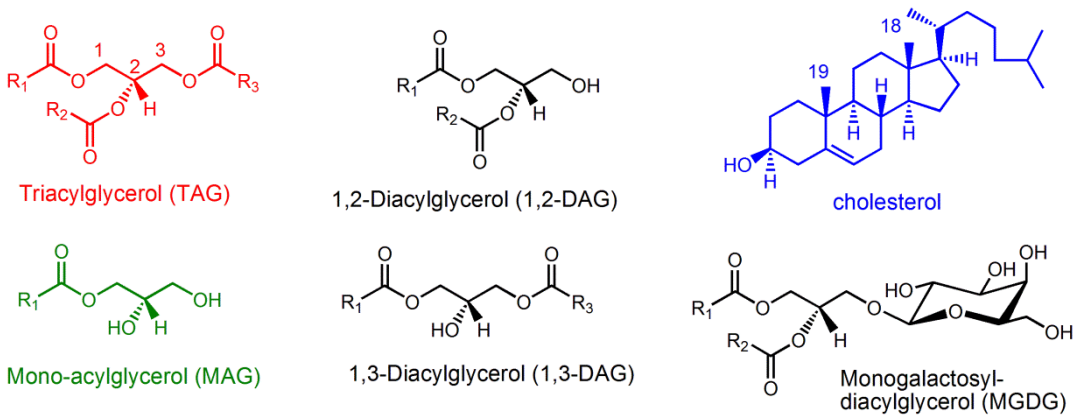

Fig. 2 Main neutral lipids classes

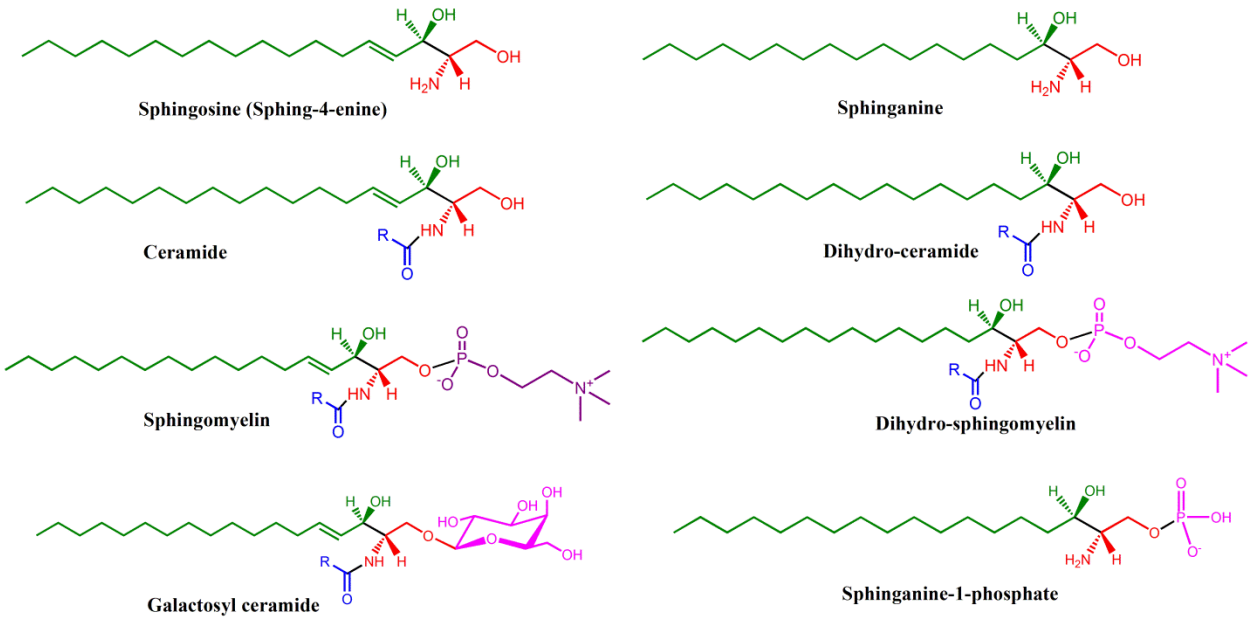

Fig. 3 Main sphingolipids classes

Another important membrane lipid in mammalian cells is sphingomyelin (SM, Fig. 3), which is a sphingosylphospholipid comprised of a ceramide moiety linked to a phosphocholine group [4]. The presence of various molecular species of SM is tissue specific in mammals. SM is particularly abundant in lipid rafts, known as specialized plasma membrane microdomains organized by glycosphingolipids and specific proteins. They serve for assembly of signaling molecules, influence membrane fluidity and trafficking of membrane proteins, and regulate different cellular processes [6]. As a highly diverse group of bioactive compounds, sphingolipids (SL) which contain a backbone of sphingoid long-chain base (sphinganine and sphingosine, Fig. 3) play important role not only in building cellular membranes but also in cell physiology and pathology being capable of eliciting apoptosis, differentiation, chemotaxis, and other responses in mammalian cells [7]. In particular, in signal transduction pathways where SL are involved, ceramide is regarded as an apoptotic mediator and sphingosine-1-phophate (S1P) is the first messenger mediating calcium homeostasis, cell growth, tumorogenesis and suppression of

apoptosis as an intracellular second messenger [8-10]. In Mammals, the most important group of glycolipids (GL), an essential component of the living cell surfaces [11], is glycosphingolipids (GSL), the basic structural characteristic of which is the attachment of one or more sugar bases to a sphingolipid moiety (see galactolsyl-ceramide as an example in Fig. 3). Due to the structural complexity and diversity of glycosyl base as well as the hydrophobic part, there are dozens of structural GSL variants in mammalian cellular membranes, which also vary in abundance and chemical stability [12, 13]. All such GSL variants lead to cell type specific GSL pattern, fundamentally reflecting the membrane microdomain composition enriched of GSL [14]. Several studies have related GSL functions to cancer, for example, the observation of anti-carcinogenic effects upon increasing ceramide levels by slowing its conversion to GlcCer via GlcCer synthase [15, 16] and the involvement of GSL in cancer pathogenesis [8]. The proposed association of malignant transformation with abnormal glycosylation may lead to the synthesis and expression of altered GSL variants and the increase of such compounds in malignant cells is ineluctable outcome of the malignant transformation of cells [17]. The review of above mentioned SL or GSL functions causes fundamental interest in some topics of my thesis and may serve as inspiration to explain the results obtained so far.

The progress in exploring information in genomics and proteomics directed research, for example, in diseases pathogenesis or progression including cancer, diabetes, cardiovascular disease, neurodegenerative disorder and inflammatory disease, has left behind the corresponding advancement of knowledge about lipids, which are as previously described highly rated but structural diverse [2]. Therefore, systems-level qualitative and quantitative analysis of lipids (i.e lipidomics, usually deemed as a branch of the field of metabolomics) and the interrelated proteins as well as intracellular pathways in a variety of biological samples are highly required

and promising. An important mission for lipidomics is to study the interaction of individual lipid molecular species and their effects on metabolic disorders and, to a broader extent, on the biological system as a whole. The most promising aspect arising from this field is to inspire investigations aimed to elucidate a network of the roles of genes, proteins and metabolites which can describe cellular functions in an integrative manner [18].

Recent reviews have pointed out a couple of driving forces for the renaissance in lipid studies. One is revealed to be the understanding of biophysical properties of lipids and membranes in particular of lipid–lipid and lipid–protein interactions. As one of the most representative biological model systems, cellular lipidomics requires establishing a framework pinpointing the relationships of the aforementioned cellular components as well as manipulating the roles of lipids [19].

This thesis moves within the wide-field cellular lipidomics with special focus on untargeted quantitative analysis of the individual lipid molecular species. Interaction of lipids with some relevant proteins will be also mentioned in chapter 4 with respect to epithelial cellular lipidomics. Another highlighted driving force has been attributed to the availability and rapid development of advanced analytical tools including nuclear magnetic resonance (NMR) spectroscopy and mass spectrometry (MS) [2, 18, 19], which facilitate to observe the variations in cellular lipidome due to external stimulus or cellular differentiation as well as different cancer metastatic stages, etc. The development of analytical methodology and its application in studying HeLa cellular lipidome affected by external hypoxia stimulation will be discussed in detail in chapter 3 and the comparative lipidomic studies on urothelial cancer metastasis will be presented in chapter 4.

2.2 NMR and Mass spectrometry

As previously introduced, the prompt and prominent advancement in analytical tools has pushed forward lipidomics research to a new era. NMR spectroscopy as a powerful tool for structural elucidation of molecules has been employed to study lipid structures as well as lipid-protein interactions and therefore can provide information on biomembrane structure and dynamics [2, 20]. As introduced before, together with GPL and SL, the cholesterol as one major sterol in mammalian cells is an essential component to build up the cell membrane matrix [21]. However; different from other classes of membrane lipids, cholesterol is a neutral and apolar lipid which makes it inappropriate for MS analysis. Although NMR has only moderate sensitivity compared with MS its role in cholesterol analysis of raw lipid extracts must be absolutely appreciated. In a simple ^{1}H-NMR spectrum of these extracts, cholesterol can be easily detected since its angular methyls resonances (sharp singlets for Me-18 and Me-19, Fig. 4) are clearly distinguished from phospholipids signals. Thus, as shown in Fig. 4 for the raw lipids extract of HeLa cells, the normalized area ratio of Me-18 cholesterol signal (δ_H 0.723, 3H) with respect to $-N^+(CH_3)_3$ signal (δ_H 3.226, 9H) attributable to choline-containing lipids allowed to promptly establish the relevant [Chol]/[PC+SM-PC] molar ratio.

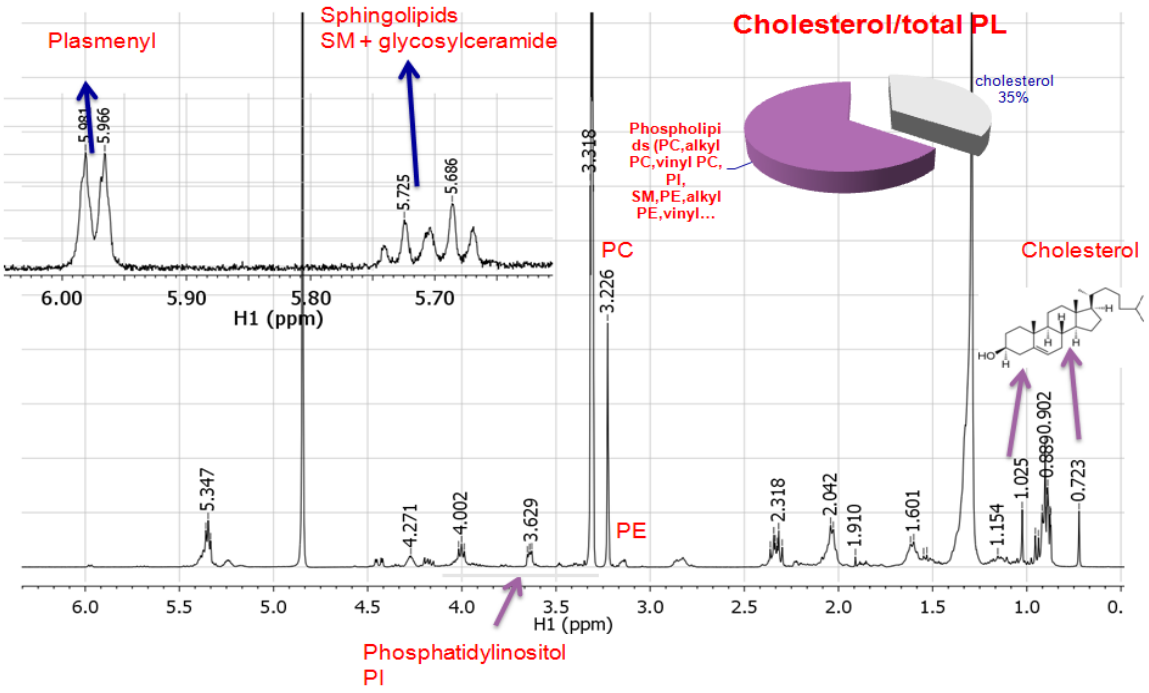

Fig. 4 ^{1}H-NMR spectrum of HeLa cellular lipids in CD_3OD with some peak assignments to species belonging to different GPL, neutral and SL lipid classes

So far NMR has been employed in metabolomic studies in several successful cases [22-24], but it has not found extensive uses in cellular lipidomics research. Although modern lipidomics approaches mainly rely on the wide arsenal of MS techniques, NMR represents a powerful tool for the qualitative analysis and often it is crucial in the elucidation of their structural details. First of all, the sample preparation for NMR measurements is rather simple and rapid not implying any derivatization of components. Moreover, NMR analyses carried out on lipids raw extract give an immediate perception of the main lipids therein present. Although the number of compounds detected in a raw lipid extract is limited, the NMR spectra give a good picture of what really is present, minor compounds might not be seen, but the major trends are clear. As a non-destructive method, NMR technique is advantageous in quantitative analysis of lipid mixtures isolated from different biological matrices, as the first snapshot of the lipidome. In fact, several structural features can be reliably established by ^{1}H-NMR (Fig. 4) such as the

presence/ absence of a) species belonging to the major GPL and SL classes (in particular the presence of 1Z-plasmenly-PL by characteristic ^{1}H signals at δ_H 5.998), b) neutral lipids such as cholesterol (Chol), triglycerides (TAG) and diglycerides (DAG) and c) the overall unsaturation index of their acyl chains. When ^{1}H-NMR analysis is coupled to ^{31}P-NMR measurements it becomes an even more powerful tool in phospholipids analysis [25]. In particular, through ^{31}P-NMR it is possible to differentiate the membrane lipids in distinct PL classes and to obtain reliable and reproducible quantitative data such as the molar fractions of all the PL classes (see Fig. 5). Nevertheless, the application of NMR techniques in cellular lipidomics studies still remains to be developed and further investigated. It will be discussed in chapter 3 in my thesis.

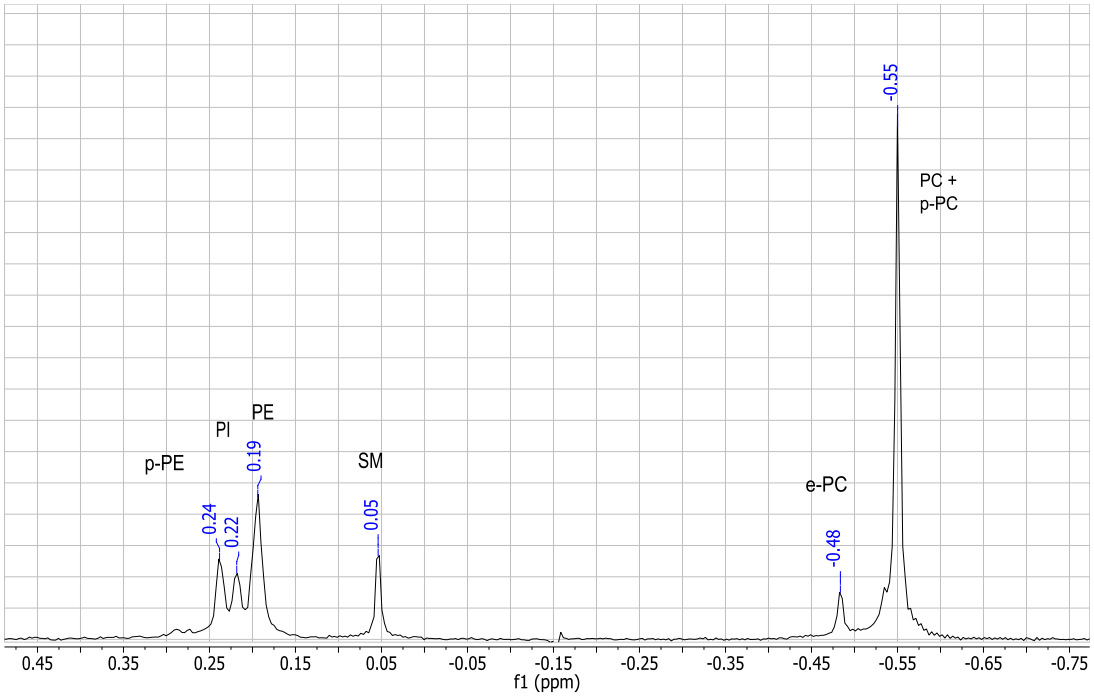

Fig. 5 ^{31}P-NMR spectrum of HeLa cellular lipids in CD_3OD with the assignments of signals attributable to different GPL classes

As previously discussed, there are enormous combinatorial structures of lipids, leading to several classes of lipids and thousands of lipid molecular species. Due to its moderate sensitivity and to the intrinsic structure-similarity among lipids (leading to strong overlap of NMR), NMR

cannot provide information about individual lipid species. Thus, MS-based techniques have to be called on. In fact, it is the rapid advancement of MS that has recently driven lipidomics research forward [18]. Similar to metabolomics, there are mainly two approaches in MS-based development for lipidomics research – *targeted lipidomics* and *global lipidomics* (or *untargeted lipidomics*). Targeted lipidomics refers to the identification and quantification focused on one or a few classes of lipid candidates while the latter term involves the characterization of hundreds or even thousands of lipid molecular species within a biological system [18, 26].

There are several MS-based methods for lipid analysis, namely 1) gas chromatography–mass spectrometry (GC-MS) with electron ionization (EI), 2) matrix-assisted laser desorption/ionization (MALDI) time-of-flight (TOF) MS, 3) electrospray ionization (ESI) MS and 4) desorption electrospray ionization (DESI) as well as 5) rapid evaporative ionization mass spectrometry (REIMS). Each of these methods has been developed and applied depending on different lipid- or sample-type. Due to its intrinsic soft-ionization feature and capability of analyzing intact lipid molecules, the most prevalent and important is ESI MS. ESI MS measurements can be carried, basically, by two approaches: a) direct infusion of the sample into the ESI ion source (*shotgun lipidomics*); b) injection of the sample into the ESI ion source via high-performance liquid chromatography (HPLC).

During the work described in my thesis, direct infusion ESI MS has been applied to study and to optimize ionization efficiency of standard, commercially available, samples from each class of lipid, while HPLC-ESI MS methodology has been used for the analysis of the raw lipids extracts obtained by different biological matrices. Generally speaking, the second approach is much more powerful from the analytical point of view since it allows chromatographic separation of the different lipid (eventually, also isomeric) species avoiding the strong ion

suppression effects imposed by the complex chemical matrix and it allows an increased dynamic range of MS measurements, very important for the detection of minor lipids components.

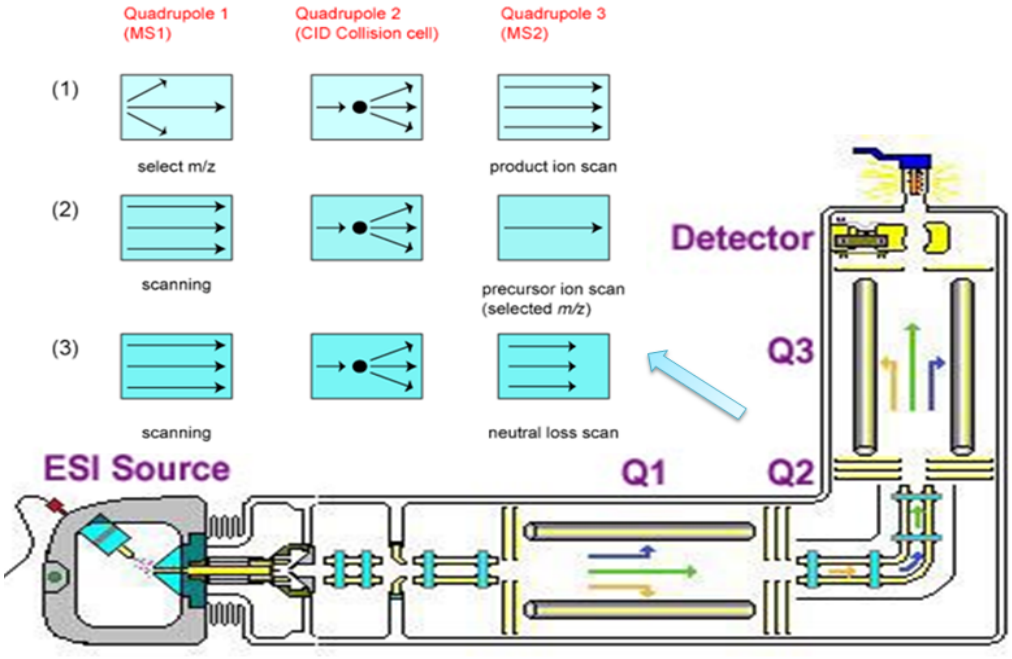

Fig.6 Schematic representation of QQQ MS configuration and operation modes for lipid analysis

Various MS analyzer configurations have been employed in lipid characterization. In all the work described in this thesis we used a triple quadruple mass spectrometer (QQQ MS) that is largely used and appreciated in several MS-lipidomics investigations reported in modern literature both for GPL analysis [27] and SL characterization [28]. QQQ MS is a type of tandem-in-space MS, which allows various MS/MS scan modes such as product ion scanning, precursor or parent ion scanning and neutral loss scanning [29]. The schematic representation of the configuration and operation modes of QQQ MS for lipid characterization is shown in Fig. 6. As presented in this scheme chart, in a typical product ion scanning procedure, the first quadruple (Q1) functions to select a molecule of lipid species with a defined m/z. The selected ions pass into Q2, where the collision-induced dissociation (CID) occurred and the dissociated fragments

are determined in Q3. In my thesis, this procedure is primarily applied to study and optimize fragmentation behavior of different lipids with common classified structures (eg: head group characters, sphingosine bases or glycosyl bases). Converse to it, precursor ion scanning (PIS) is performed in such a way that Q3 is fixed to a required fragment (with defined m/z) and in Q1 the corresponding precursor ions are scanned. PIS is very powerful to identify specific lipid classes or species with characteristic fragmentation of either head group (GPL classes or GSL with various sugar bases) or backbones (sphingosine based SL). In the case of Neutral Loss Scanning (NLS) mode, both Q1 and Q3 are scanned across a specific mass range and the ions pass into Q2 where they are fragmented. The offset of Q1 and Q3 is the neutral mass of the diagnostic fragment; thus, the ionized lipid molecular species that passing through Q1 loss this neutral mass will be transmitted through Q3 and detected. Various PIS and NLS modes will be optimized for lipid identification and quantification.

2.3 Sample preparation for lipidomics analysis

Usually, depending on different types of biological systems, the preparation of starting materials has to change by changing the biological matrix (cell culture, sub-cellular organelle, tissue, biofluids). A critical factor affecting the possibility to exploit NMR in lipidomics study is the availability of an adequate amount of total lipid extract (approximately 1 mg is required in our investigations). To ensure NMR measurements, the optimal number of cells is firstly tested. In chapter 4 of urothelial lipidomics study, we find the possible number of cells for NMR measurement can be as low as ~$3*10^7$ (2 to 3 T75 flasks of cell cultures) while for MS analysis, down to 1 T75 flask of cell culture is enough. General lipidomics workflow is presented in Fig.7 (adapted from [30]) wherein the starting cell cultures or tissue samples are extracted according to different procedures depending on the types of lipids to be analyzed as well as types of biological

samples [31]. Different procedures for lipid extraction will be discussed in chapter 3 and 4, respectively. The total lipid extract is initially dissolved in 700 ml of perdeuterated methanol (CD_3OD) for NMR measurements, after which the MS analysis will be performed as shown in Fig. 7. Both shotgun lipidomics and LC-MS methods have been applied for the work described in this thesis. In particular LC-MS runs have been always performed with reversed phase liquid chromatography (RP-HPLC) by using an optimized methanol/water (ammonium acetate) gradient as mobile phase (chapter 3 for details).

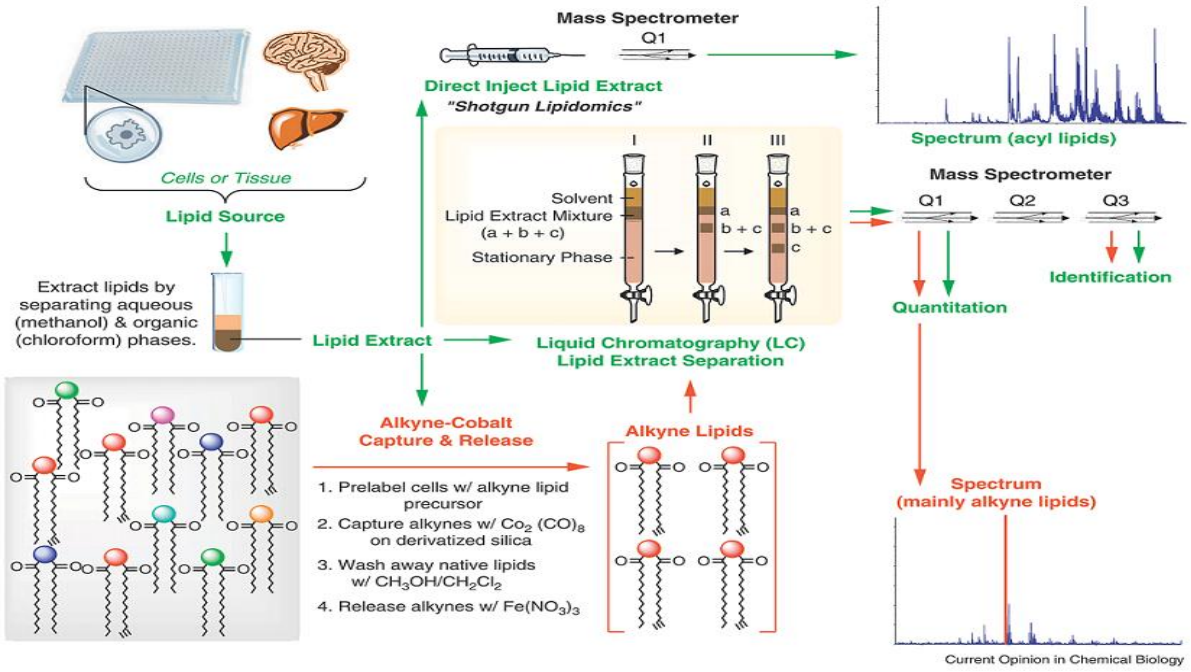

Fig. 7 Overview of lipidomics procedures (adapted from [30])

2.4 Lipidomics data processing

The generated enormous amount of data requires the rapid development of appropriate computational bioinformatics tools, which underwent great advancements in last years [32]. As mentioned before, lipids profile may vary due to several different factors including

environmental stressors, differentiation states of cells or progress of cancer metastasis [33]. The comprehensive understanding and explanation of such variations as well as the relevant regulatory factors through the analysis of complex lipidomics datasets need to be carefully addressed, especially in some issues such as a) data pre-processing (meanwhile with lipid identification), b) establishment of MS-based lipidomic data matrix regarding each lipid species as a variable, c) subsequent multivariate and univariate statistical analysis, d) data interpretation in term of lipid metabolism and finally e) eventual significance of some lipid species as biomarkers of pathology or pathogenesis [34, 35].

Despite the distinction of analytical platforms to generate various types of raw lipidomic datasets, lipid identification can be achieved by resorting to tools provided from LIPID MAPS consortium [http://www.lipidmaps.org/tools/]. By using tandem MS to define lipid classes, the candidate lipid species can be reliably established even in absence of high resolution MS-data which can be obtained only by TOF and/or Orbitrap mass analyzers. Several software packages have been developed for pre-processing MS-based lipidomics data, such as LipidProfiler™ for data acquired in MS/MS mode (eg. multiple PIS and NLS) [36] and some free software developed for data obtained in LC/MS based full-scan mode such as MZmine [37] or XCMS [38]. Of course, even instrument vendor based softwares can perform data-processing steps such as peak detection and smoothing, alignment and normalization. Spectral data is presented with features of m/z and time as well as quantity (expressed in intensity or in area) indicating lipid species. After spectra acquisition and processing, spectral data is transformed into a data matrix with lipid species as variables and samples as objects. A wealth of data yielded thereby is beyond the scope of conventional statistical analysis. In order to systematically analyze and extract more useful information with a deep biochemical understanding, multivariate data analysis (MVDA) is

applied, by which the interaction between individual lipid species and its effect on the whole lipid metabolism can be investigated.

MVDA has demonstrated its powerful applicability to the metabolomics and lipidomics data interpretation [34, 39] by highlighting important patterns hidden in the measurements. Generally, MVDA can be divided into unsupervised and supervised methods. In the unsupervised approach, the prior knowledge or classification of sample groups are not applicable. Principal component analysis (PCA) is the most common one, which can be firstly (and necessarily) used to reduce dimensionality of datasets and indicate sample grouping, trends of variation, outliers and systematic patterns. Representing one of the most common supervised methods, the partial least squares discriminant analysis (PLS-DA) can be employed when the sample group classification is known. Besides the information on major trends, PLS-DA can also be used to figure out lipid markers responsible for the trends and discrimination among different sample groups. Orthogonal projections to latent structures discriminant analysis (OPLS-DA) as a modification of PLS-DA method can generate results with much improved and easier interpretability. In my thesis, I have tried to explore the capabilities of various MVDA methods to study lipid profile of a given biological system (problem), to highlight changes in lipid profile and to discover potential lipid markers. Univariate statistical tools have been also used to analyze the discovered lipid markers for further validation.

2.5 Aim of the thesis

The main aim of the thesis is to exploit the applications of lipidomics methodologies in cell biology through advanced Mass Spectrometric and high-resolution NMR techniques. In the first part of my thesis I had to do with the development of reliable analytical methodologies

capable of relating environmental stressor-induced cell responses to changes in lipids distributions. In particular, a quantitative characterization of lipids composition in HeLa cells upon hypoxia-induced conditions has been done and the main results are presented in Chapter 3. The second-stage study aims to investigate possible roles and relevant differential changes of membrane lipids with respect to urinary bladder metastasis progress. This has been done by comparing the urothelial cell line RT4 (derived from the papilloma urinary bladder, a model system of a benign tumor) with the cell line T24 (derived from the malignant tumor of urinary bladder, a model system of a metastatic tumor). Some interesting preliminary results will be presented in chapter 4.

Chapter 3 is comprised of the publication entitled *"A lipidomics investigation of the induced hypoxia stress on HeLa cells by using MS and NMR techniques"* recently published on *"Molecular Biosystems"*. As the first author, I have helped with cell cultures and performed lipid extraction. I have conducted MS analysis and prepared samples for NMR analysis. Finally, I have managed lipidomic data analysis. I have given a major contribution to the writing of the manuscript preparing Figures 3-8 as well as Tables 1-4.

2.6 References

[1] Fahy E, Subramaniam S, Brown HA *et al.* A comprehensive classification system for lipids. Journal of lipid research 2005; 46:839-861.

[2] Wenk MR. The emerging field of lipidomics. Nature reviews. Drug discovery 2005; 4:594-610.

[3] Bou Khalil M, Hou W, Zhou H *et al.* Lipidomics era: accomplishments and challenges. Mass spectrometry reviews 2010; 29:877-929.

[4] Leray C. Phospholipids. In: Introduction to Lipidomics. CRC Press; 2012. pp. 213-242.

[5] Leray C. Simple Lipids with Only One Component. In: Introduction to Lipidomics. CRC Press; 2012. pp. 3-168.

[6] Korade Z, Kenworthy AK. Lipid rafts, cholesterol, and the brain. Neuropharmacology 2008; 55:1265-1273.

[7] Haynes CA, Allegood JC, Park H, Sullards MC. Sphingolipidomics: methods for the comprehensive analysis of sphingolipids. Journal of chromatography. B, Analytical technologies in the biomedical and life sciences 2009; 877:2696-2708.

[8] Lahiri S, Futerman AH. The metabolism and function of sphingolipids and glycosphingolipids. Cellular and molecular life sciences : CMLS 2007; 64:2270-2284.

[9] Spiegel S, Milstien S. Sphingosine-1-phosphate: an enigmatic signalling lipid. Nature reviews. Molecular cell biology 2003; 4:397-407.

[10] Huwiler A, Zangemeister-Wittke U. Targeting the conversion of ceramide to sphingosine 1-phosphate as a novel strategy for cancer therapy. Critical reviews in oncology/hematology 2007; 63:150-159.

[11] Merrill AH, Jr. Sphingolipid and glycosphingolipid metabolic pathways in the era of sphingolipidomics. Chemical reviews 2011; 111:6387-6422.

[12] Farwanah H, Kolter T. Lipidomics of Glycosphingolipids. Metabolites 2012; 2:134-164.

[13] Merrill AH, Jr., Stokes TH, Momin A *et al.* Sphingolipidomics: a valuable tool for understanding the roles of sphingolipids in biology and disease. Journal of lipid research 2009; 50 Suppl:S97-102.

[14] Hakomori S. Structure, organization, and function of glycosphingolipids in membrane. Current opinion in hematology 2003; 10:16-24.

[15] Gouazé V, Liu Y-Y, Prickett CS *et al.* Glucosylceramide Synthase Blockade Down-Regulates P-Glycoprotein and Resensitizes Multidrug-Resistant Breast Cancer Cells to Anticancer Drugs. Cancer Research 2005; 65:3861-3867.

[16] Basu S, Ma R, Mikulla B *et al.* Apoptosis of human carcinoma cells in the presence of inhibitors of glycosphingolipid biosynthesis: I. Treatment of Colo-205 and SKBR3 cells with isomers of PDMP and PPMP. Glycoconj J 2003; 20:157-168.

[17] Kannagi R, Izawa M, Koike T *et al.* Carbohydrate-mediated cell adhesion in cancer metastasis and angiogenesis. Cancer Science 2004; 95:377-384.

[18] Blanksby SJ, Mitchell TW. Advances in mass spectrometry for lipidomics. Annual review of analytical chemistry 2010; 3:433-465.

[19] van Meer G. Cellular lipidomics. The EMBO journal 2005; 24:3159-3165.

[20] Gawrisch K, Eldho NV, Polozov IV. Novel NMR tools to study structure and dynamics of biomembranes. Chemistry and physics of lipids 2002; 116:135-151.

[21] Ohvo-Rekila H, Ramstedt B, Leppimaki P, Slotte JP. Cholesterol interactions with phospholipids in membranes. Progress in lipid research 2002; 41:66-97.

[22] Fernando H, Bhopale KK, Kondraganti S *et al.* Lipidomic changes in rat liver after long-term exposure to ethanol. Toxicology and applied pharmacology 2011; 255:127-137.

[23] Griffin JL, Walker LA, Garrod S *et al.* NMR spectroscopy based metabonomic studies on the comparative biochemistry of the kidney and urine of the bank vole (Clethrionomys glareolus), wood mouse (Apodemus sylvaticus), white toothed shrew (Crocidura suaveolens) and the laboratory rat. Comparative biochemistry and physiology. Part B, Biochemistry & molecular biology 2000; 127:357-367.

[24] Nicholson JK, Wilson ID. Opinion: understanding 'global' systems biology: metabonomics and the continuum of metabolism. Nature reviews. Drug discovery 2003; 2:668-676.

[25] Marsh D, Pali T. The protein-lipid interface: perspectives from magnetic resonance and crystal structures. Biochimica et biophysica acta 2004; 1666:118-141.

[26] Han X. Lipidomics: developments and applications. Journal of chromatography. B, Analytical technologies in the biomedical and life sciences 2009; 877:2663.

[27] Busik JV, Reid GE, Lydic TA. Global analysis of retina lipids by complementary precursor ion and neutral loss mode tandem mass spectrometry. Methods in molecular biology 2009; 579:33-70.

[28] Shaner RL, Allegood JC, Park H *et al.* Quantitative analysis of sphingolipids for lipidomics using triple quadrupole and quadrupole linear ion trap mass spectrometers. Journal of lipid research 2009; 50:1692-1707.

[29] Farwanah H, Kolter T, Begley TP. Lipidomics. In: Wiley Encyclopedia of Chemical Biology. John Wiley & Sons, Inc.; 2007.

[30] Alex Brown H. Lipidomics: when apocrypha becomes canonical. Current Opinion in Chemical Biology 2012; 16:221-226.

[31] Astarita G, Ahmed F, Piomelli D. Lipidomic Analysis of Biological Samples by Liquid Chromatography Coupled to Mass Spectrometry. In: Lipidomics. Edited by: Armstrong D. Humana Press; 2009. pp. 201-219.

[32] Niemelä PS, Castillo S, Sysi-Aho M, Orešič M. Bioinformatics and computational methods for lipidomics. Journal of Chromatography B 2009; 877:2855-2862.

[33] Hakomori S-i. Glycosphingolipids as differentiation-dependent, tumor-associated markers and as regulators of cell proliferation. Trends in Biochemical Sciences 1984; 9:453-459.

[34] Orešič M. Bioinformatics and computational approaches applicable to lipidomics. European Journal of Lipid Science and Technology 2009; 111:99-106.

[35] Yetukuri L, Ekroos K, Vidal-Puig A, Oresic M. Informatics and computational strategies for the study of lipids. Molecular BioSystems 2008; 4:121-127.

[36] Ejsing CS, Duchoslav E, Sampaio J *et al.* Automated Identification and Quantification of Glycerophospholipid Molecular Species by Multiple Precursor Ion Scanning. Analytical Chemistry 2006; 78:6202-6214.

[37] Pluskal T, Castillo S, Villar-Briones A, Oresic M. MZmine 2: modular framework for processing, visualizing, and analyzing mass spectrometry-based molecular profile data. BMC bioinformatics 2010; 11:395.

[38] Smith CA, Want EJ, O'Maille G *et al.* XCMS: processing mass spectrometry data for metabolite profiling using nonlinear peak alignment, matching, and identification. Anal Chem 2006; 78:779-787.

[39] Kaiser KA. Metabolic Profiling of Primary and Secondary Biosynthetic Pathways in Angiosperms: Comparative Metabonomics and Applications of Hyphenated LC-NMR and LC-MS. In: 2012.

Chapter 3. A lipidomics investigation of the induced hypoxia stress on HeLa cells by using MS and NMR techniques

Yang Yu[1,b], Laura Vidalino[b], Andrea Anesi[a], Paolo Macchi[b] and Graziano Guella [*a,b,c]

3.1 Abstract

Induced hypoxia stress on cervical cancer derived cells (HeLa cells) can lead to significant changes of their membrane lipid profiles. The lipidome of HeLa cells was characterized by a joint approach wherein liquid chromatography-mass spectrometry (LC-MS) analysis was followed by high resolution NMR measurements. Multivariate data analysis showed apparent separation between control and hypoxia-treated HeLa cells and thus demonstrated hypoxia effects on lipid metabolism. The most striking finding was that hypoxia stimulation significantly reduced the total amount of cellular phosphoinositols (PI) but caused a prominent increase of the amount of lyso phosphocholines (lyso-PC) and lyso phosphoethanolamines (lyso-PE). The observed attenuation of PI amount upon hypoxic conditions is probably due to the accumulation of cellular myo-inositol, which is known to play a critical role in d*e novo* synthesis of PI. Moreover, our study suggests that polyunsaturated phospholipids species are stronger biomarkers for discriminating the effect of hypoxia treatment. The evaluation of changes in the average unsaturation index (UI) of the membrane lipids acyl chains reveals that UI slightly increases in several lipid classes, thus affecting membrane fluidity and further membrane-dependent

[1] *Bioorganic Chemistry Laboratory, Department of Physics, University of Trento, Trento, Italy*
[b] *Molecular and Cellular Neurobiology lab, CIBIO Centre for Integrative Biology, University of Trento, Trento, Italy*
[c] *CNR, Istituto di Biofisica, Trento, Via alla Cascata 56/C, 38050 Povo (TN) – Italy*
**Email :graziano.guella@unitn.it*
Fax :+39 461281696
Tel :+39 461 281536

functions. The plausible mechanisms by HeLa cells to adapt to hypoxia conditions are also briefly reported.

Key words: HeLa/ hypoxia/ lipidomics/ NMR/ mass spectrometry/multivariate analysis

3.2 Introduction

As an emerging field, lipidomics represents the global identification and quantitative assessment of the vast array of lipids, or lipidome, within a given biological system.[1,2] To achieve such a comprehensive description, lipidomics involves system-level analysis of thousands of pathways and networks of cellular lipid species as well as their interactions with other factors including other lipids or proteins.[3] Cellular membranes are composed of complicated arrangements of lipids which participate in vital cellular functions. Phospholipids (PL) and sphingolipids (SL), the major components of cellular membranes, exert important cellular functions associated with cell proliferation, apoptosis, signal transduction pathways and regulation of membrane trafficking.[4] The major PL classes present in mammalian cellular membranes are 1,2 diacyl-glycerophospholipids such as glycerophosphocholines (PC), glycerophosphoethanolamines (PE), glycerophosphoinositols (PI), glycerophosphoglycerols (PG), glycerophosphoserines (PS), glycerophosphatidic acids (PA) as well as the corresponding 1-alkenyl,2-acyl analogues such as plasmenyl-PC (pPC) and plasmenyl-PE (pPE). Among the sphingosine-based (SL) membrane lipids, N-acylated ceramides (Cer), sphingomyelins (SM which are 1-O phosphocholine ceramide derivatives) and galactosylceramides (Gal-Cer) are usually found as important membrane components in eukaryotic cells. The structural diversity of all these lipid classes, often leading to several hundreds of individual molecular species, is essentially caused by the acyl chains structural diversity which in turn derives from diversity in

their chain length and degree of unsaturation. Other important cellular lipids are lyso-phospholipids (lyso-PL) bearing only one acyl chain at the sn-1 position (usually) of the glycerol backbone which are involved in important signaling pathways. Growing evidence has correlated the perturbation of lipid metabolism as well as dysfunctions of specific lipid species to a variety of diseases including cancer, obesity, hypertension, diabetes and neurodegenerative diseases.[5] Thus, lipidomics represents an important tool to study alterations in lipid metabolism and can facilitate the discovery of lipid biomarkers as useful indicators of disease progression or metabolic cellular response to various environmental stressors.

The greatest advances in lipidomics investigations have been relied on two main analytical techniques, the nuclear magnetic resonance (NMR) and the mass spectrometry (MS), the latter often coupled to a liquid chromatography (LC) system. As a non-destructive and highly reproducible technique,[6] NMR is often used in lipids analysis for *ab initio* structural elucidation of new lipid species; however, due to its intrinsically quantitative response, it can be, used even for reliable quantifications of lipids mixtures obtained by tissues, body fluids and cell cultures.[4,7] In particular, ^{31}P-NMR spectroscopy is a very powerful technique in the quantitation of PL classes due to the fact that, at least in principle, within a given PL class the phosphorous nucleus feels a different chemical environment with respect to that of a different PL class. Owing to the high sensitivity and resolution for characterization of intact lipid species, electrospray ionization mass spectrometry coupled with liquid chromatography (LC-ESI MS) can supply the most comprehensive and informative data set for cellular lipidome studies.[8] Tandem MS measurements, for example, through precursor ion scanning and neutral loss scanning, are also often required for identification of all lipid molecular species. This latter methodology is usually

much better than full scan MS due to its higher sensitivity and enhanced signal/noise ratio and, therefore, can facilitate the characterization of minor but biologically relevant lipid species.[9]

HeLa cellular lipidome has been rarely studied. As a model system, lipidomic analysis of HeLa cells has been performed to analyze the response of eight classes of phospholipids to paclitaxel-induced apoptosis by combing normal phase liquid chromatography (NPLC)/ESI (negative ionization)/MS^n-based lipidomic strategy with multivariate statistical analysis.[10] The aim of this study was to explore the relation between phospholipids metabolism and paclitaxel-induced apoptosis as well as phospholipase changes to better understand the anticancer mechanisms of chemotherapeutic agents. HeLa cellular lipidome study has been also conducted using the shotgun lipidomic approach to investigate cell cycle dependent changes in membrane stored curvature elastic energy by analyzing lipid composition alterations in different cell phases, revealing that HeLa cells can modify the membrane stored elastic energy through cell cycles.[11] These previous works have suggested HeLa cell line is a good model in lipidomic research with respect to anticancer drug effects on global lipid metabolism and to energy homeostasis related lipid profile alterations.

Increasing evidence shows that cancer cells are correlated with specific alterations in lipid metabolism. In fact, changes in lipid composition are strongly related to many cellular processes, including cellular growth, proliferation, energy homeostasis and motility.[12] Cells derived from prokaryotic and eukaryotic organisms have the abilities to sense and respond to oxygen alterations to maintain their homeostasis. In particular, cancer cells have developed oxygen-sensing capability to adapt to chronic low-oxygen conditions,[13] known as hypoxia. Previous studies have demonstrated that tumor hypoxia has been associated with changes in carbohydrate and lipid metabolism. For cancer cells, low oxygen availability can lead to the

activation of hypoxia-inducible factor (HIF), which causes the switch of cellular metabolic processes to anaerobic energy production including prevention of glucose-derived lipid synthesis and requirement of glutamine as carbon source for lipid synthesis.[12] Recently, few studies proposed phospholipids as reliable markers for hypoxia that induces alterations in tumor cell proliferation[14] and it is believed that lipidomics tool is promising for future and more comprehensive studies of cancer cellular lipid profile alterations induced by hypoxia. Nevertheless, more information and global phospholipids profile analysis as well as its interrelated cellular pathways still remain to be revealed.

In order to address the hypoxia-mediated alterations in cancer cellular phospholipid profile, to elucidate the corresponding pattern, and to further reveal the underlying mechanisms as well as molecular pathways involved, we performed a lipidomics investigation using HeLa cell line as a model system. First, we characterized each phospholipid class and individual phospholipid molecular species in control and hypoxia-stressed HeLa cells by resorting to the high resolution NMR and high performance liquid chromatography (HPLC) – ESI QqQ MS/MS tecniques. Second, multivariate data analysis (MVDA) was used to differentiate control and hypoxia-stressed cells and to understand how (existence of potential lipid biomarkers) and how much the changes in phospholipid profile are able to get light into the targeted biological problem (hypoxia). Finally, the trends and the possible mechanisms for such changes have been investigated by analyzing changes in the overall unsaturation index of PL classes. Taken together, our data show for the first time how the cell membranes lipids of HeLa cancer cells are affected by induced-hypoxia states and provide a preliminary insight into the corresponding mechanisms.

3.3 Materials and Methods

Chemicals

Methanol was of hypergrade for LC-MS with purity 99.9% (Merck). Chloroform with purity 99.8% and water were of HPLC grade (VWR). Ultrapure water was obtained from Milli-Q system (Millipore). Methanol-D4 was with deuteration degree of min. 99.8% for NMR Spectroscopy (Merck). Lipid standards DLPC (1,2-dilauroyl-*sn*-glycero-3-phosphocholine), DOPC (1,2-dioleoyl-*sn*-glycero-3-phosphocholine), DOPS (1,2-dioleoyl-*sn*-glycero-3-phospho-L-serine), DOPA (1,2-dioleoyl-*sn*-glycero-3-phosphate), DSPG (1,2-dioctadecanoyl-sn-glycero-3-phospho-(1'-rac-glycerol)) and standards SM (sphingomyelin, Brain, Porcine), L-α-PE (Egg, Chicken), L-α-PI (Soy) with purity >99% were all purchased from Avanti Polar Lipids (Alabaster). Standard lipids and extracted cellular lipids were prepared and dissolved in glass vials.

Cell culture and Hypoxia treatment

HeLa cells were cultured in DMEM (supplemented with 10% heat-inactivated FBS, 1% L-glutamine and 1% penicillin/ streptomycin) in an incubator at 37 $^{\circ}$C with 5% CO_2. 24 hours before hypoxia treatment, HeLa cells were synchronized by serum starvation. Hypoxia was induced with 200 μM Cobalt (II) chloride ($CoCl_2$) added to cell cultures for 3h. Untreated cells were used as negative controls. In order to achieve sufficient biomass for NMR analysis, approximately $1x10^8$ cells were used, while $1x\ 10^7$ cells were sufficient for MS analysis. Since cell cultures are growing in strictly controlled conditions, their variability is smaller than the one expected for other type of samples, thus allowing the use of smaller sample sizes (n=4).

Immunocytochemistry and fluorescence microscopy

Cell cultures were carried out as described previously (Vidalino *et al.*, 2012). After $CoCl_2$ treatment, HeLa cells were washed in pre-warmed PBS and then fixed in 4% PFA for 15 minutes at room temperature. After permeabilization in 0.1% Triton X100 for 5 minutes, cells were immunostained. The following antibodies were used: mouse anti-HIF1α (dilution 1:50; Abcam), rabbit anti-ACTIN (dilution 1:500, Sabta Cruz. The following secondary antibodies (1:500, Invitrogen) were used: Alexa Fluor 488-conjugated goat anti-rabbit and anti-mouse IgGs, Alexa Fluor 594-conjugated. Microscopy analysis was performed using the Zeiss Observer Z.1 Microscope implemented with the Zeiss ApoTome device and with a PlanApo oil immersion lens (63X, NA=1.4). Pictures were acquired using AxioVision imaging software package (Zeiss) and assembled with Adobe Photoshop 7.0. Images were not modified other than adjustments of levels, brightness and magnification.

Phospholipids extraction and sample preparation

Total cellular lipids were extracted according to Bligh and Dyer method with slight modifications.[15] In brief, medium was removed and cells washed with PBS twice followed by trypsin digestion. Cells were washed again with PBS and centrifuged for 10 min at r.t. at 2400 g. The pellet was then resuspended in 1 ml Milli-Q water and incubated in ice. Before lipid extraction, 10 ng/µl standard DLPC (12:0/12:0), distinct from any natural cellular lipid as previously assessed, was added in order to estimate the yield of extraction (recovery). 3 ml chloroform/methanol (v/v 2:1) was added to the resuspended pellet followed by sonication in ice (program set as total time 15 min, amplitude 20, time pulse 3 sec and time pause 5 sec). The samples were then centrifuged at 16000 g for 10 min at 4 °C and the chloroform phase (bottom layer) was carefully collected into a glass vial and the upper layer was subjected to another extraction step. The combined chloroform fractions were evaporated under a gentle stream of N_2.

The extracted lipids were initially dissolved in 700 µl of perdeuterated methanol (CD_3OD) for NMR measurements. At the end of NMR analysis the sample was then concentrated to final volume of 500 µl and used for all the MS analysis. The final standard DLPC (12:0/12:0) concentration assuming a 100% recovery was 6.25 ng/µl. Peak area of DLPC in the real sample was divided by that of DLPC in standard solution (6.25 ng/ul assuming 100% recovery) to give the value of lipid recovery.

NMR measurements

^{1}H- (400 MHz) and ^{31}P-NMR (162 MHz) spectra of the raw organic lipid extracts were recorded in d_4-methanol (99.90% CD_3OD) at 300 K on a Bruker-Avance 400 MHz NMR spectrometer by using a 5 mm BBI probe equipped with pulsed-gradient field utility. The ^{1}H-90^0 proton pulse length was found 9.3 µs with a transmission power of 0 db whilst ^{31}P-90^0 proton pulse length was 17 µs with a transmission power of -3 db. The chemical shift scale (δ) was calibrated on the residual proton signal of CD_3OD at δ_H 3.310 ppm and δ_C 49.00 ppm whilst the ^{31}P-NMR δ scale was calibrated on the PC signal at δ_P -0.550 ppm. The following experiments were done (info obtained are reported in brackets): ^{1}H-NMR (proton chemical shifts and scalar couplings J); ^{1}H-^{1}H DQCOSY (proton-proton scalar correlation); ^{1}H–^{13}C HSQC (proton-carbon one-bond correlation); ^{1}H–^{13}C HMBC (proton-carbon multiple-bond correlation). 1D NMR spectra (^{1}H and ^{31}P) of the lipid extracts were fitted and integrated by the software MestreNova 8.1 (Mestrelab Research S.L., Escondido, CA).

Optimization of precursor ion scanning and neutral loss scanning for ESI MS/MS analysis

Characteristic fragmentation of each standard phospholipid (PL) class (DOPC, DOPS, DOPA, DSPG, SM, L-α-PE (Egg), L-α-PI (Soy)) were firstly studied by triple quadruple mass

spectrometry (Applied Biosystems API 3000^{TM}, Italy) with direct infusion at 10 µl /min using a syringe pump (Harvard Apparatus, Italy). Individual standard lipid was dissolved in methanol/water (v/v 7:3) containing ammonium acetate (10 mM). Full scan and MS/MS analysis were performed both in positive and negative ionization mode. Next, equal volume of 1 mg/ml of each lipid standard were mixed and analyzed by HPLC - ESI MS/MS to optimize class-specific MS/MS head group survey scanning (Precursor Ion Scanning and Neutral Loss Scanning) for sample analysis.

HPLC-ESI MS/MS measurements

Total HeLa PL extracts were separated and analyzed with Shimadzu High Performance LC^{TM} (CBM-20 A, equipped with the binary pump LC-20AB, Italy) combined with Applied Biosystems API 3000^{TM} QQQ mass spectrometer (LC/MS/MS System, equipped with electrospray ion source). A Kinetex C_{18} column (100A pore size, 4.6 mm ID, 2.6 µm particle size, and 10 cm, Phenomenex, Italy) was used for lipid separation. The mobile phase included A: methanol/ water (v/v 7:3) with 10 mM ammonium acetate and B: methanol with 10 mM ammonium acetate. The gradient elution program started from 70% B/30% A, reached 100% B in 45 min, and maintained at 100% B for 20 min. The flow rate was 1 ml/min and 10 µl of sample was injected. The mass spectrometric analysis was carried out in positive ionization mode and MS/MS class-specific scan conditions optimized as follows: NEB (Nebulizer Gas) 9, CUR (Curtain Gas) 10, TEM (Temperature) 300 ^{0}C, IS (IonSpray Voltage) 5 kV, CAD (collision gas) 4, DP (Declustering Potential) 65, FP (Focusing Potential) 250, EP (Entrance Potential) 5, CE (Collision Energy) 40 and CXP (Collision Cell Exit Potential) 18. Unit resolution was set for both Q1 and Q3 and step size was 0.1 amu. Precursor ion scan 184 was used to characterize PC, lyso PC, pPC and SM, indicating the precursor ion form of $[M+H]^{+}$. Neutral loss scanning of

185, 115, 189, 141 and 277 Da were employed to detect PS with precursor ion $[M+H]^+$, PA with precursor ion $[M+NH_4^+]^+$, PG ($[M+NH_4^+]^+$), PE/ lyso PE/ pPE ($[M+H]^+$) and PI ($[M+NH_4^+]^+$), respectively.

Data processing

Data generated from LC/MS/MS class-specific scanning were processed with Analyst (Version 1.42) by extracting ions from TIC (Total Ion Chromatogram) and peak areas were integrated from EIC (Extracted Ion Chromatogram) after mass tolerance aligning and peak smoothing. Identification of lipid molecular species was resorted to Lipid Mass Spec. Prediction (LIPID MAPS) by surveying Mass, Mass tolerance, Head group and Precursor ion. Intra-class quantification and distribution was assessed by normalizing peak area of each lipid species to the overall area of all lipids belonging to the same lipid class. A data matrix was generated, which comprised of rows representing different samples and columns indicating relative abundance of individual PL species as variables. The data matrix was imported into software SIMCA-P 13.0 (Umetrics, Italy) for multivariate data analysis (MVDA). Pareto-scaling was used to preprocess data and principal component analysis (PCA) was an initial overview of data set about group classification and trends, which here indicated the separation between control and hypoxia-treated HeLa cells. Partial Least Squares Discriminant Analysis (*PLS-DA*) was used to better discriminate control and treated cells. *PLS-DA* was also employed to find out PL species as markers which had significant discriminatory power. Unpaired t-test of the candidate marker species was carried out with GraphPad Prism 5. For Unsaturation Index (UI) analysis, the relative abundance of individual PL species was multiplied by their corresponding unsaturation number.

3.4 Results and discussion

Cobalt (II) chloride induces hypoxia

Since cellular lipids are highly variable depending on cell cycle, we decided to investigate only the effects of hypoxia on dynamic changes of lipid profile after synchronizing cell growth at the same stage by serum starvation.[16] It has been demonstrated that hypoxia can be induced by $CoCl_2$ and both higher concentration (400 µM) and long term exposure (24h) of $CoCl_2$ induce cell apoptosis.[17] For this reason, we incubated HeLa cells with 200 µM $CoCl_2$ for 3h. Although no apoptosis was observed (data not shown), under this condition, hypoxia was induced. As shown in Fig. 1 hypoxia induction was assessed by monitoring the hypoxia-inducible factor 1-α (HIF 1-α) which accumulates in the nucleus upon exposure to hypoxic conditions.[18] No morphological changes were observed by microscope analysis after treatment with $CoCl_2$.

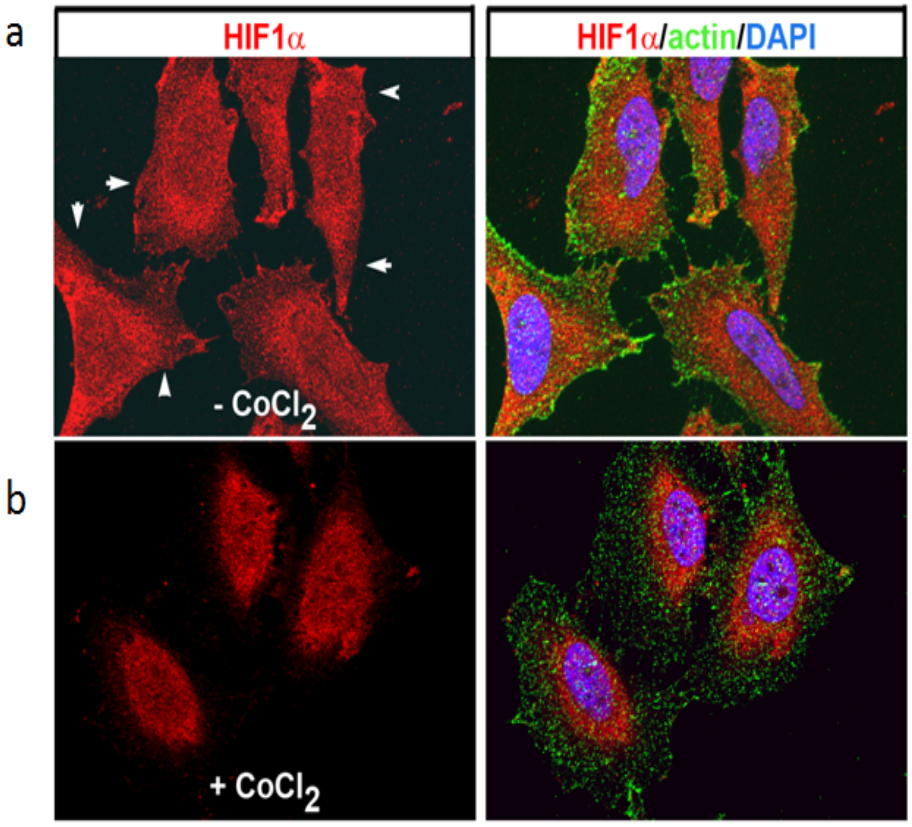

Fig. 1 $CoCl_2$-induced hypoxia in mammalian cells. HIF 1-α is a cytoplasmic protein. HeLa cells lines were treated with 200 μM cobalt chloride for 3h and then processed for immunostaining analysis. Fluorescent images were taken from representative cells. (a) Immunostaining for HIF 1-α (red) and ACTIN (green) shows the cytoplasmatic localization of HIF 1-α in normoxia conditions. (b) Under hypoxia induction, HIF 1-α shuttles from the cytoplasm and localizes within the nucleus. (63X magnification).

NMR analysis of phospholipid classes

The raw lipids extracts obtained from control and hypoxia treated HeLa cells were subjected to extensive 1D (^{1}H and ^{31}P) and 2D (HSQC and HMBC)-NMR measurements carried out at 300 K in deuterated methanol.

The ^{1}H-NMR spectrum contained information which proved to be relevant for arriving at the overall profile of the main cell membrane lipids. In fact, besides the characteristic peaks attributable to the presence of PC (δ_H 3.22 s, δ_C 54.5) and to PE (δ_H 3.16 m, δ_C 41.5), signals due to the presence of plasmenyl PC and/or plasmenyl PE (δ_H 5.96 d and 4.43q, δ_C 146.2 and 108.1, respectively), SM lipids (δ_H 5.71 dt and 5.45d, δ_C 134.9 and 131.0, respectively) were also detected. Moreover, a characteristic triplet at δ_H 3.20 (coupled to δ_C 76.1) was attributed to lipid species belonging to PI class. Worthy of mention, the latter was clearly detectable only in the untreated HeLa samples whilst it was found to be below the detection limit in the hypoxia-treated HeLa samples.

The analysis of these ^{1}H-NMR spectra allowed us i) to clearly detect also cholesterol (Chol) by the presence of the characteristic singlet signals of its angular methyl groups at δ_H 0.72 and δ_H 1.02 (coupled to δ_C 12.2 and δ_C 19.5, respectively) and ii) to establish the [Chol]/[PC+SM lipids] molar ratio by evaluation of the corresponding area of the signal at δ_H 0.72 (x 3) for Chol with respect to the area of the signal at δ_H 3.22 for PC+SM. No statistically significant change

of the value of this ratio was found in hypoxia-treated (0.52 ± 0.02) with respect to that of untreated HeLa cell extracts (0.51 ± 0.02).

Although the integration of the ^{1}H-NMR signals allowed to roughly establish also the relative molar ratio of the main PL classes, we used only the results of the corresponding ^{31}P-NMR spectra for the relative quantitative analysis of PL classes in HeLa cell extracts.

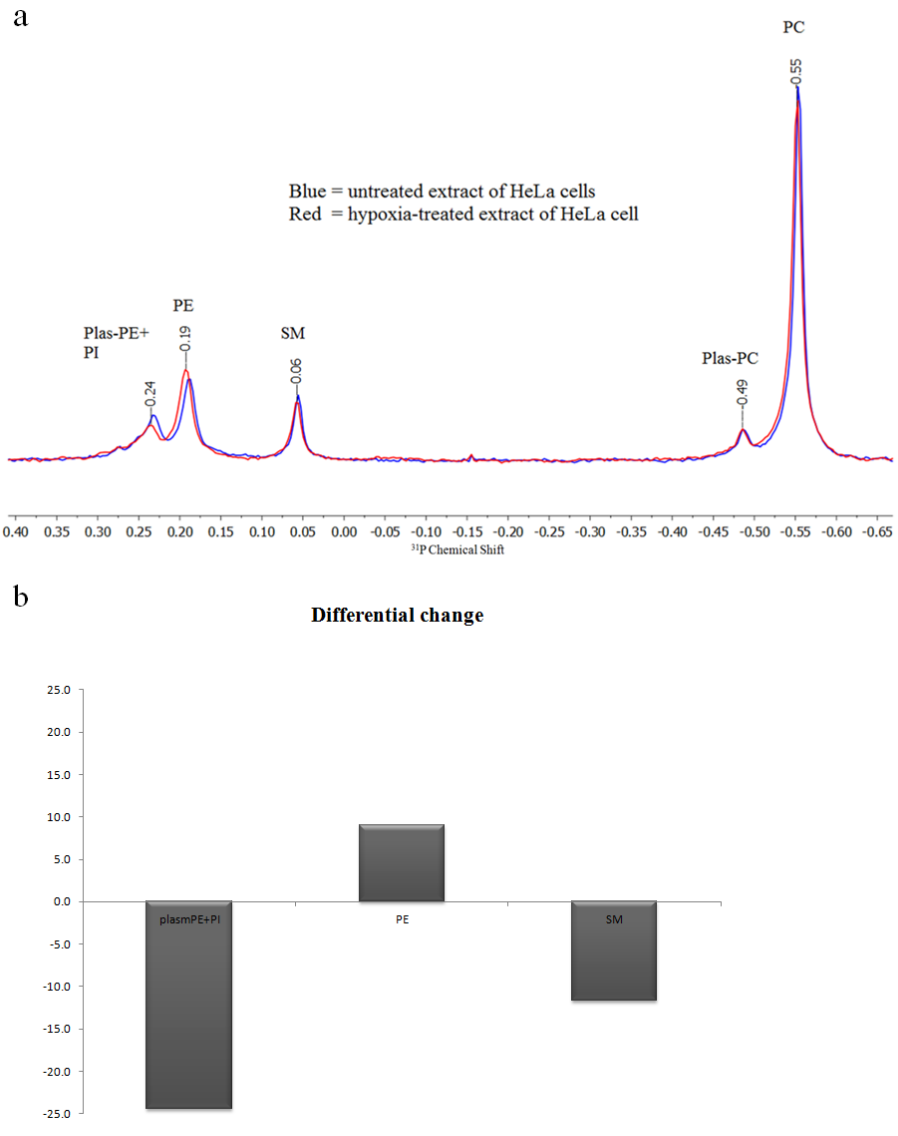

Fig. 2 NMR analysis of PL composition in control and hypoxia-stressed HeLa extracts. (a) Overlay of the high resolution ^{31}P-NMR spectra of untreated (blue) and hypoxia-stressed (red) HeLa extracts (b) Relative % changes of selected PL classes.

The ^{31}P-NMR spectra of untreated (blue spectrum) and $CoCl_2$-treated (red spectrum) HeLa samples are reported in Fig. 2a. The spectral assignment of every resonance to a given PL class was done with reference to the ^{31}P chemical shift scale measured at 300K on 10 mM solutions (CD_3OD as solvent) containing commercially available lipids such as PC, pPC, PE, pPE, PI, PG, PS and SM. ^{31}P-NMR measurements gave reliable clues to the main PL classes present in the raw HeLa lipid extracts and was used to establish the quantitative changes in PL classes distribution after hypoxia-induced conditions. In particular, the ^{31}P NMR spectra showed the presence of the following classes in order of increasing ^{31}P chemical shifts (δ_P values in ppm, % molar ratio in parenthesis): PC (–0.55, 53%), pPC (–0.49, 6.5%), SM (+0.06, 10%), PE (+0.19, 16.5%), PI and pPE (+0.24, 14%) with the latter two classes, unluckily, not resolved each other in spite of high resolution conditions of our ^{31}P measurements ($W_{1/2} \leq$ 2 Hz). The relative changes in lipid distribution after $CoCl_2$ treatment were obtained by ^{31}P–NMR spectra simulations followed by comparison of the corresponding peak area integrations. As shown in Fig. 2b, a significant decrease was found for the overall amount of PI+pPE, small and opposite trends were found for SM (slight decrease, -10%) and PE (slight increase, +10%) whilst PC and pPC kept almost unchanged. Although a small decrease in the total amount of pPE class was clearly observed in the ^{1}H-NMR spectra, since pPE represented only 2-3% of the overall PL content, the most significant contribution to the decrease of the PI+pPE area (-25%) in the ^{31}P-NMR spectra must be attributed to PI lipid species.

Due to the intrinsically low sensitivity and low dynamic range of NMR measurements, minor PL classes such as PS, PG, lyso PL, ceramides and DAGs were or not detected or not further characterized. Anyhow, NMR spectra of lipids do not contain structural information (i.e. chain length, number of unsaturations, double bonds positions) of the acyl chains present in all

PL molecular species. In our study, NMR technique was adopted to estimate inter-class distribution while mass spectrometric analysis was performed to determine intra-class distribution of PL and SL molecular species.

Lipid class-specific (head groups) survey scans through MS/MS measurements

In order to get more comprehensive information about individual PL species, we carried out a detailed mass spectrometric analysis whereby diagnostic fragmentation patterns for all PL classes were established in order to arrive at the complete annotation of lipid species (data not shown). In presence of ammonium ion, the ESI positive ion-mode was found to get clear results for PL identifications; in particular, precursor ion scanning (PIS) of the fragment ion at m/z 184 (phosphocholine head group) was used to identify the protonated molecular ion $[M+H]^+$ of all the PC (including pPC) and the SM lipid species. On the other hand, measurements through the neutral loss scanning (NLS) of 185, 115, 189, 141 and 277 Da were employed to detect PS, PA, PG, PE and PI, respectively. To sum up, Table 1 showed MS/MS scanning methods with diagnostic fragmentations as well as the corresponding precursor ions for PL identification. These preliminary studies were crucial to establish the class-specific MS/MS methods for PL identification and quantification; a mixture of standard PL from different classes was used for HPLC-ESI MS/MS analysis to validate these methods for sample analysis.

Table 1 Characteristic fragmentation patterns of each PL class

Phospholipid Class	Precursor Ion	MS/MS Type	Characteristic Fragment
Phosphatidylcholine (PC)	$[M+H]^+$	Precursor ion scan (PIS) 184	Phosphocholine
Sphingomyelin (SM)	$[M+H]^+$	PIS 184	Phosphocholine
Phosphatidylethanolamine (PE)	$[M+H]^+$	Neutral loss scan (NLS) 141	Phosphoethanolamine
Phosphatidylserine (PS)	$[M+H]^+$	NLS 185	Phosphoserine
Phosphatidylinositol (PI)	$[M+NH_4^+]^+$	NLS 277	Phosphoinositol $+NH_3$
Phosphatidylglycerol (PG)	$[M+NH_4^+]^+$	NLS 189	Phosphoglycerol $+NH_3$
Phosphatidic acid (PA)	$[M+NH_4^+]^+$	NLS 115	Phosphoric acid $+NH_3$

The chromatographic separation and the mass-spectrometric characterization of individual molecular species in the standard PL mixture were optimized by the combination of RP-HPLC (reversed phase liquid chromatography), full scan ESI positive ion-mode assisted by ammonium ions present in the mobile phase and finally by MS/MS precursor ion scanning (PIS) or neutral loss scanning (NLS). As shown in the total ion chromatograms (TIC) in Fig. 3a, the identified PS 18:1/18:1 (by NLS of 185 Da) eluted at 14.04 min while lipids eluted at 20.61 min and 18.31 min were established (PIS of m/z 184) to be PC 18:1/18:1 and SM (d18:1/18:0), respectively. Similarly, PE and PI components were well separated and identified by diagnostic head group survey scan (NLS 141 Da and NLS 277 Da, respectively), which are shown in the TIC in Fig. 3b. Finally, the characterization of PA 18:1/18:1 and PG 18:0/18:0 (by NLS 115 Da and NLS 189 Da, respectively) is shown in Fig. 3c.

Our study confirms that the combination of RPLC and various MS/MS scanning methods is able to target specific PL classes more efficiently than full scan detection.[9,19,20] Moreover, the addition of ammonium ions gives better response factors for each PL class in ESI positive ion-mode by MS/MS with respect to the most used ESI negative ion-mode methodology. Due to ammonium ions in mobile phase, the sodium adducts formation was greatly reduced, leaving the protonated species $[M+H]^+$ for PE and PS and the $[M+NH_4^+]$ adducts for PG, PI and PA as the dominant pseudo-molecular ions, an outcome in keeping with some previous studies.[9,21,22] We also applied this methodology to estimate intra-class PL distribution and to further determine their contributions to the relative changes in lipid composition profile by extra-cellular stimulation.

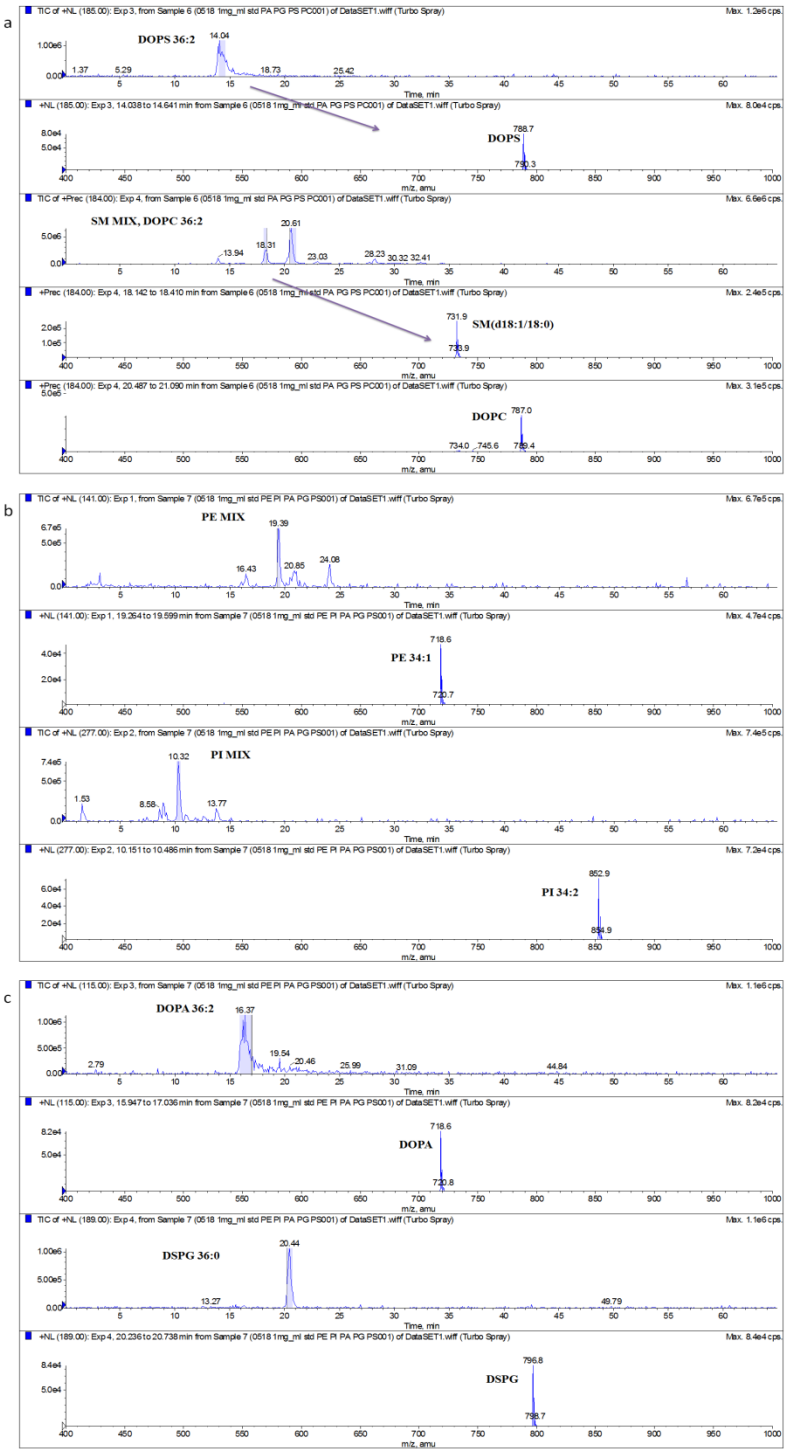

Fig. 3 RPLC MS/MS determination of standard lipid mixtures (DOPC, DOPS, DOPA, DSPG, SM (Brain, Porcine), L-α-PE (Egg, Chicken), L-α-PI (Soy)) in ESI positive mode. (a) Detection of DOPS by NLS at 185 Da and DOPC, SM (d18:1/18:0) by PIS of m/z 184; (b) Identification of PE 34:1 by NLS of 141 Da and PI 34:2 by NLS of 277 Da; (c) Detection of DOPA by NLS of 115 Da and DSPG by NLS of 189 Da.

HeLa cellular phospholipids profiling and hypoxia-induced lipid alterations

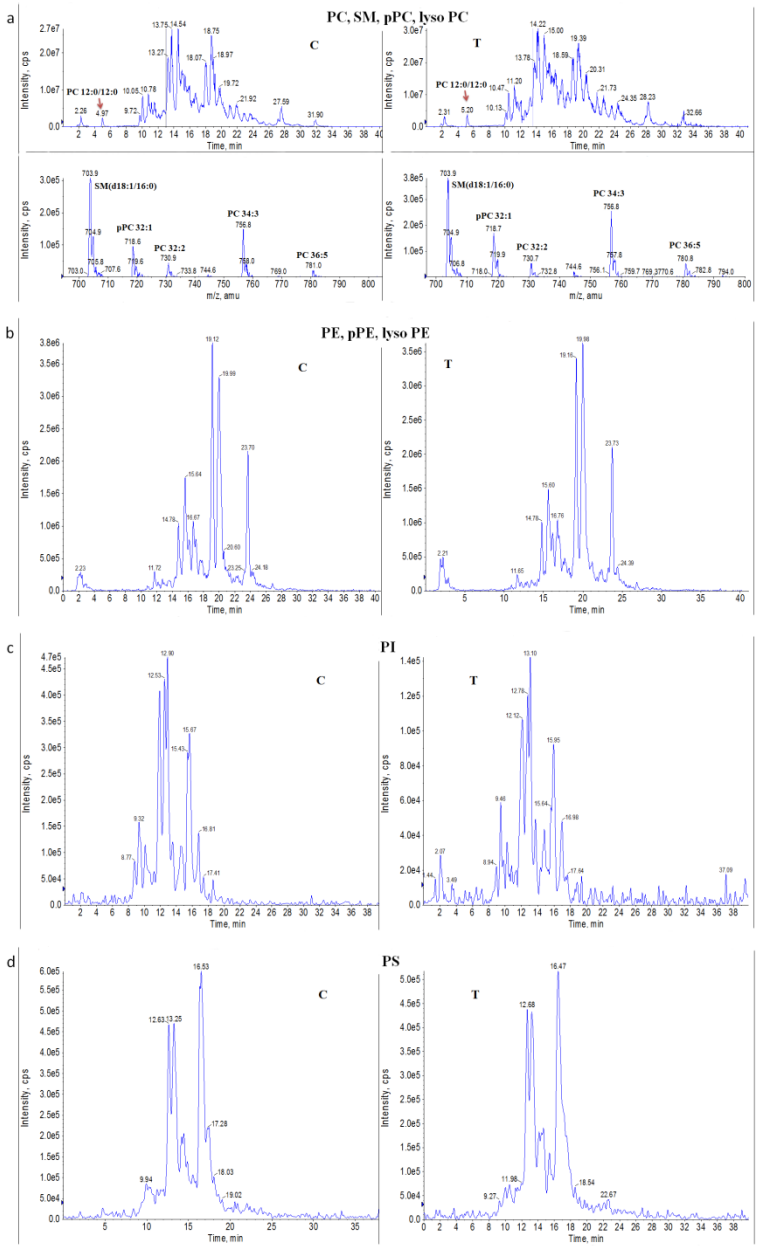

Fig. 4 Ion chromatograms obtained by LC-MS analysis of control HeLa cellular lipids (designated as "C", left) and $CoCl_2$-treated HeLa cellular lipids (designated as "T", right) for (a) top: PC, SM, LPC and pPC, as detected through PIS of m/z 184; bottom: lipid species detected within the time retention windows 13.01–13.12 min (C) and 13.52–13.62 min (T); (b) PE, pPE and LPE, as detected through NLS of 141 Da; (c) PI as detected through NLS of 277 Da; d) PS as detected through NLS of 185 Da. Note that the intensities of PI signals in treated are almost 3 times lower than in untreated HeLa cells.

The efficiency of total cellular lipid extraction was another key point in order to reliably assess the relative changes upon hypoxia stress. To tackle it, a known amount of PC 12:0/12:0 (DLPC) was added before solvent extraction (chloroform/methanol 2:1) in order to estimate the recovery both for control and hypoxia-stressed cells. The estimated lipid recovery was about 60% for both control and treated samples.

Our RPLC-ESI (+) MS/MS methodology allowed a direct relative quantitation of the precursor ion mass spectra of all the lipids bearing the phosphocholine groups (PC, SM, lyso PC and plasmenyl PC) contained in HeLa cells after $CoCl_2$ treatment with respect to those from normal HeLa cell cultures; some examples of identified species are presented in Fig. 4a. As a first outcome, no significant changes of these PC species in hypoxia stressed cells were detected (Fig. 4a) as well as for PE and plasmenyl PE (Fig. 4b). The most relevant effect of $CoCl_2$ treatment was instead observed on PI lipids which were found to strongly decrease (almost 3 folds change, Fig. 4c), in good agreement with results from the above reported ^{31}P-NMR experiments. Similar to PC and PE, there were no significant changes of PS lipids (Fig. 4d).

In total, 189 membrane lipid species were characterized, including 42 species of PC, 33 pPC, 13 lyso-PC (LPC), 39 PE, 15 pPE, 14 PI, 10 SM, 10 lyso-PE (LPE), 4 PG and 9 PS. With the class-specific survey scanning, quantitative data were generated from the peak area of detected precursor ions on the assumption that all the species belonging to the same class had almost identical ESI-MS response factors.[9] In particular, the total amount of each class (after normalization by previously added standard DLPC) was evaluated for control and $CoCl_2$ treated HeLa cells. As shown in Fig. 5a, the amount of LPC increased significantly upon hypoxia stimulation (with p value 0.0085) and the same trend was also clear for LPE (Fig. 5b). On the contrary, the overall amount of PI lipids strongly decreased after hypoxia stimulation, which was

shown in Fig. 5c. The total amount of PG and DAGs in both control and treated cells was found so low that either a reliable analysis was completely hindered (PG) or their presence (DAG) was uncertain. Concerning PS, a class of membrane lipids expected to play an important role in many cellular signaling, they kept almost unchanged with the exception of PS 36:3 and PS 40:5 after hypoxia treatment (Table 3). Few ceramide-derivatives, namely ceramide (d18:0/C18:0)-1P, ceramide (d18:0/C24:1), ceramide (d18:1/C24:0), 1-galactolsyl-ceramide (d18:1/C24:1) and 1-galactolsyl-ceramide (d18:1/C24:0) were identified but the total amount of all these lipids was less than 1% and remained almost unchanged after the treatment.

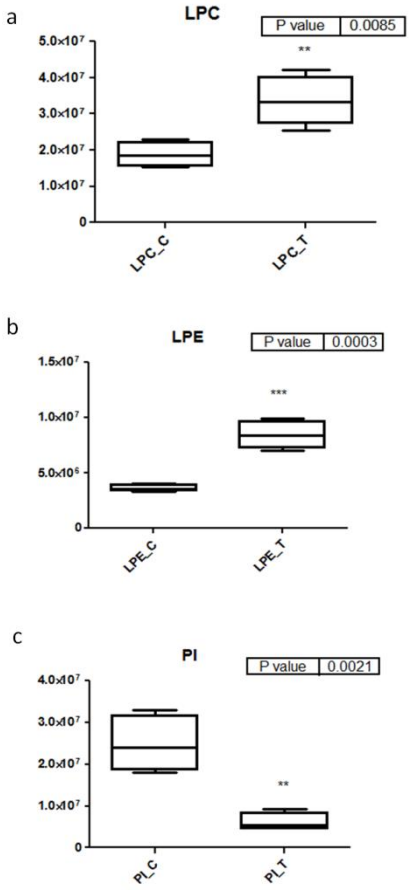

Fig. 5 Amount **o**f overall PL classes (values expressed in term of areas obtained from MS/MS experiments) of control and hypoxia-stressed HeLa cells. Upon hypoxia treatment (a) LPC increases, (b) LPE increases and (c) PI decreases. The superscript (*) shows significant differences of treated (T) with respect to control (C) at $p < 0.05$ (n=4).

Table 2 Relative abundances and number of species of different PL classes in control (C) and hypoxia-treated HeLa cells (T) with a double bond number (N) on the acyl chains higher than 3 or with a double bond number lower than 3.

Double Bonds	PC		pPC		PE		pPE		PI		PS	
	Relative abundance (%)	Nr. of species	Relative abundance (%)	Nr. of species	Relative abundance (%)	Nr. of species	Relative abundance (%)	Nr. of species	Relative abundance (%)	Nr. of species	Relative abundance (%)	Nr. of species
N ≥ 3 (C)	12.4 ± 0.7	***27***	6.1 ± 0.6	***6***	30.9 ± 1.1	***26***	25.6 ± 1.6	***6***	40.1 ± 3.0	***8***	9.4 ± 1.1	***3***
N < 3 (C)	87.6 ± 0.7	***15***	93.9 ± 0.6	***27***	69.1 ± 1.1	***13***	74.4 ± 1.6	***9***	59.9 ± 3.0	***6***	90.6 ± 1.1	***6***
N ≥ 3 (T)	16.0 ± 1.4	*27*	5.4 ± 0.3	*6*	32.6 ± 1.4	*26*	25.2 ± 1.4	*6*	42.1 ± 3.4	*8*	9.3 ± 0.5	*3*
N < 3 (T)	84.0 ± 1.4	*15*	94.6 ± 0.3	*27*	67.4 ± 1.4	*13*	74.8 ± 1.4	*9*	57.9 ± 3.4	*6*	90.7 ± 0.5	*6*

Meanwhile, a relative quantitative analysis was performed by normalizing the peak area of each identified lipid to the overall peak area of all lipids belonging to the same class in order to establish the intra-class distribution of each PL and SL molecular species. The most abundant PC species (% relative abundance in parenthesis) were 34:1 (18.9±1.5), 32:1 (18.7±0.6) and 34:2 (11.1 ± 0.3); the acyl chain length of all the PC species ranged from 28 to 42 whereas the number of double bonds varied from 0 up to 9. Table 2 presented the relative abundances and number of different PL classes in control (C) and hypoxia-treated HeLa cells (T) with a double bond number (N) on the acyl chains higher than 3 or with a double bond number lower than 3. The ratio between polyunsaturated PL species (N ≥3) and PL species with N < 3 varied remarkably in different classes. As shown in Table 2, polyunsaturated PC, pPC and PS species accounted for only 12.4%, 6.1% and 9.4%, respectively whilst the proportion of polyunsaturated species significantly increased in PE (30.9%), pPE (25.6%) and PI (40.1%).

It has been reported that some metabolites which are involved in the biosynthesis and catabolism of phospholipids and other lipids could be affected by the enhanced expression of hypoxia-induced factor (HIF) in hypoxic tumor cell lines, for example, in AML cell lines[23] and prostate cancer cell lines.[24] Generally, hypoxia is able to induce variation in phosphatidylcholine turnover or in myo-inositol level in different cell lines.[23,25,26] For example, it has been reported

that under hypoxic conditions, the accumulation of myo-inositol in AML cells might be related to the phosphatidylcholine turnover.[23] Our investigation seems to suggest that the significant decrease of the amount of PI lipids upon hypoxic condition is probably due to the accumulation of cellular myo-inositol, which played a critical role in d*e novo* synthesis of phosphatidylinositol (PI). The changed level of myo-inositol, which has important functions in mammalian cells, has been associated to adjust phospholipid levels.[27] Myo-inositol is also able to participate in up-regulation of glucose metabolism which can affect glycolytic intermediates synthesis.[28] Furthermore, some previous studies have demonstrated that the synthesis of PI from *myo*-inositol was markedly inhibited by hypoxia in the rabbit carotid body.[29] The researchers speculate that during hypoxia several second messenger cascades are activated, which can directly or indirectly influence PI turnover. Another proposed possibility is attributed to the diminution of ATP levels, which is supported by the report that anoxia in isolated hamster heart or permeabilized adrenal chromaffin cells can both cause a decrease in PI biosynthesis paralleled by a decrease in ATP levels.[30,31] Such modulation and variation in cellular PI may indicate an adaptive response in energy homeostasis of hypoxia-stressed HeLa cells.

Multivariate analysis and individual potential marker analysis

As shown in Table 2 there is no clear evidence of difference in the unsaturation distribution within a given class between treated and untreated cells. We wondered if such a difference could become evident by looking at individual phospholipid within a given class under normal or hypoxia conditions. The plots in Fig. 6 illustrate the multivariate data analysis (MVDA) conducted on the 42 phosphatidylcholine species detected in HeLa. Principal component analysis (PCA), an unsupervised multivariate method, was firstly used to analyze the generated MS data. The first two components of PCA model cumulatively described 84% of the

total variability. The PCA scores plot (Fig. 6a) showed a clear-cut separation between control and hypoxia-treated HeLa cells in PC2 dimension, thus suggesting that hypoxia treatment induced a significant change in phosphatidylcholine profile. The contribution of each phosphatidylcholine species to the discrimination was further investigated in the corresponding loadings plot (Fig. 6b), which displayed the discrimination pattern. Along the second component to the upper part, the variables represented the more abundant phosphatidylcholine species in hypoxia-treated HeLa cells, whilst in the opposite side are reported the more abundant phosphatidylcholine species in the control cells. On the other hand, mono- or di-unsaturated phosphatidylcholine species are much more representative for the untreated HeLa cells.

Partial least squares discriminant analysis (PLS-DA) model, a supervised multivariate technique, was further applied to enhance class separation and to characterize phosphatidylcholine species responsible for such separation. As illustrated in the PLS-DA scores plot (Fig. 6c), a clearer class separation between control and hypoxia-treated cells could be obtained by the first component. Along the first component of the corresponding loadings plot (Fig. 6d), phosphatidylcholine species further away from the main cluster had stronger influence on class separation[32] and show the most significant changes between control and treated cells. Therefore, the metabolism changes of lipid species associated with hypoxia stimulation could be explained. Further looks at how each phosphatidylcholine specie contributed to the separation could give insights into the importance of each species (variable) and thus variable influence on projection (VIP) plot was displayed (Fig. 6e). This VIP plot summarized the importance of each variable accounting for hypoxia effects. In fact, variables with higher VIP values ($\geq$1) were most influential and accordingly picked out as potential markers (9 candidate phosphatidylcholine

species). In order to confirm that we were dealing with "true lipid markers", univariate analysis (unpaired t-test) was finally carried out.

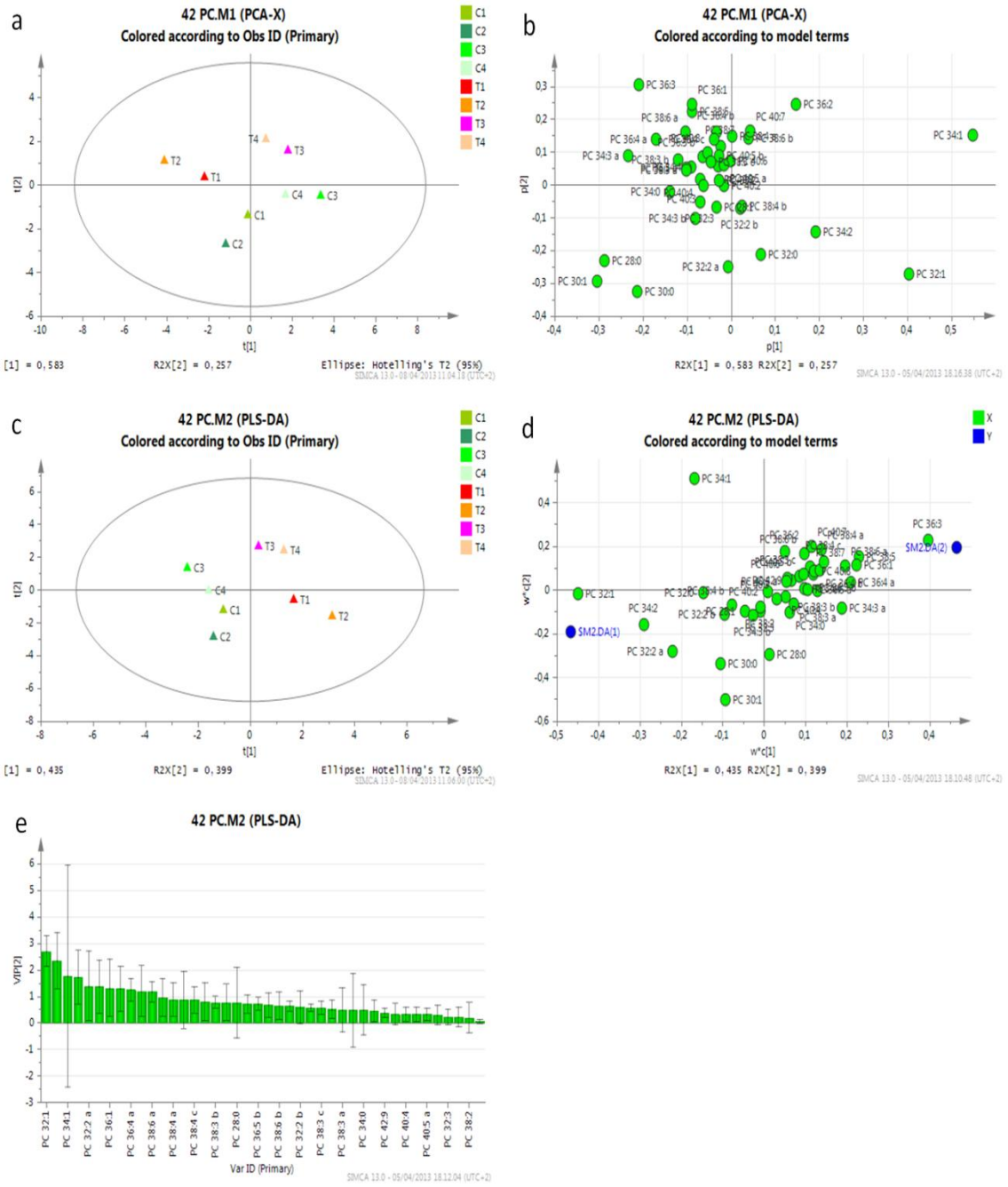

Fig. 6 Multivariate data analysis of 42 species of HeLa cellular phosphatidylcholine (PC). (a) PCA scores plot, and (b) Loadings plot of the control and hypoxia-treated HeLa cells (designated as "C" and "T" respectively, n=4) (c) PLS-DA scores plot and (d) Loadings plot (e) VIP plot from PLS-DA.

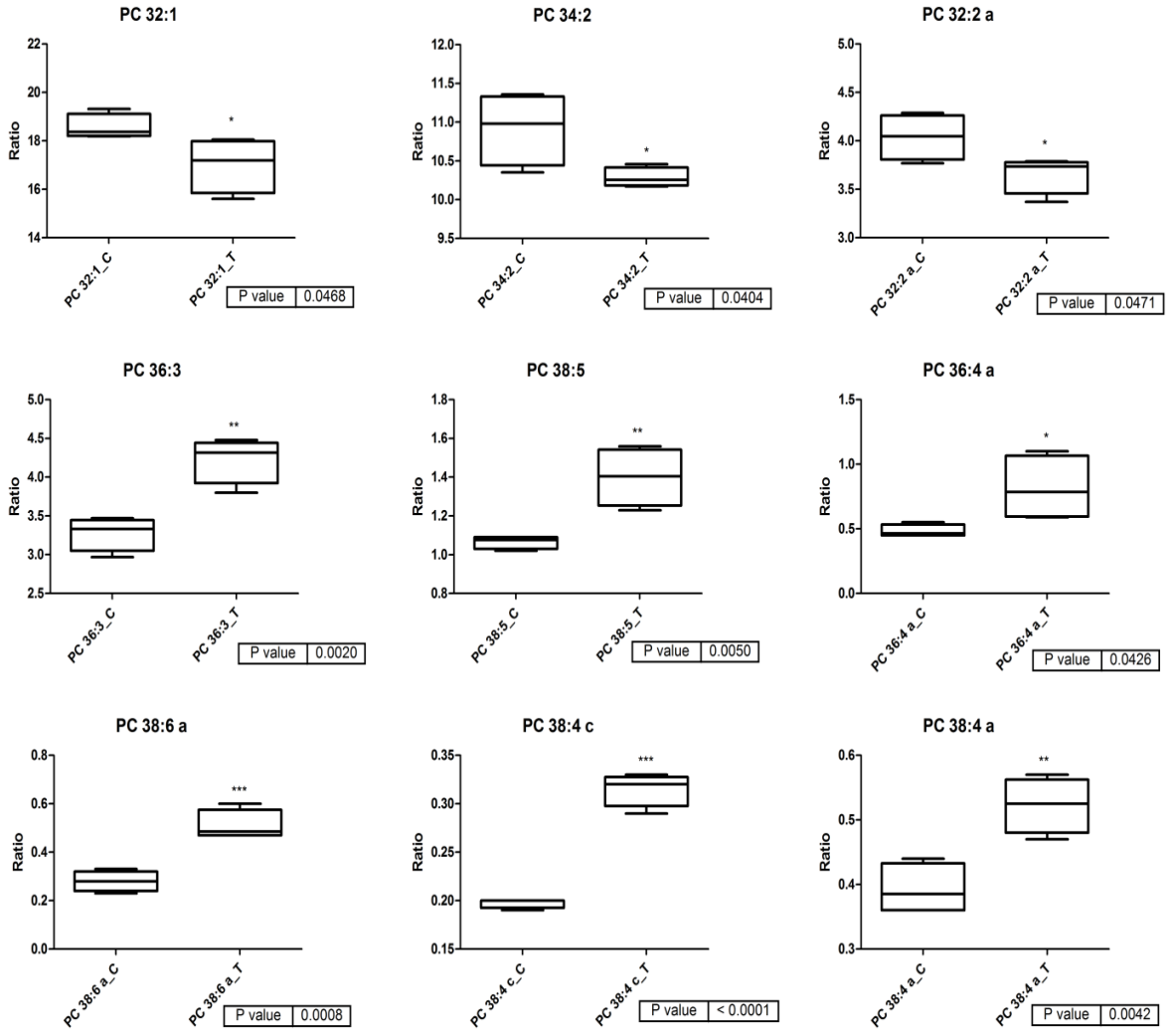

Fig. 7 Univariate analysis of potential PC markers obtained from PLS-DA. Mono- or di-unsaturated PC (32:1, 34:2, 32:2a) decreased whilst poly-unsaturated PC species (36:3, 38:5, 36:4a, 38:6a, 38:4c, 38:4a) increased upon hypoxia stress. The superscript (*) shows significant differences of treated (T) with respect to control (C) at $p < 0.05$ (n=4).

As shown in the individual marker analysis in Fig. 7, hypoxia-stress induced a remarkable decrease in mono- and di-unsaturated PC species (32:1, 34:2 and 32:2a), whereas polyunsaturated PC species (36:3, 38:5, 36:4a, 38:6a, 38:4c, 38:4a) were increased compared to the corresponding level of control samples. MVDA of PL molecular species from other classes and individual marker analysis were performed in a similar workflow as previously described.

The results of MVDA and the univariate confirmation by t-test can show the effects of hypoxia stress on HeLa cells. The identified candidate PL markers and their qualitative changes are presented in Table 3. Moreover, most of LPC and LPE species exhibited pronounced variations and discriminatory power, as reported in Table 4. These analyses showed that hypoxia stress could alter metabolism of PL species from different classes (PC, PE, pPE, pPC, PI, PS, LPC and LPE) and also revealed a general trend induced by hypoxia treatment: PL species with polyunsaturated acyl chains greatly increased whilst mono- and di-unsaturated species reduced. Based on such findings, Unsaturation Index (UI) analysis of each PL class was performed.

Table 3 Identified potential PL markers and their corresponding qualitative changes in hypoxia-treated (T) or control HeLa cells (C).

Lipid Class	Identity of PL molecular species	Higher abundance in Control (C) or Treated (T)
PE	PE 34:2	C
Plasmenyl PE	pPE 34:1	T
Plasmenyl PE	pPE 36:5	C
Plasmenyl PE	pPE 38:6	T
Plasmenyl PC	pPC 36:2	T
Plasmenyl PC	pPC 36:1	T
Plasmenyl PC	pPC 36:3	C
Plasmenyl PC	pPC 34:2	T
Plasmenyl PC	pPC 36:5	C
Plasmenyl PC	pPC 38:6	C
PI	PI 32:1	C
PI	PI 38:4	T
PI	PI 38:3	T
PS	PS 36:3	T
PS	PS 40:5	C

Table 4 Potential LPC, LPE markers and their corresponding distributions in hypoxia-treated or control HeLa cells

Lipid Class	Identity of PL molecular species	Higher abundance in Control (C) or Treated (T)
LPC	LPC 20:1, LPC 22:5, LPC 14:0, LPC 22:6, LPC 22:4, LPC 16:1, LPC 20:5, LPC 18:2, LPC 20:3	T
LPE	LPE 20:4, LPE 22:5, LPE 22:4, LPE 20:3, LPE 24:4,	T
LPE	LPE 18:0, LPE 18:1	C

Unsaturation Index analysis of each phospholipid class

The intra class unsaturation index (UI) represents the sum of the number of double bonds of each lipid molecular species averaged by their molar fraction within a given class. It was indicated in Fig. 8 that by hypoxia stimulation, UI of LPC, PC, PE and LPE increased (Fig. 8a, b, d and e), while on the contrary, the UI of pPC decreased as compared with the control HeLa cells (Fig. 8c). Results shown in Fig. 8 were in accordance with individual marker analysis presented in Table 3 and 4, which indicated a clear trend of increasing UI for most of the PL molecular species due to hypoxia stress. Such analyses demonstrated that hypoxia had great effect to alter the fatty acid compositions of different classes of PL in HeLa cellular membrane with an overall enhancement of the acyl chain unsaturations.

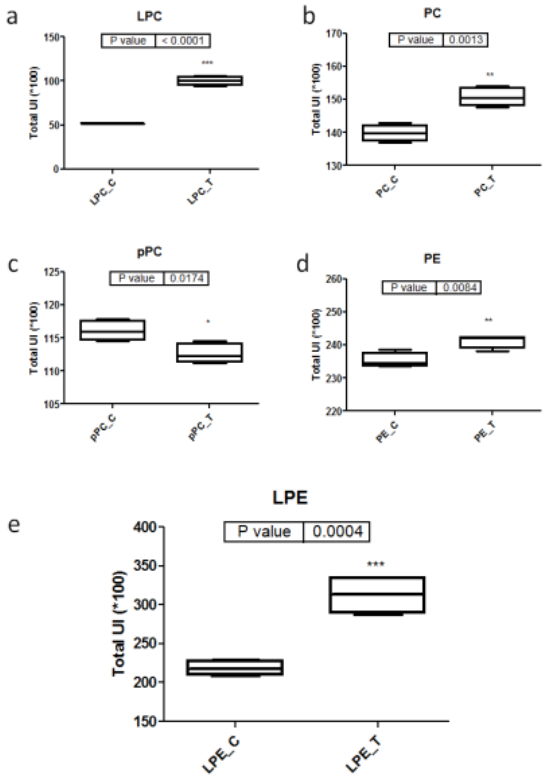

Fig. 8 Unsaturation Index (UI) analysis for each PL class. By hypoxia treatment UI of (a) LPC, (b) PC, (d) PE and (e) LPE increased whilst (c) pPC decreased. The superscript (*) shows significant differences of treated (T) with respect to control (C) at $p < 0.05$ (n=4).

The membranes lipids are built from fatty acyl chains of various degree of (un)saturation displaying different effects on membrane fluidity and permeability[33] in order to adapt the cell itself to environmental changes. Such adjustment of cellular membrane fluidity might impact several membrane-dependent functions including cell signaling.[34] Previous studies demonstrated that perturbations of the order-state of membranes were critical for physiological properties of cells such as membrane dynamics as observed in different disease states.[35]

Mechanisms associated with hypoxia-stimulated membrane fluidity and dynamics changes are not clear yet, while such changes might be linked to the enhanced function of fatty-acyl CoA desaturases or the involvement of cellular triglycerides turnover, the unsaturation properties of the latter could also be altered by hypoxia.[36] Another interesting mechanism underlying the alteration of membranes was that the plasma membrane had more abundant sphingolipids, sterols and saturated PL species; instead, the endoplasmic reticulum (ER) contained primarily unsaturated PL species. Such lipids distribution determined that the plasma bilayer membrane was more rigid and impermeable with promoted compartmentalization of specific proteins involved in cellular signaling and cell-cell adhesion. On the other hand, unsaturated PL species would make the ER membrane more fluid and available for the incorporation of newly synthesized proteins.[4] Taken together, the observed increase in membrane PL unsaturation might attribute to the enhanced ER activity in comparison with plasma membrane activity by hypoxia stimulation. In order to confirm this hypothesis, however, a lipidomics analysis on different cell components (plasma, ER, mitochondria, nucleus, and Golgi apparatus) is clearly required but their separation/purification is still a challenging task.

3.5 Conclusions

We have developed an RPLC-MS/MS-based methodology for precise identification and characterization of cellular lipids. Cervical cancer derived cells (HeLa cells) were selected as a model to study the effects of hypoxia on tumor lipid profile alterations. Phospholipid profiles of control and hypoxia-stressed cells have been compared by combining NMR and LC-MS data with multivariate and univariate data analysis tools. In particular, our research is the first report of cellular lipidomics study combining NMR with MS technique. Although modern lipidomics approaches mainly rely on the wide arsenal of MS techniques, NMR represents a powerful tool for the qualitative analysis and often it is crucial in the elucidation of their structural details. First of all, the sample preparation for NMR measurements is rather simple and rapid, not implying any derivatization of components. Moreover, NMR analyses carried out on lipids raw extract give an immediate perception of the main lipids therein present. Although the number of compounds detected in a raw lipid extract is limited, the NMR spectra give a good picture of what really is present, minor compounds might not be seen, but the major trends are clear. In particular, through ^{31}P-NMR it is possible to differentiate the membrane lipids in distinct PL classes and to obtain reliable and reproducible quantitative data such as the molar fractions of all the PL classes. It is worth of mention that in all the (only) MS-based approaches these data are difficult to obtain since PL classes have quite different response factors in ESI source and a direct comparison among all these classes is often hindered by several other factors. Among the latter, neutral membrane lipids (PC, pPC,ePC,SM) are usually detected and quantified in positive ESI ion-mode whilst anionic membrane lipids (PE,PS,PG,PI,CL) require negative ESI ion-mode conditions. The comparison of data obtained in such different conditions is often quite cumbersome and, even worst, eventually unreliable. Of course NMR on lipids shows also some

elements of weakness. First, due to its intrinsically low sensitivity, it is necessary to deal with an adequate number of cells, at least a magnitude order higher than used in MS measurements. More importantly, lipids belonging to the same class show almost the same ^{1}H- and/or ^{31}P-NMR spectra no matter of the acyl chain length, number and position of unsaturations. This limitation completely prevents to establish the intra-class chemical diversity. But, the latter information is rather easily achieved by MS measurements, in particular by exploiting the modern LC-MS marriage, making the two techniques highly complementary. In the case discussed here, this joint approach allowed us to characterize up to 189 PL molecular species.

Interestingly, our data showed that hypoxia stimulation significantly reduced the total amount of cellular PI. In contrast, we observed a prominent increase of the amount of LPC as well as LPE in the same samples. Another interesting finding was that hypoxia stress affected cell membrane fluidity and dynamics by increasing the unsaturation of the acyl chains in several lipid classes. Statistical analysis revealed the membranes lipid markers that had discriminatory power. Such analysis might explain the changes of membrane fluidity and dynamics observed in cells in the presence of hypoxia. On the whole, the alterations in lipids amount and the fluidity enhancement in HeLa cellular membrane induced by hypoxia are of vital importance for membrane-dependent functions and the adaptive response of HeLa cells to hypoxia environment. Taken together, our results have proved that lipidomics approach could be explored as an important and integrative tool to investigate effects of stress inducers on lipid distribution and dynamics. Further investigations are required to understand the underlying biochemical mechanisms whereby lipids distribution can be altered; besides, studies on lipid biosynthesis through the aid of genomics/transcriptomics/proteomics tools will open new perspective for tumor treatment or cancer prevention.[37]

3.6 Acknowledgments

We thank Mr. Adriano Sterni (University of Trento) for LC-MS analyses, and technical assistance. We are grateful to dr. Pietro Franceschi (Edmund Mach Foundation, TN) for the helpful discuss and support with the data analysis. The financial supports from Department of Physics and CIBIO (Centre for Integrative Biology) at the Univeristy of Trento are also acknowledged.

3.7 Notes and References

1. M. C. Culf, D. A. Barnett, A. S. Culf and I. Chute, *Drug Discov. Today*, 2010, **15**, 610-621.

2. M. R. Wenk, *Nat. Rev. Drug Discov*., 2005, **4**, 594-610.

3. K. Tripathy, *J. Comput. Sci. Syst. Biol.*, 2011, **4**, 93-98.

4. M. B. Khalil, W. M. Hou, H. Zhou, F. Elisma, L. A. Swayne, A. P. Blanchard, Z. M. Yao, S. A. L. Bennett and D. Figeys, *Mass Spectrom. Rev.*, 2010, **29**, 877-929.

5. M. P. Wymann and R. Schneiter, *Nat. Rev. Mol. Cell Biol.*, 2008, **9**, 162-176.

6. M. E. Dumas, E. C. Maibaum, C. Teague, H. Ueshima, B. F. Zhou, J. C. Lindon, J. K. Nicholson, J. Stamler, P. Elliott, Q. Chan and E. Holmes, *Anal. Chem.*, 2006, **78**, 2199-2208.

7. G. F. Pauli, B. U. Jaki and D. C. Lankin, *J. Nat. Prod*., 2005, **68**, 133-149.

8. O. Yanes, R. Tautenhahn, G. J. Patti and G. Siuzdak, *Anal. Chem.*, 2011, **83**, 2152-2161.

9. R. Taguchi, T. Houjou, H. Nakanishi, T. Yamazaki, M. Ishida, M. Imagawa, T. Shimizu, *J. Chromatogr. B*, 2005, **823**, 26-36.

10. X. Li and Y. J. Yuan, *OMICS*, 2011, **15**, 655-664.

11. C. V. Hague, A. D. Postle, G. S. Attard and M. K. Dymond, *Farad. Discuss.*, 2013, **161**, 481-497.

12. C. R. Santos and A. Schulze, *FEBS J.*, 2012, **279**, 2610-2623.

13. A. J. Giaccia, M. C. Simon and R. Johnson, *Genes Dev.*, 2004, **18**, 2183-2194.

14. A. M. Weljie and F. R. Jirik, *Int. J. Biochem. Cell Biol.*, 2011, **43**, 981-989.

15. E. G. Bligh and W. J. Dyer, *Biochem. Cell Biol.*, 1959, **37**, 911-917.

16. C. V. Hague, PhD thesis, Faculty of Engineering, Science and Mathematics, *University of Southampton*, 2009, 271 pp.

17. S. J. Yang, J. Pyen, I. Lee, H. Lee, Y. Kim and T. Kim, *J. Biochem. Mol. Biol.*, 2004, **37**, 480-486.

18. G. L. Semenza, *Curr. Opin. Cell Biol.*, 2001, **13**, 167-171.

19. X. Han, J. Yang, H. Cheng, H. Ye and R.W. Gross, *Anal. Biochem*., 2004, **330**, 317-331.

20. K. Ekroos, I. V. Chernushevich, K. Simons and A. Shevchenko, *Anal. Chem*., 2002, **74**, 941-949.

21. M. Koivusalo, P. Haimi, L. Heikinheimo, R. Kostiainen and P. Somerharju, *J. Lipid Res.*, 2001, **42**, 663-672.

22. J. V. Busik, G. E. Reid and T. A. Lydic, *Methods Mol. Biol*., 2009, **579**, 33-70.

23. A. Lodi, S. Tiziani, F. L. Khanim, M. T. Drayson, U. L. Gűnther, C. M. Bunce and M. R. Viant, *ACS Chem. Biol.*, 2011, **6**, 169-175.

24. K. Glunde, T. Shah, P. T. Winnard, V. Raman, T. Takagi, F. Vesuna, D. Artemov and Z. M. Bhujwalla, *Cancer Res.*, 2008, **68**, 172-180.

25. E. Ackerstaff, D. Artemov, R. J. Gillies and Z. M. Bhujwalla, *Neoplasia*, 2007, **9**, 1138-1151.

26. F. Podo, *NMR Biomed.*, 1999, **12**, 413-439.

27. A. Ferretti, S. D'Ascenzo, A. Knijn, E. Iorio, V. Dolo, A. Pavan and F. Podo, *Br. J. Cancer*, 2002, **86**, 1180-1187.

28. R. Mendelsohn, P. Cheung, L. Berger, E. Partridge, K. Lau, A. Datti, J. Pawling and J. W. Dennis, *Cancer Res.*, 2007, **67**, 9771-9780.

29. R. Rigual, M. T. G. Cachero, A. Rocher and C. González, *Pflügers Arch., Eur. J. Physiol.*, 1999, **437**, 839-845.

30. J. T. Wong, R. Y. K. Man and P. C. Choy, *Lipids*, 1996, **31**, 1059-1067.

31. D. A. Eberhard, C. L. Cooper, M. G. Low and R. W. Holz, *Biochem. J.*, 1990, **268**, 15-25.

32. H. Zhang, J. R. Wang, L. F. Yau, H. M. Ho, C. L. Chan, P. Hu, L. Liu and Z. H. Jiang, *Mol. BioSyst.*, 2012, **8**, 3208-3215.

33. E. Busse, G. Zimmer, O. Bartsch and B. Kornhuber, *Oncology*, 1993, **50**, 241-244.

34. E. J. Helmreich, *Biophys. Chem.*, 2003, **100,** (1-3), 519-534.

35. J. M. Ntambi, *Prog. Lipid Res.*, 1995, **34**, 139-150.

36. M. Ståhlman, C. S. Ejsing, K. Tarasov, J. Perman, J. Borén and K. Ekroos, *J. Chromatogr. B*, 2009, **877**, 2664-2672.

37. T. Mashima, H. Seimiya and T. Tsuruo, *Br. J. Cancer*, 2009, **100**, 1369-1372.

Chapter 4. Comparative Lipidomic studies of in vitro urinary bladder cancer models RT4 and T24: an investigation on urothelial metastasis

4.1 Abstract

Comparative lipidomic studies of urothelial cancer cell line RT4 as a model system of a benign tumor and T24 as a model system of a metastatic tumor [1] was performed to investigate how and how much changes in lipids profile are related to urothelial metastasis. RT4 cell line derives from the papilloma urinary bladder and such cells are not malignant, which display normal epithelial cell characteristics while the malignant cell line T24 displays spreading and invasive motility, which represents the development of urothelial cancer. Such metastasis progression was proposed to correlate with specific mutations [2] and significant changes of the lipids metabolism. Our study, here reported for the first time, points out that the malignant cell type shows a strong decrease (3-fold) of ether PC species complemented by a sharp increase of the length and the average unsaturation number of their acyl chains. Also ceramide-based sphingolipids show different profiles in these two types of cells. Further analyses are in progress and more information will be acquired in the near future.

4.2 Introduction

The specific structural characteristics of urothelial cells which cover the mammalian urinary tract enable the tight organization of urothelium to form blood – urine barrier as the tightest and most impermeable barrier in the body. In urinary bladder, the normal urothelium consists of roughly 3 to 5 layers of cells composed of a thick layer (at the apical membrane) of specific glycoprotein “uroplakin” incorporated with lipid membranes. As a special type of

epithelium, the structure and functionality of related proteins are broadly studied [3-5]; however, the lipid directed research still remains far behind, not even mentioned lipid hallmarks in the relevant pathologic states. Originated as epithelial cells in urinary bladder which can get more access for extended periods to urine in which chemicals are concentrated, urothelium is much susceptible to carcinoma. So the exposure of urinary bladder to certain chemicals can lead to urinary bladder cancer in which specific alterations in lipid profiles may occur.

In the pathogenic state of malignancy, epithelial tumor is able to form vascularized colonies (metastases) at different sites in the body, whereas benign tumors cannot. Thus, *in vivo* definition, cancers can be invasive and metastasize, instead, benign tumors can principally be divided into two groups as those associated with progressing to cancer and those without [6]. As pointed out by C.A. Klein (2013), the molecular differences between benign and malignant tumors are poorly studied and appreciated. Following malignant transformation at the genetic and epigenetic levels, an observed metastatic phenotype is dependent on varied behavior at different cellular levels. As protection to cytoplasmic components, plasma membrane can perform endocytosis and is able to increase mechanical stability during cell division. During cancer metastasis the separation of individual cells from tumor is common and the flexible features of membrane lipids can aid to decrease shear forces in such separation [7]. Besides, cellular plasma membrane provides specific domains for protein-lipid interactions, some of which are involved in structural and signaling alterations during cell proliferation or cell death [8]. For example, proteins of the receptor tyrosine kinases (RTK) family members and other signaling proteins such as Ras, caveolins and CD44 have been demonstrated to mediate cell motility and migration in association with lipid rafts [9-11]. Despite important roles of lipids in tumor metastasis, systematic studies on lipid characteristics and variations related to this

progress have rarely been mentioned. And therefore, extensive interest in lipidomic studies arises due to such close relations between metastatic progress and changes in lipid profiles.

With respect to urinary bladder, there are two types of pathological *in vitro* model systems: 1) urothelial cell line RT4 as a model system of benign tumor, and 2) urothelial cell line T24 as a model system of a metastatic tumor. In particular, RT4 cell line derives from a transitional cell papilloma of urinary bladder (a grade I urothelial carcinoma) [12, 13] where cells are nonmalignant displaying similar growth and motility characteristics to normal epithelial cells [1]. Compared to RT4, T24 cells derive from poorly differentiated (grade III) transitional urinary bladder carcinoma [12, 14], in which cells display malignant characteristics such as non-self-limited growth with extensive invasiveness and pervasion. These two models are very representative in the metastatic progression and such comparative studies between benign and malignant bladder model system may reveal a continuous process for urinary bladder cancer development [1]. So far the two representative models have been extensively employed in bladder cancer research such as mutation-related studies or morphological comparisons [15], whereas no systematic lipid studies have yet been performed.

As described in the introduction of this thesis, several studies have linked the involvement of GSL in cancer pathogenesis [16], as well as it has been also proposed association of malignant transformation with abnormal glycosylation and the subsequent GSL variations [17]. Moreover, a certain biophysical characterization of RT4 and T24 has demonstrated that T24 cells possess lower stiffness due to reorganization of their molecular network [12]; however, no further studies have related global lipid variations which may contributes to such biophysical alterations. Thus, more information on global lipid profile analysis including GSL characterization need to be investigated.

In order to address the metastatic related alterations in urothelial bladder lipid profile, to elucidate the associated variation pattern, and to open further investigations on relevant cellular function as well as development of the therapeutic potential in bladder cancer treatment, we performed a comparative lipidomic study employing RT4 and T24 as model systems. Firstly we characterized the main PL and GSL (only d18:1 ceramides based GSL) classes and individual molecular species as well as cholesterol in RT4 and T24 cells by our multi-technique approach where high resolution NMR measurements were combined with classical HPLC–ESI QqQ MS/MS techniques. Furthermore, MVDA was also applied to discriminate RT4 and T24 illustrating lipid variation patterns and discovering potential lipid markers in association with urothelial bladder metastasis. To sum up, our data for the first time elucidate how the bladder cancer development is linked to lipid variations and provide a preliminary insight into the corresponding mechanisms.

4.3 Material and methods

Chemicals

All the solvents and lipid standards are the same as described in chapter 3, and moreover, another GSL standard of C16 Galactosyl (ß) Ceramide (d18:1/16:0) (D-galactosyl-ß-1,1' N-palmitoyl-D-*erythro*-sphingosine) was purchased from Avanti Polar Lipids (Alabaster).

Urothelial cell cultures of RT4 and T24

Urothelial cell cultures were performed as in Imani et al. (2012). Briefly, both of human urothelial cell lines RT4 and T24 were cultured in a 1:1 mixture of Advanced-Dulbecco's modified essential medium (ADMEM, Invitrogen, Gibco, Paisley, UK) and Ham's F-12 medium (Sigma-Aldrich, St. Louis, MO, USA), supplemented with 10% fetal bovine serum (FBS, Gibco,

Invitrogen, Carlsbad, CA, USA), another 5 µg/ml insulin-transferrin-selenium supplement (Gibco, Invitrogen), 100 µg/ml streptomycine and 100 units/mL penicillin. Both types of cell culture were plated with seeding density of 5×10^4 cells/cm^2 in cell culture flasks with 75cm^2 available growth areas (T75). To achieve sufficient biomass for NMR analysis, 3 flasks of T24 cultures and 2 flasks of RT4 cultures would be necessary (approximately $3*10^7$ cells in each case). Cells were incubated at 37°C in a humidified atmosphere of 5% CO2 (v/v) in air for one week. After one week growth to confluence, cells were detached by incubation with TrypLE Select (Gibco, nvitrogen) at 37°C, resuspended in the medium, centrifuged at 200g for 5 minutes and collect the pellets for further lipid extraction and analysis.

Lipid extraction and sample preparation

The total lipid extraction procedures previously described in chapter 3 was modified as a two-step protocol in order to expand lipid recovery to also highly polar lipids (eg.GSL) from biological matrix [18, 19]. In short, the collected pellets are dissolved in 1 ml Milli-Q water by gently pipetting and moved to a glass bottle. Before lipid extraction, 60 ul of 100 ng/ul standard DLPC (12:0/12:0) distinct from any natural cellular lipid as previously described was added to the solution. 5 ml of chloroform/methanol (v/v 10:1) was added to the resuspended pellet followed by sonication in ice and shaking for 2 h. After that, the samples were centrifuged at 2500 rpm for 10 min. The lower organic phase was carefully collected into a glass vial and the upper aqueous phase was subjected to another extraction with 3 ml of chloroform/methanol (v/v 2:1) under shaking for 1h. Finally, all the combined lower organic phase was evaporated by Rotovapor and the lipid extracts were initially dissolved in 700 ul perdeuterated methanol (CD_3OD) for NMR measurements. At the end of NMR analysis the sample was fluxed with N_2 to reconstitute in 300 ul MeOH for all the MS analyses

NMR analysis and MS measurements

As described in detail in chapter 3, the analytical conditions (both NMR and LC-MS/MS analysis) are similar except for a certain modifications and improvements. Characteristic fragmentation of GSL standard C16 Galactosyl (ß) Ceramide (d18:1/16:0) was studied and optimized using triple quadruple mass spectrometry (Applied Biosystems API 3000^{TM}, Italy). Full scan and MS/MS scanning were performed both in positive and negative ionization mode. The sphingosine-based (d18:1) class-specific Product Ion Scan of the ions at m/z 264 and dihydrosphingosine-based (d18:0) PIS of the ions at m/z 266 in ESI-positive mode [20] were optimized to characterize d18:1-based and d18:0-based GSL indicating the precursor ion form of $[M+H]^+$. Both this daughter ions are attributable to dehydrated sphingosine (264 Da) or dehydrosphingosine (266 Da) backbone deriving from the loss of the N-acyl chain and 2 water molecules from the corresponding $[M+H]^+$ parent ion. Analytical parameters were as follows: NEB 9, CUR 10, TEM 300 ^{0}C, IS 5 kV, CAD 4, DP 65, FP 250, EP 5, CE 50 and CXP 18. Unit resolution was set for both Q1 and Q3 and step size was 0.1 amu. Meanwhile, the characteristic fragmentation pattern of another important lipid class diacylglycerols (DAG) was studied demonstrating NLS 35 able to achieve DAG identification and quantification with precursor ion $[M+NH_4^+]^+$. Analytical parameters for DAG analysis were the same as for other GPL NLS condition.

Data processing

All the data processing procedures are the same as described in chapter 3. In brief, after pre-processing the acquired raw MS/MS spectral data and identification of individual lipid species, data matrices comprised of rows representing different samples and columns indicating relative ratio of individual lipid molecular species as variables were subjected to MVDA to discriminate

RT4 and T24. Potential lipid species markers observed by PCA which had significant discriminatory power were subjected to univariate unpaired t-test carried out with GraphPad Prism 5.

4.4 Results and discussions

Morphological comparison between RT4 and T24

At first, morphological features of nonmalignant RT4 cell cultures and malignant T24 cell cultures were compared (Fig. 1). Originated as epithelia, RT4 cells (bottom panel) firmly bound to each other and showed typical epithelial shape similar to the phenotype of normal urothelial cells, which was termed polygonal cell shape. In contrast, as invasive urothelial carcinoma, T24 cells (top panel) tend to separate from each other and showed irregular fibroblastic shape with elongated filopodia, plasma membrane elongations typical for extensive motility. So the morphological comparison between RT4 and T24 showed different features, which might be associated with differences in lipids comprising biological membranes.

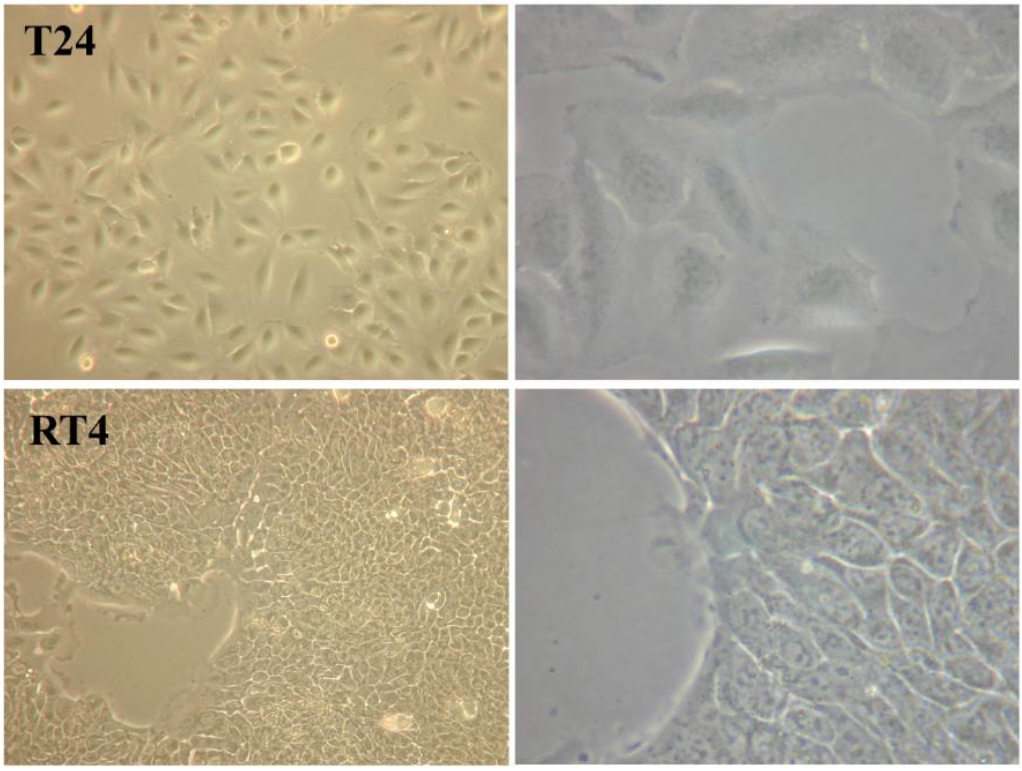

Fig. 1 Phase-contrast microscopic images for T24 (top) and RT4 (bottom) morphological comparison: Left column (100x magnification, scale bar 20 µm), right column (400x magnification, scale bar 20 µm).

^{1}H-NMR and ^{31}P-NMR analysis of RT4 and T24 lipid extracts

The lipids extracted from cultured RT4 and T24 cells were both dissolved in deuterated methanol (CD_3OD, 700 µl) for 1D (^{1}H and ^{31}P) and 2D (HSQC and HMBC)-NMR determinations at 300 K. The ^{1}H-NMR spectrum (128 transients and 5 sec of relaxation delay) provided information to study the overall lipid profile of cellular membrane, including PL as well as TAG and cholesterol. First of all, a careful inspection of ^{1}H-NMR spectra of these lipid extracts shows (Fig. 2a, where spectra are normalized on the characteristic singlet peak at δ_H 3.224 s of all (PC+ SM) species) a very significant difference in the overall distribution of unsaturations in the acyl chains. In fact, whilst in RT4 extract (red line) the peak area of the signals at δ_H ~2.84 attributable to bis-allylic protons (present only in PUFA chains) are much

lower than the corresponding signals in the T24 sample, the opposite change is observed for the mono-allylic protons (present also in MUFA chains) at $\delta_H \sim 2.04$. This is a strong evidence that polyunsaturated chains are somehow recruited or ex novo biosynthesized during cancer development. Concerning the structures of PUFA chains ^{1}H-NMR spectrum of T24 cell extracts clearly indicated that they must be ω-6 type polyunsaturated since the downfield triplet (δ_H 0.97) expected for terminal Me in ω-3 type is absent and no long-range coupling was found in this region neither with olefinic protons (δ_H 5.34) nor with bis-allylic protons (δ_H 2.84) in the corresponding TOCSY-2D spectrum. Another striking difference between the two cell lines that can be promptly appreciated in their ^{1}H-spectra (Fig. 2b, spectra normalized as Fig. 2a) relies on the relative amount of TAGs. In fact, the relative amount of TAG as estimated by the relative intensity signals (2H, $\delta_H \sim 4.36$, dd) attributable to isochronous protons at C1 and C3 positions of the glycerol backbone is much higher in RT4 than in T24. In fact, by TOCSY-2D analysis it was easily established that the residual signals present in this region in T24 ^{1}H- NMR spectrum were mainly due to the shielded olefinic proton of 1Z-alkenyl chains of p-PC and p-PE species. Other minor changes were also detected such as an increase of SM but, essentially, the main structural information was that PUFA lipids species increase whilst TAG neutral lipids decrease in T24 with respect to RT4. Worth of note, the molar ratio [Chol]/ [all PC+SM] as obtained by peak-normalized-area ratio of the corresponding Me's signals was found slightly lower in T24 (0.50±0.01) than in RT4 (0.54 ±0.01) cell line (Fig. 2a).

^{31}P-NMR analysis (Fig. 2c), however, again shows its complementarity to ^{1}H-NMR by adding another important piece of information concerning the relative amount of 1-alkyl (ether)-2-acyl PC species (specifically indicated as e-PC, to distinguish from plasmenyl PC indicated as p-PC). Concisely, *while in RT4 e-PC lipids are a significant part (~ 17%) of the overall PL*

species, they are almost depleted in T24 cells. Moreover, this analysis confirms the ^{1}H-NMR derived information that the relative molar fraction of SM is higher in T24 (~6.5%) than in RT4 (~3.5%); finally the area of the signal attributable to unresolved PC + plasmenyl-PC at δ_P = -0.55 is slightly higher in T24 (~45%) than in RT4 (~40%) but still not sufficient to account for the overall strong reduction of e-PC lipids observed in malignant T24 cells. Although further biosynthetic experiments are required to understand the mechanism of lipid trafficking, our results seem to suggest that, at least partially, the tumor progression leads to a rewiring of 1-saturated alkyl-2-acyl PC into 1-PUFA-acyl,2 acyl PC.

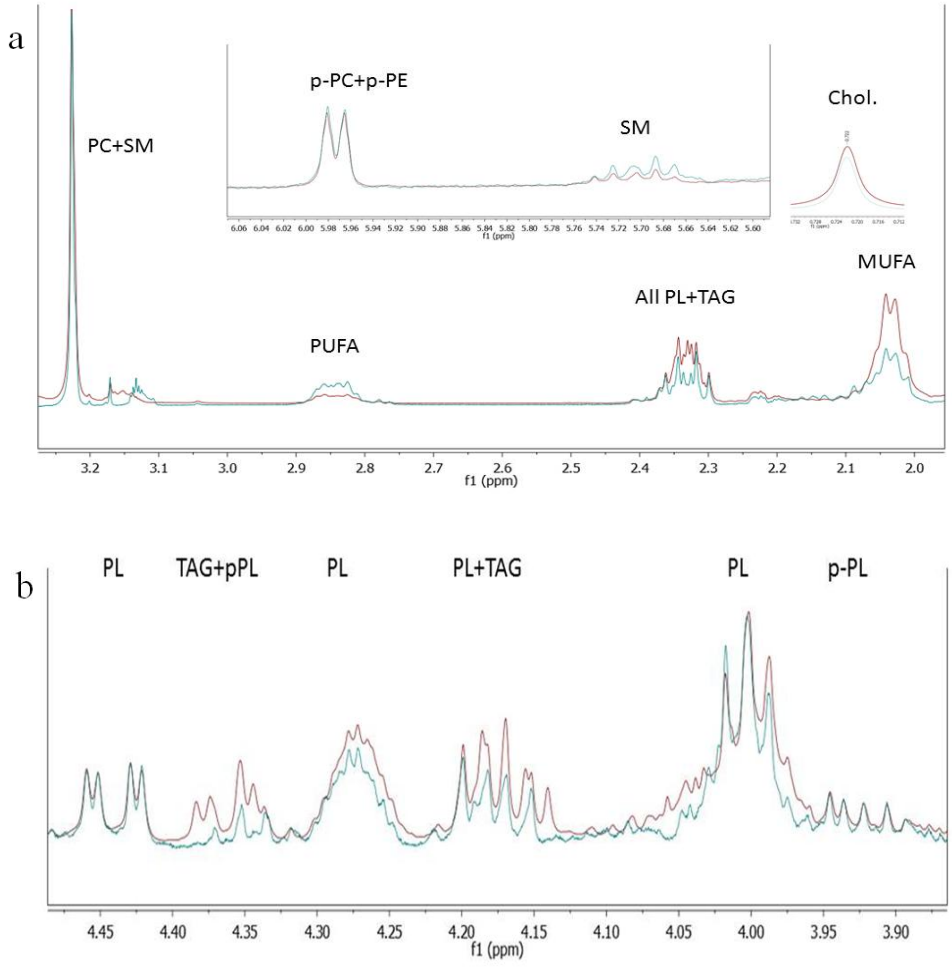

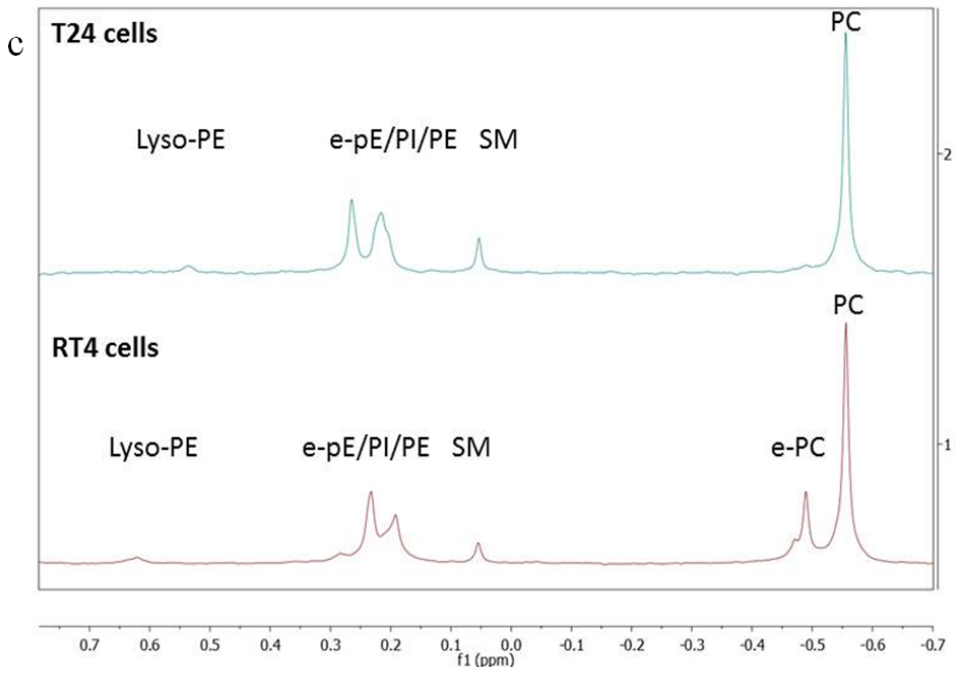

Fig. 2 NMR analysis of composition and characteristics of lipid extracts from RT4 and T24 cells**.** (a) Overlay of ^{1}H-NMR spectra showing intermediate region of RT4 (red line) and T24 (blue line) indicating comparisons of mono-unsaturated acyl chain (from MUFA), polyunsaturated acyl chain (from PUFA), TAG and cholesterol (Chol). (b) Overlay of ^{1}H-NMR spectra of intermediate region of RT4 (red line) and T24 (blue line) showing TAG comparison. (c) ^{31}P-NMR spectra comparing RT4 (red line) and T24 (blue line) cellular PLs.

As the first snapshot of cellular lipid profile, the extensive NMR analysis provided useful information in several aspects including structural alterations of fatty acyl chains, estimation of PL and TAG ratios as well as the quantitative variations in PL classes.

To summarize, compared with nonmalignant urothelial cell type (RT4), the malignant cells (T24) have molar ratio/fractions:

1) Much lower in TAG, as defined by [TAG]/[all PC+SM]
2) Much lower in 1-alkyl(ether) -2-acyl PC
3) Similar in 1-alkenyl-2-acyl (plasmenyl) PL
4) Higher in ω-6 PUFA acyl-chains of PL
5) Slightly higher in SM (18:1 based-ceramides), as defined by SM /[all PC+SM]

6) Slightly lower in cholesterol, as defined by [Chol]/[all PC+SM]
7) Slightly higher in the total PC+plasmenyl PC, as defined by [PC+plasmenyl PC]/[all PC+SM]

Since changes of TAG and PUFA are inversely related, the increase of PUFA in malignant cells must not attributed to the TAG acyl chains but, instead, to a re-wiring of the acyl chains of PL and/or SM. Such interesting earmarks might be indication of malignancy of urinary bladder cancer. Similar investigation was performed by Stenman. K *et al* (2009) to characterize PUFA in human malignant prostate tissue, in which they had proposed as relevant factors of the malignancy a) the dietary effects and b) the variations in mitochondrial membrane breakdown during cell death and/or fast turnover of lipid regions [21]. As we discussed in previous chapter, the increase of the overall unsaturation might attribute to the enhanced ER activity (containing primarily unsaturated PL species) in comparison with plasma membrane activity. In a word, during the bladder cancer development, the malignant urothelial carcinoma would have higher amount of PUFA ω-6 acyl chains together with reduced TAG content probably for facilitating their invasiveness.

Despite the important structural information obtained by NMR measurements, more comprehensive information on lipid molecular species (eg. Lipid ID, chain length and number of unsaturations) was obtained by carrying out our optimized HPLC-ESI MS/MS methodology.

Cellular lipids comparison between RT4 and T24 via HPLC-ESI MS/MS measurements

As described in chapter 3, our RPLC/ESI (+) MS/MS methodology enabled lipids identification and relative quantification; in particular, precursor ion scanning (PIS) of the fragment ion at m/z 184 (phosphocholine head group specific) was used to characterize the

protonated molecular ion $[M+H]^+$ of PC, LPC, plasmanyl and plasmenyl PC (here both were indicated as pPC) and SM lipid species. As shown in the total ion chromatogram (TIC) in Fig. 3, there were strong changes in the relative peak intensities of the choline-containing PL species in RT4 (red line-spectrum) with respect to T24 (blue line-spectrum). First of all, great variations occurred in PC species with short chain length, among which the identified PC 28:0 was shown in the middle panel of Fig. 3; in T24 these species dramatically decreased with respect to RT4. Another significant difference was presented in the bottom panel in Fig. 3 (within the retention time window 20.2–20.4 min) indicating the lipid species identified as indicated here in Fig. 3 pPC 34:1 belonging to ether-PC (alkyl 18:0/acyl 16:1) class. Even in this case the relative amount of ether PC was much lower in T24, in fair agreement with the above-discussed ^{31}P-NMR data.

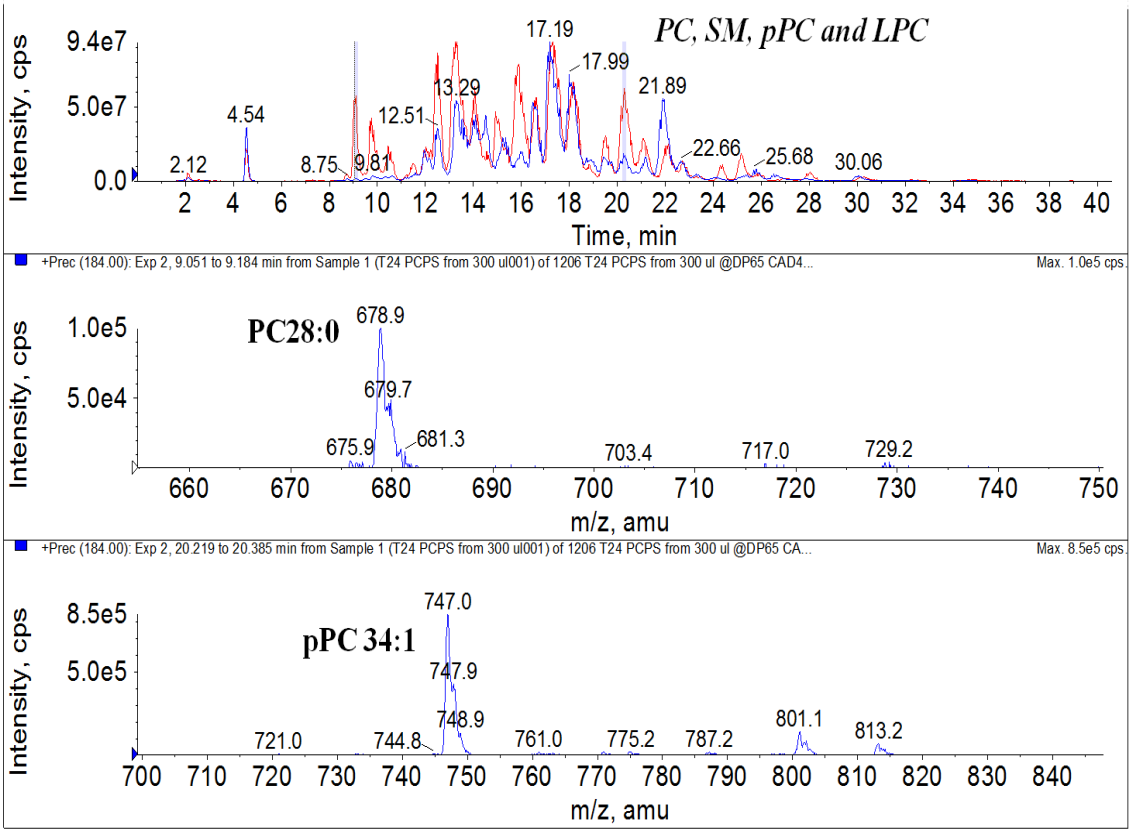

Fig. 3 Ion chromatogram obtained by RPLC/ESI (+) MS/MS PIS 184 comparing cellular PC, SM, LPC and pPC in RT4 (red line) with respect to T24 (blue line). Top panel: spectra overlay for PC, SM, LPC and pPC comparison; Middle panel: lipid species detection within the time retention window 9.05–9.18 min identified as PC 28:0; Bottom panel: identified pPC 34:1 within the retention time window 20.22–20.39 min.

The amount of pPC and relative ratio of pPC with respect to all choline-containing PL were evaluated for RT4 and T24. As shown in Fig. 4a, the amount of pPC decreased significantly in T24 comparing with RT4 (with p value < 0.0001), which confirmed the alterations as revealed in spectral comparison in Fig. 3 as well as in NMR analysis. It was presented in Fig. 4b that comparing T24 with RT4, the ratio of pPC was also lowered dramatically with respect to all choline-containing lipid classes, while in contrast, the proportion of PC increased in T24.

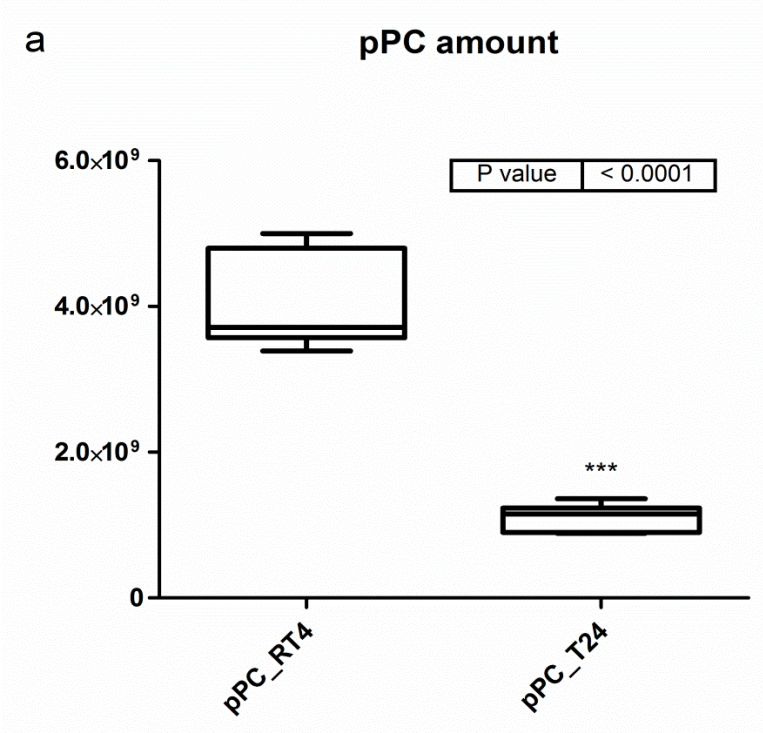

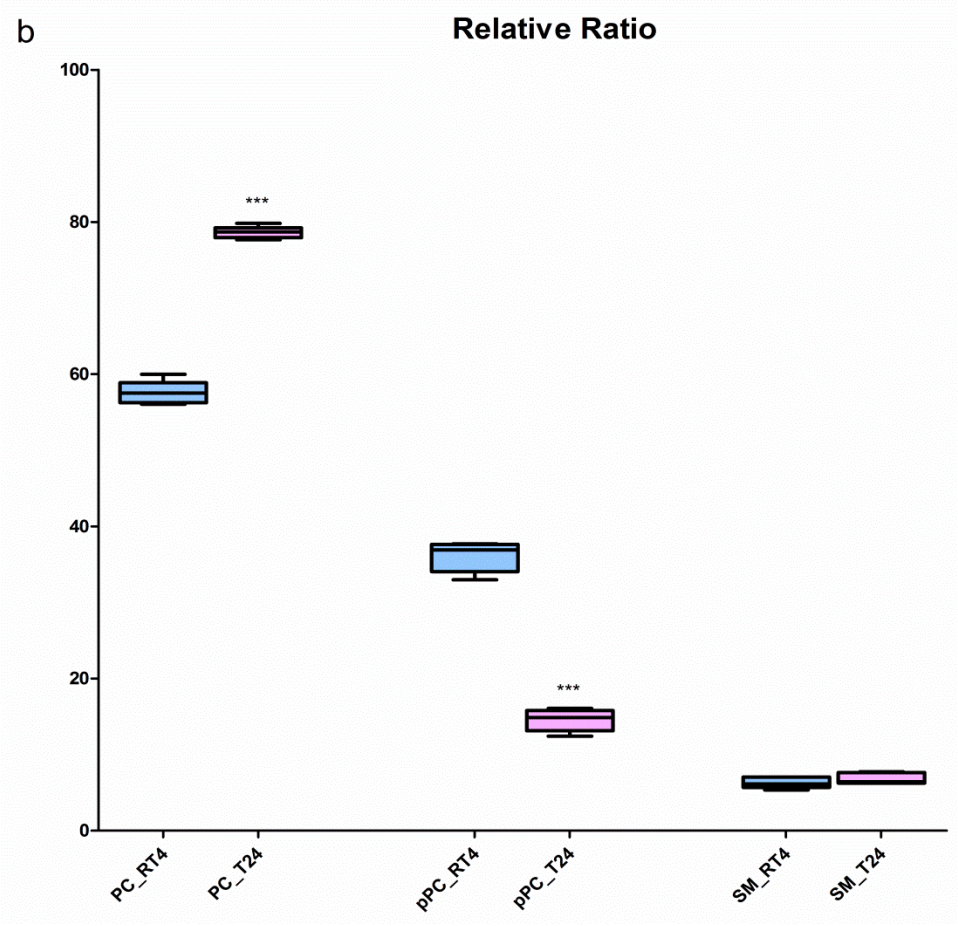

Fig. 4 Comparison of PC, SM and pPC between RT4 and T24 (a) pPC amount (values expressed in terms of areas obtained from MS/MS experiments) in RT4 and T24 cells, (b) Relative ratio of pPC, SM and PC (values expressed in terms of number of percentage) in RT4 and T24 cells. The superscript (*) shows significant difference of T24 with respect to RT4 at $p < 0.05$ (n=6).

It has been known that specific genetic alterations that go along with malignant transformation may intervene in the synthesis and breakdown of choline–containing PLs and so far higher choline metabolite level is used as a diagnostic marker of malignancy for breast cancer [22]. During malignant transformations, choline metabolism and choline-derived metabolites may go through alterations via various metabolic pathways. This study, performed by Katz-Brull *et al* (2002), demonstrated that the reduced levels of a choline-ether-PL may serve as a metabolic marker of breast cancer. Similarly, we have found a sharp decrease (about 3-fold) of 1-alkyl,-2-acyl PC species in urinary bladder malignant cells comparing with the benign counterpart. The

role ether PC in the malignant transformation of urothelial carcinoma is not clear, but their strong reduction during epithelium malignancy (RT4 and T24 are originated as epithelium in urinary bladder) may find a reasonable explanation within the biochemical scenario highlighted in recent literature reports [23]. In fact, according to findings there reported, the faster choline uptake and kinase activity in malignant cells is related to the over-expression of the biochemical precursor free phosphocholine ($^{-}O_3POCH_2CH_2N^{+}(CH_3)_3$) leading to a strong perturbation of the biosynthesis of all the PC species, including their ether analogues. Thus, the substantial decrease of ether PC in the malignant urothelial T24 cells not only can be used as a biochemical feature of the bladder cancer malignancy but also indicate that in the progress of malignant bladder carcinoma the biosynthesis of 1-alkyl, 2-acyl PC is strongly suppressed. On the other hand, the biosynthesis of these ether phospholipids starts in peroxisomes with the acylation of dihydroxyacetonephosphate (DHAP) by the enzyme dihydroxyacetonephosphate acyltransferase (DHAPAT) followed by the formation of the ether linkage by the enzyme alkyl-DHAP synthase, that catalyzes the exchange of the acyl-chain in acyl-DHAP for a long chain fatty alcohol [24]. Furthermore ether-PC lipids have been demonstrated to be the biogenetic precursors of the, well known, strong biologically active 1-alkyl,2-acetyl PC (PAF, platelet-activating factor), a family of naturally occurring acetylated phospholipid mediators involved in inflammation processes.

As mentioned in the introduction of my thesis, since GSL is an important class of lipid especially in epithelium and ceramides-metabolism has been extensively proved to play an important role in cancer pathogenesis, an RPLC ESI (+) MS/MS method was developed also for their characterization. In particular, we exploit the fact that ESI positive ion-mode Product Ion Scans of the daughter ions at m/z 264 and m/z 266 are class-specific fragmentation routes of the $[M+H]^+$ precursor ions, respectively, in sphingosine-based (d18:1) and in dihydrosphingosine-

based (d18:0) GSL lipids. However, since the amount of dihydrosphingosine-based (d18:0) GSL in these two cells were found very low (data not shown), their characterization through PIS 266 was not further investigated. As shown in Fig. 5, the contents of Cer (d18:1/16:0) (Fig. 5 middle panel) and Cer (d18:1/18:0) (Fig. 5 bottom panel) were found much higher in T24 comparing with RT4 cells, thus suggesting that also some specific ceramides played important roles in urinary bladder cancer metastasis especially in signaling transduction pathway in cancer progression. Further analyses on differential changes in GSL profile between RT4 and T24 need to be investigated.

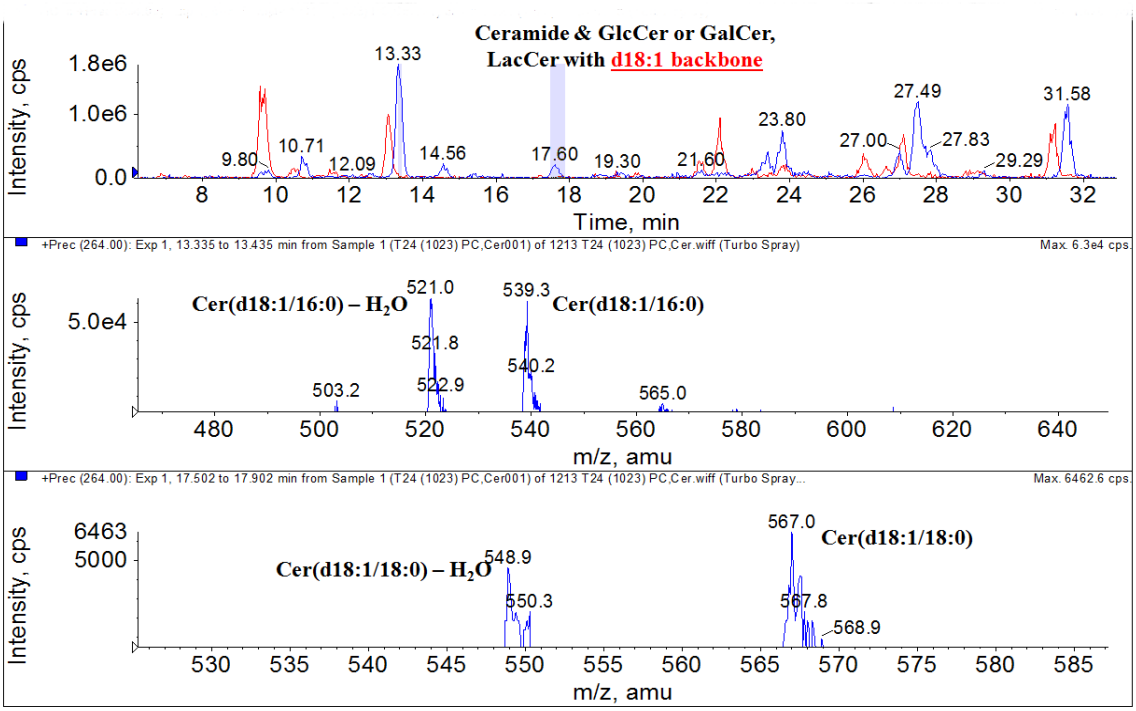

Fig. 5 Ion chromatogram obtained by RPLC/ESI (+) MS/MS PIS 264 comparing cellular Ceramide (Cer), glycosyl-ceramide (GalCer or GlcCer) and lactosyl-ceramide (LacCer) in RT4 (red line) cells with respect to T24 (blue line) cells. Top panel: spectra overlay for Cer, GalCer or GlcCer and LacCer comparison; Middle panel: higher abundant lipid species in T24 cells detected within 13.34–13.44 min with ID Cer (d18:1/16:0) and its dehydrated form; Bottom panel: identified Cer (d18:1/18:0) and its dehydrated form within 17.50–17.90 min in T24 cells.

Multivariate analysis and individual potential marker analysis

According to Fig. 3, there were relevant changes in choline-containing lipid species with shorter chain length. In order to reveal such variation pattern and further to analyze the corresponding markers responsible for discriminating T24 from RT4 cells, multivariate data analysis (MVDA) was performed by systematically looking at individual lipid species. The plots in Fig. 6 illustrate the multivariate data analysis (MVDA) conducted on the 42 PC species characterized in both types of cells. Principal component analysis (PCA), an unsupervised multivariate method, was firstly adopted to visualize the preprocessed MS/MS data. As for data scaling, Pareto scaling is used through all analysis and UV scaling is not optimal because it tends to overestimate the low intensity lipids. The PCA scores plot (Fig. 6a) showed a clear-cut separation between RT4 cells and T24 cells in PC1 dimension, thus suggesting that during malignant progress, PC lipid profiles varied significantly. The first two components of PCA model cumulatively described 92% of the total variability, which demonstrated the great discrimination between RT4 and T24 cells. There were some biological variation between the replicates T24_03 and other T24, which were observed as their separation in the PC2 dimension, however, the differences in RT4 and T24 cells were the major one. The contribution of each species to the discrimination was further investigated in the corresponding loadings plot (Fig. 6b), where the discrimination pattern would be overviewed. Along the first component to the right part, the variables represent the more abundant PC species in the nonmalignant RT4 cells, whilst in the opposite side are reported the more featured PC species in the malignant T24 cells. PC species further away from the central part have stronger power for discrimination and show the most substantial changes between two cell types. As seen obviously in Fig. 6b, PC species with shorter chain length and low unsaturation index (any or just one double bond) are much

more representative for RT4 cells while PC species with relatively longer chain length and higher unsaturation index are enriched in T24 cells. In Fig. 6c, a PCA biplot which displayed sample RT4 and T24 replicates and 42 PC species as variables in the same graphic could show similarly the distinctive separation between two cell types with their corresponding responsible PC lipid species.

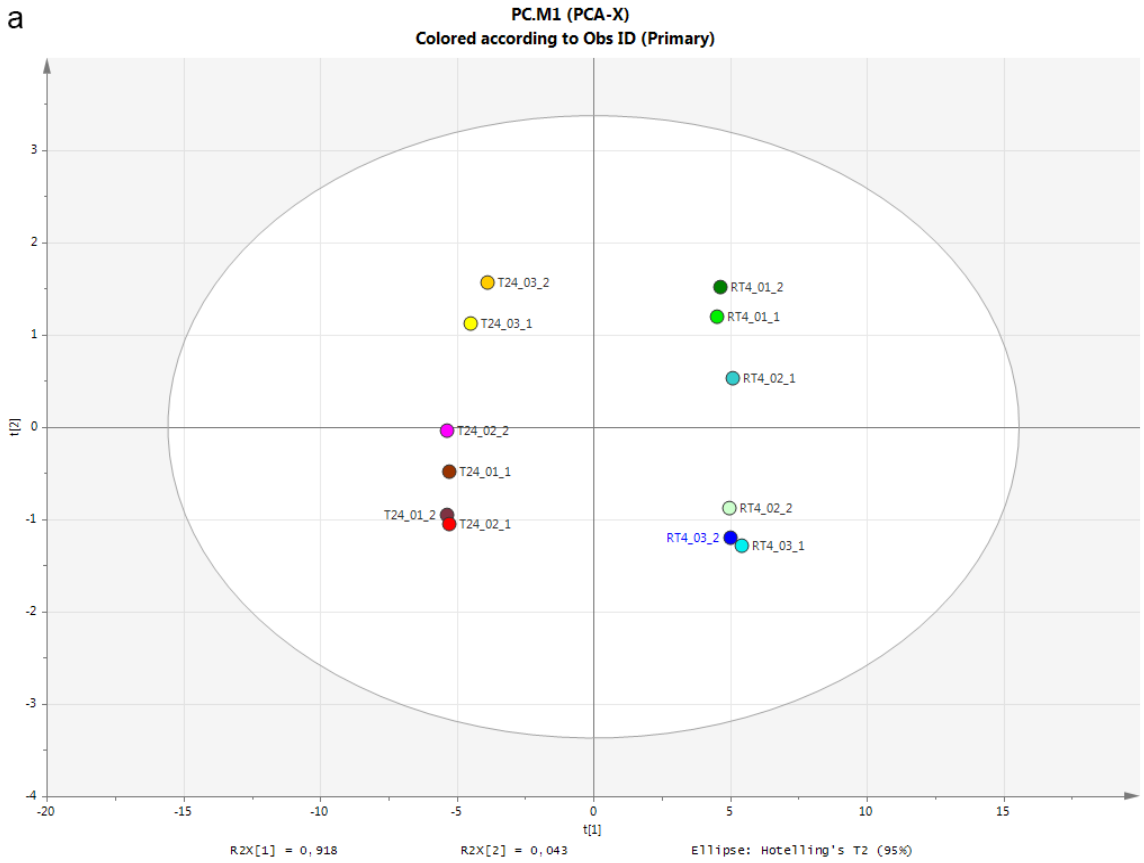

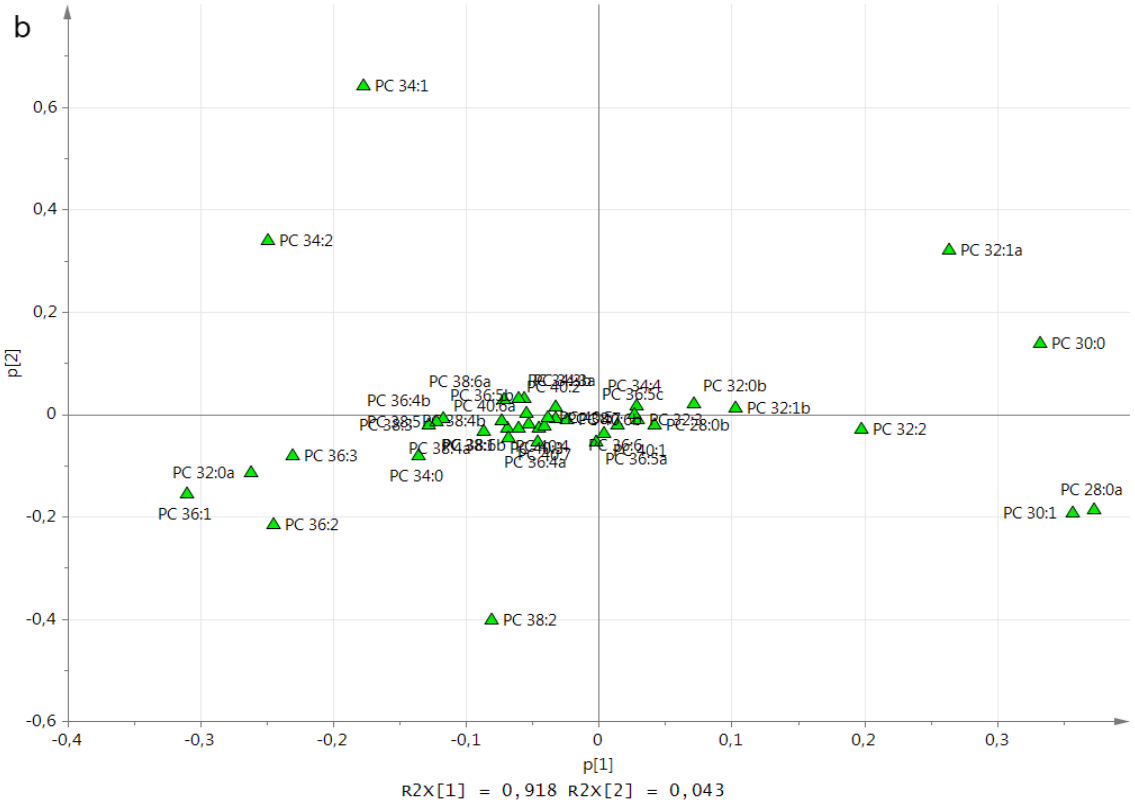
b
PC 34:1
PC 34:2
PC 32:1a
PC 30:0
PC 38:6a
PC 36:4b
PC 40:6a
PC 34:4
PC 32:0b
PC 32:1b
PC 28:0b
PC 32:2
PC 36:3
PC 32:0a
PC 34:0
PC 36:4a
PC 36:5a
PC 36:1
PC 36:2
PC 28:0a
PC 30:1
PC 38:2
p[2]
p[1]
R2X[1] = 0,918 R2X[2] = 0,043

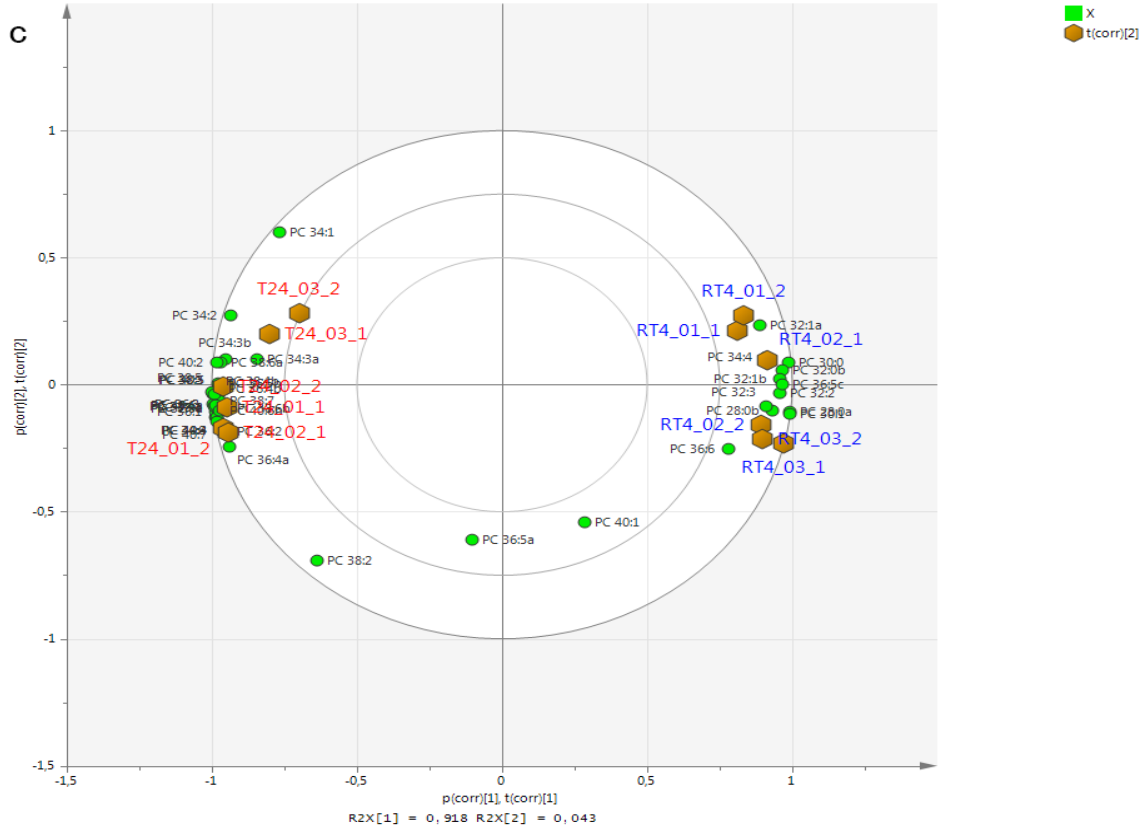
c
x
t(corr)[2]
PC 34:1
T24_03_2
PC 34:2
T24_03_1
PC 34:3b
PC 34:3a
PC 40:2
T24_02_2
T24_01_1
T24_02_1
T24_01_2
PC 36:4a
RT4_01_2
RT4_01_1
PC 32:1a
RT4_02_1
PC 34:4
PC 30:0
PC 32:0b
PC 32:1b
PC 36:5c
PC 32:3
PC 32:2
PC 28:0b
RT4_02_2
RT4_03_2
PC 36:6
RT4_03_1
PC 40:1
PC 36:5a
PC 38:2
p(corr)[2], t(corr)[2]
p(corr)[1], t(corr)[1]
R2X[1] = 0,918 R2X[2] = 0,043

Fig. 6 Multivariate data analysis of 42 cellular phosphatidylcholine (PC) species in RT4 and T24. (a) PCA scores plot, (b) Loadings plot and (c) PCA biplot of the RT4 and T24 cells. (n=6)

Further analysis of the main PC lipid markers revealed from the loadings plot (Fig. 6b) was performed with univariate unpaired t-test and therefore would testify how and how much individual PC molecular species changed in malignant urothelium comparing with the nonmalignant counterpart. As presented in the analysis of individual PC species in Fig. 7, the urinary bladder carcinoma malignancy was accompanied with a remarkable decrease in PC species bearing fatty acids with shorter chain up to 32 carbon and lower unsaturation index (28:0a, 30:0, 30:1, 32:1) with an exception of 32:2, which had two double bonds in its fatty acyl chain. However, a reverse example was 32:0a, which dramatically increased in T24 comparing with RT4. Except for this shorter saturated species, in T24 cells there was a trend in fatty acyl chain length as well as unsaturation increase compared to the corresponding level of RT4 cells. Similarly, an exceptional example was discovered to be a low abundant species PC 34:0 (< 2%), a longer saturated species which increased in T24 cells. MVDA and UVDA of PL molecular species from other classes were carried out in a similar workflow.

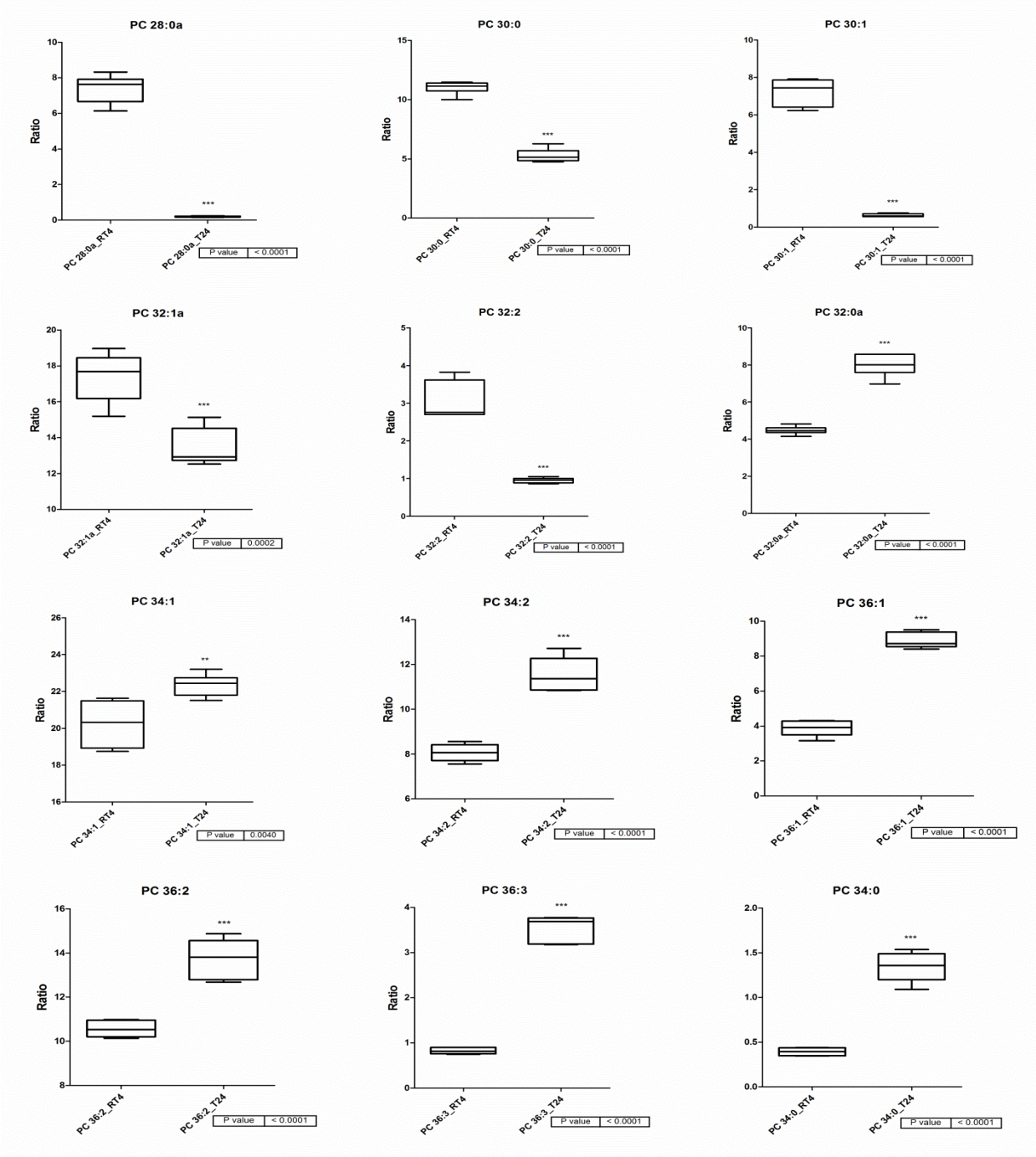

Fig. 7 Univariate analysis of potential PC marker revealed from Fig. 6b. Shorter PC species (i.e. with < 32 carbon chain length, 28:0a, 30:0, 30:1, and 32:1a, 32:2) decreased whilst PC species with > 32 carbon chain length increased in malignant cell line T24. The superscript (*) shows significant differences of T24 with respect to RT4 at $p < 0.05$ (n=6).

Fatty acyl (FA) carbon chain length, double bonds (db) distribution/variation and Unsaturation Index (UI) analysis

In order to reveal general variations in fatty acyl chain length and/or double bonds in a more systematic way, univariate data analysis of the fatty acyl carbon chain length (Fig. 8), distribution as well as variation of unsaturations (double bonds, Fig. 9) and Unsaturation Index (Fig. 10) was performed.

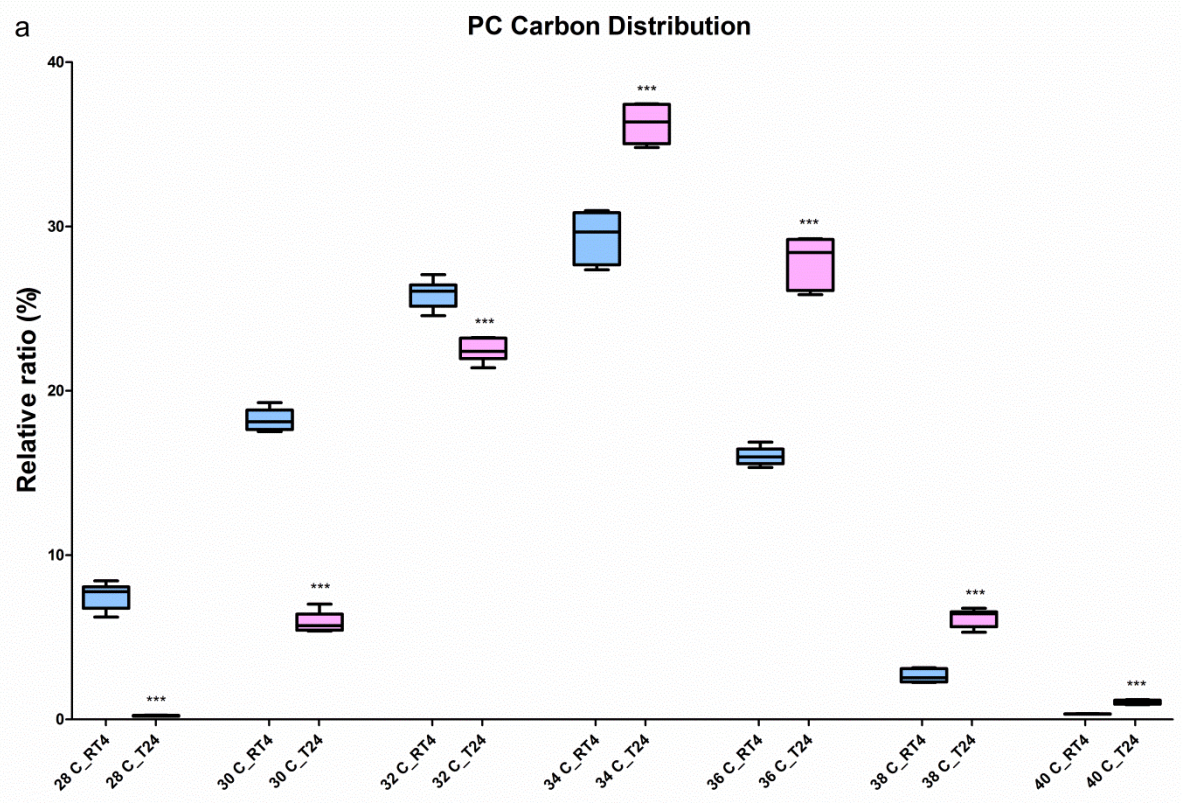

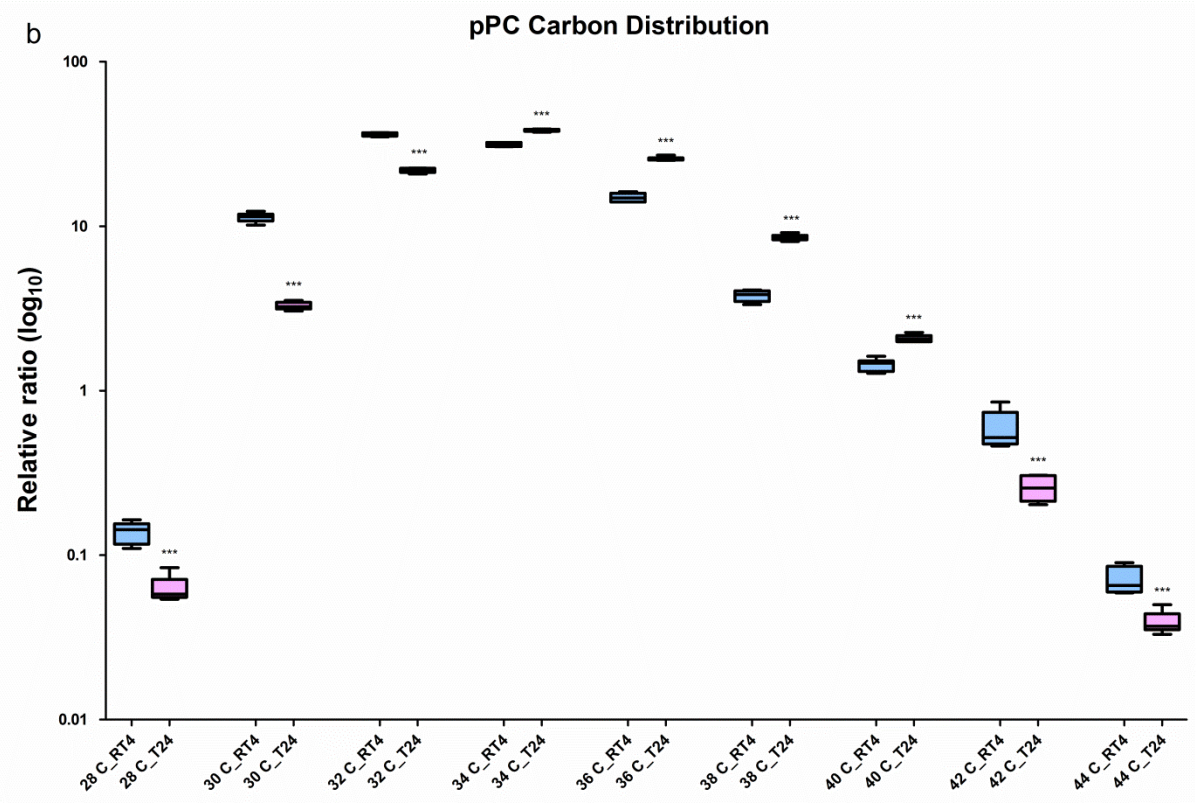
b
pPC Carbon Distribution
Relative ratio (log10)
100
10
1
0.1
0.01
***
28 C_RT4
28 C_T24
30 C_RT4
30 C_T24
32 C_RT4
32 C_T24
34 C_RT4
34 C_T24
36 C_RT4
36 C_T24
38 C_RT4
38 C_T24
40 C_RT4
40 C_T24
42 C_RT4
42 C_T24
44 C_RT4
44 C_T24

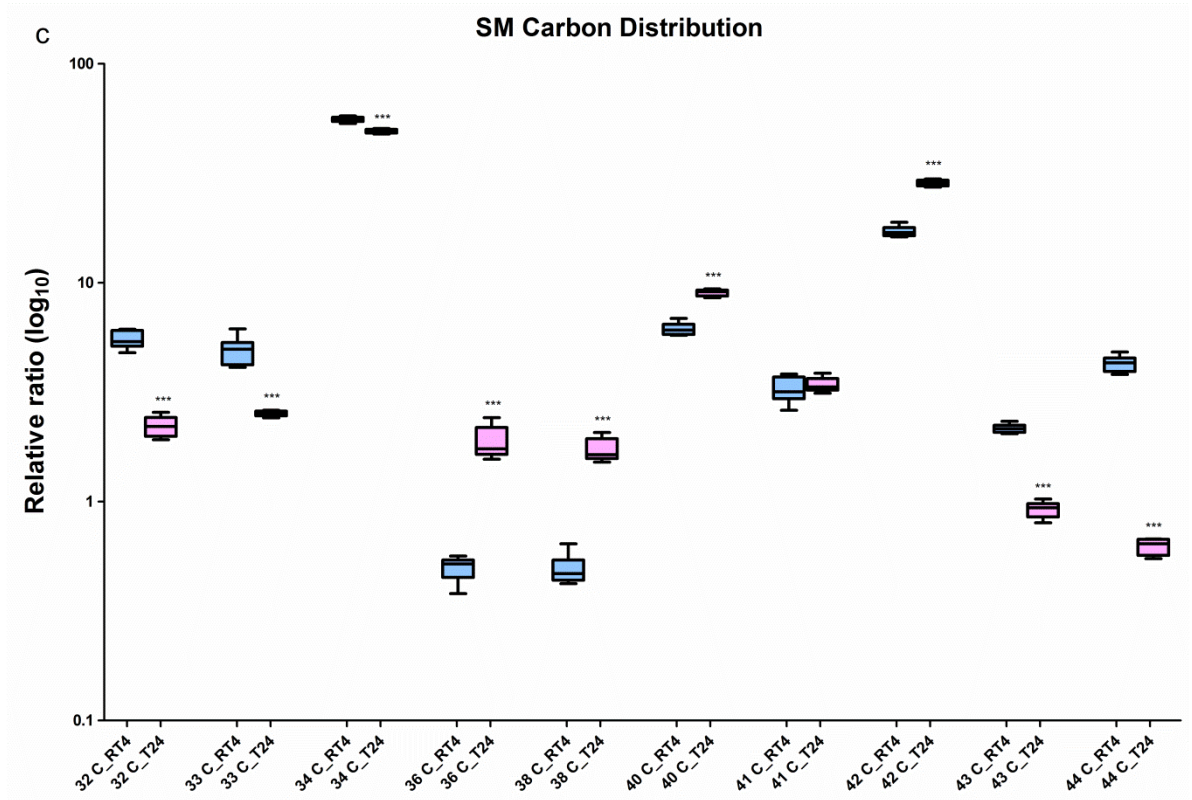
c
SM Carbon Distribution
Relative ratio (log10)
100
10
1
0.1
***
32 C_RT4
32 C_T24
33 C_RT4
33 C_T24
34 C_RT4
34 C_T24
36 C_RT4
36 C_T24
38 C_RT4
38 C_T24
40 C_RT4
40 C_T24
41 C_RT4
41 C_T24
42 C_RT4
42 C_T24
43 C_RT4
43 C_T24
44 C_RT4
44 C_T24

Fig. 8 Fatty acyl carbon chain length distribution and variation in T24 comparing with RT4. (a) Characterization of PC fatty acyl chain with carbon number from 28 to 40 (values expressed in terms of number of percentage), (b) The ether PC (pPC) carbon chain lenth distribution (28-44 C) and variation (values expressed in terms of $\log_{10}$), (c) SM carbon number distribution (32-44 C) and variation (values expressed in terms of $\log_{10}$). The superscript (*) shows significant difference of T24 with respect to RT4 at $p < 0.05$ (n=6).

As indicated in Fig. 8a, PC lipids have fatty acyl chain with carbon number ranging from 28 to 40, among which, the dominant ones were those with 34 C. It was clearly revealed in such analysis that the proportion of those PC lipids with less than 32 C dramatically decreased in the malignant T24 cells comparing with nonmalignant RT4 cells, whereas the PC lipids with 34-40 C significantly increased in T24 cells. Very similar phenomenon was also discovered in ether PC (pPC) except for the fact that pPC lipids with 42 C and 44 C decreased again in T24 cells (Fig. 8b). As for SM, there were three trends in different carbon number distribution blocks (Fig. 8c). The proportion of SM within 32-34 C decreased in T24 cells comparing with that in RT4 whereas SM within 36-42 C significantly increased upon malignancy in T24 cells. SM with the longest chain (43 C and 44 C) decreased again in the malignant T24 cells comparing with the nonmalignant counterpart RT4 cells. To sum up, the general trends from the above analysis reflect the fact that T24 cells have reduced amounts of shorter lipids and reversly enriched longer lipids but reduced proportion of the longest lipids. The possible explanation is that in order to facilitate their invasiveness to the surrounding cells or environment, the malignant urinary bladder carcinomas (eg. T24 cells) choose to keep an optimal cellular membrane skeleton. The fact that the optimal carbon numbers of SM differed from those of PC (pPC) might be due to the ceramide backbone specificity.

Apart from carbon number distribution and variation, another important feature of lipids, the unsaturation distribution (double bonds, db) was also worthy of investigations (Fig. 9).

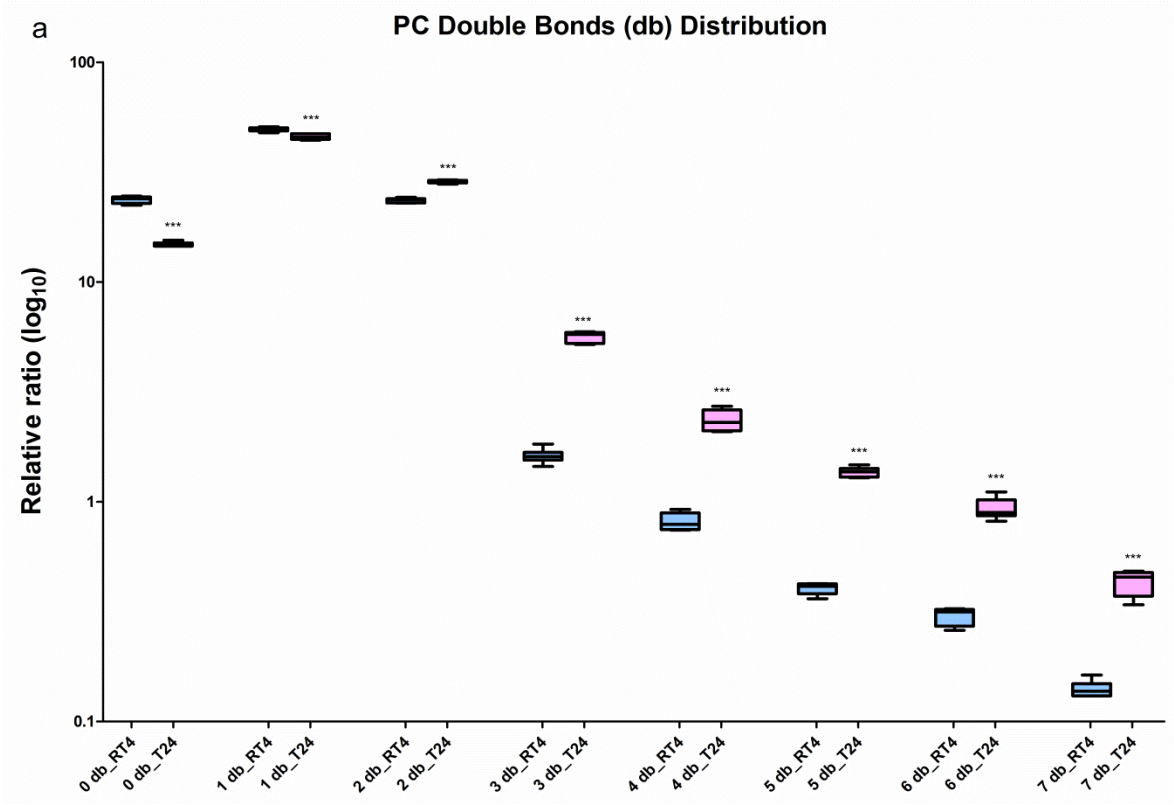
a
PC Double Bonds (db) Distribution
Relative ratio (log10)
100
10
1
0.1
***
0 db_RT4
0 db_T24
1 db_RT4
1 db_T24
2 db_RT4
2 db_T24
3 db_RT4
3 db_T24
4 db_RT4
4 db_T24
5 db_RT4
5 db_T24
6 db_RT4
6 db_T24
7 db_RT4
7 db_T24

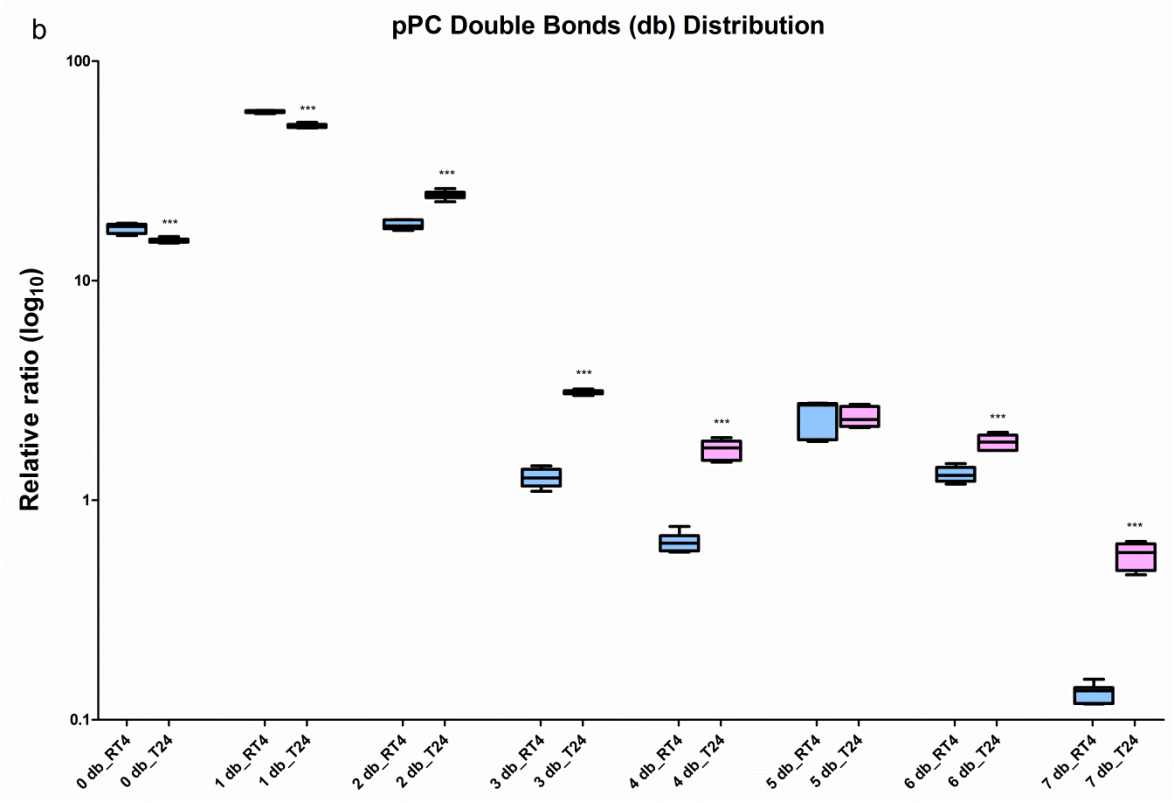
b
pPC Double Bonds (db) Distribution
Relative ratio (log10)
100
10
1
0.1
***
0 db_RT4
0 db_T24
1 db_RT4
1 db_T24
2 db_RT4
2 db_T24
3 db_RT4
3 db_T24
4 db_RT4
4 db_T24
5 db_RT4
5 db_T24
6 db_RT4
6 db_T24
7 db_RT4
7 db_T24

Fig. 9 Fatty acyl double bonds (db) distribution and variation in T24 cells with respect to RT4 cells. (a) Analysis of PC double bonds (0-7 db) distribution (values expressed in terms of relative ratio $\log_{10}$), (b) The ether PC (pPC) double bonds (0-7 db) distribution (values expressed in terms of relative ratio $\log_{10}$). The superscript (*) shows significant difference of T24 with respect to RT4 at $p < 0.05$ (n=6).

A clearer pattern and trend in unsaturation (db) variations due to urinary bladder metastasis can be reliably established: the malignant cell line T24 has reduced fractions of saturated or mono- unsaturated (0 and 1 db) PC species (Fig. 9a) as well as the ether forms (pPC, Fig. 9b) while di-unsaturated and polyunsaturated PC, pPC species are much more enriched in T24 cells (2-7 db). A further UI analysis was performed to reveal the total unsaturation variation in T24 cells with respect to RT4 cells (Fig. 10). As illustrated in both Fig. 9 and 10, T24 cells have increased unsaturation (db) in their fatty-acyl chains of PL, thus suggesting that the malignant carcinoma may require less stiffness for its movement and invasiveness [12]. Such findings were in accordance with the previous NMR analysis that T24 has higher amount of PL with PUFA acyl-chains.

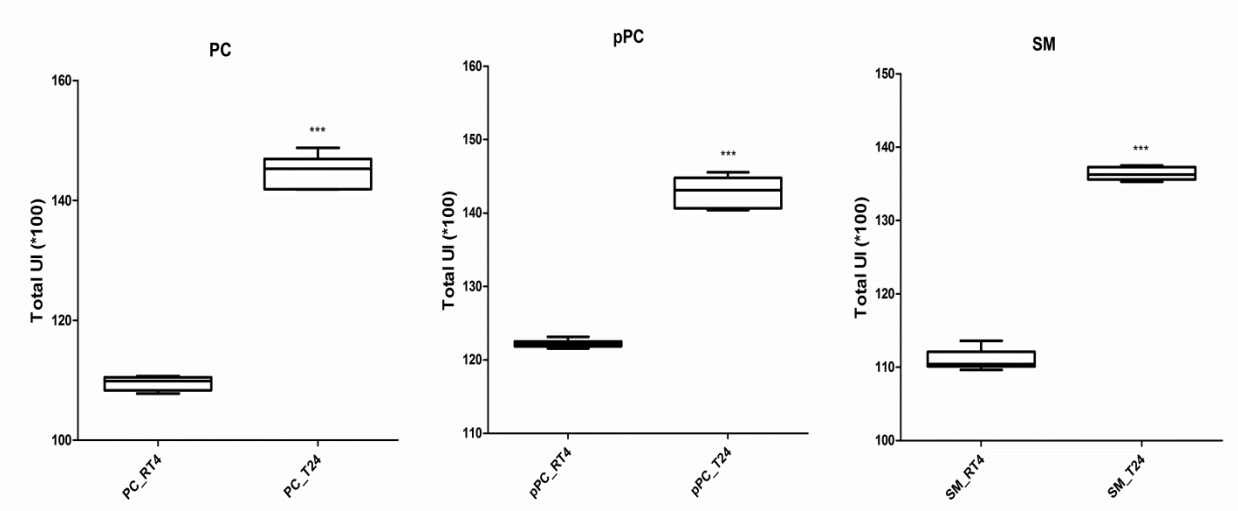

Fig. 10 Unsaturation Index (UI) analysis of PC, pPC and SM. The malignant urinary bladder cell line T24 has increased UI of (a) PC, (b) pPC and (c) SM compared with nonmalignant urinary bladder cell line RT4. The superscript (*) shows significant differences of T24 with respect to RT4 at $p < 0.05$ (n=6).

Being in accord with the previous analysis, it was clearly demonstrated that shorter and saturated or mono-unsaturated lipids are dominant in benign urothelial cell type while the malignant urothelial cells have lipids with longer and more unsaturated fatty acyl chains.

4.5 Conclusions and perspectives

The previously developed NMR and RPLC-MS/MS-based methodology was used to characterize cellular lipids. An *in vitro* model of two human urothelial cell types, RT4 representing low grade non metastatic tumor cells and T24 as high grade metastatic urinary bladder carcinoma, was used to study changes in lipids profile associated to urothelial metastasis. Interestingly, during the urothelial metastasis our LC-MS data showed: a) a significant decrease of the relative amount of ether PC species; b) a selective decrease of lipid species with shorter and saturated/mono-unsaturated acyl chains; c) a significant increase of lipid species with longer chain length, di-unsaturated and polyunsaturated fatty acyl chains and d) an increase of some specific GSL species. To summarize, the cells may carry out some significant re-organization of cellular membrane when undergoing malignant cell transformation, involving variations in compositional lipid structures as well as possible signaling transduction pathways. The molecular pathways whereby they afford these large variations remain to be elucidated; extensive biosynthetic experiments are clearly required in order to explain our findings but this goal was absolutely out of my thesis project. Anyhow, the observed depletion (almost total) of the 1-alkyl PC species and the chain shortening of the PC and ether PC as well as SM species might serve as a tool in urinary bladder cancer intervention.

Since data analysis is now in accelerated progress, a more complete description of our investigated biological problem will be published in a new paper whose preparation is in

progress. In fact, some data concerning the characterization of normal urothelial lipidome have been recently obtained in our Lab. Thus, in the next months, we would be able to compare these data with those obtained on tumor cells and to obtain an even better lipidomics view on the urinary bladder cancer development. Finally, since metastatic progression is certainly triggered by changes in cellular signaling transduction pathways associated with lipids, studies on lipid metabolism through the aid of genomics/ transcriptomics/ proteomics tools will be very helpful.

4.6 References

[1] Kabaso D, Lokar M, Kralj-Iglic V *et al.* Temperature and cholera toxin B are factors that influence formation of membrane nanotubes in RT4 and T24 urothelial cancer cell lines. International journal of nanomedicine 2011; 6:495-509.

[2] Alberts SR. Updated Options for Liver-Limited Metastatic Colorectal Cancer. Clinical Colorectal Cancer 2008; 7, Supplement 2:S58-S62.

[3] Višnjar T, Kocbek P, Kreft M. Hyperplasia as a mechanism for rapid resealing urothelial injuries and maintaining high transepithelial resistance. Histochem Cell Biol 2012; 137:177-186.

[4] Kreft ME, Di Giandomenico D, Beznoussenko GV *et al.* Golgi apparatus fragmentation as a mechanism responsible for uniform delivery of uroplakins to the apical plasma membrane of uroepithelial cells. Biology of the Cell 2010; 102:593-607.

[5] Kreft M, Hudoklin S, Jezernik K, Romih R. Formation and maintenance of blood–urine barrier in urothelium. Protoplasma 2010; 246:3-14.

[6] Klein CA. Selection and adaptation during metastatic cancer progression. Nature 2013; 501:365-372.

[7] Patra S. Involvement of Lipid Rafts in Growth Factor Receptors-Mediated Signaling for Cancer Metastasis. In: Signal Transduction in Cancer Metastasis. Edited by: Wu W-S, Hu C-T. Springer Netherlands; 2010. pp. 209-224.

[8] Patra SK. Dissecting lipid raft facilitated cell signaling pathways in cancer. Biochimica et Biophysica Acta (BBA) - Reviews on Cancer 2008; 1785:182-206.

[9] Patra SK. Ras regulation of DNA-methylation and cancer. Experimental Cell Research 2008; 314:1193-1201.

[10] Murai T. The Role of Lipid Rafts in Cancer Cell Adhesion and Migration. International Journal of Cell Biology 2012; 2012.

[11] Babina I, McSherry E, Donatello S *et al.* A novel mechanism of regulating breast cancer cell migration via palmitoylation-dependent alterations in the lipid raft affiliation of CD44. Breast Cancer Research 2014; 16:R19.

[12] Liu H, Tan Q, Geddie WR *et al.* Biophysical characterization of bladder cancer cells with different metastatic potential. Cell biochemistry and biophysics 2014; 68:241-246.

[13] Franks LM, Rigby C. Letter: HeLa cells and RT4 cells. Science 1975; 188:168.

[14] Bubenik J, Baresova M, Viklicky V *et al.* Established cell line of urinary bladder carcinoma (T24) containing tumour-specific antigen. International journal of cancer. Journal international du cancer 1973; 11:765-773.

[15] Imani R, Kabaso D, Erdani Kreft M *et al.* Morphological alterations of T24 cells on flat and nanotubular TiO2 surfaces. Croatian medical journal 2012; 53:577-585.

[16] Lahiri S, Futerman AH. The metabolism and function of sphingolipids and glycosphingolipids. Cell. Mol. Life Sci. 2007; 64:2270-2284.

[17] Kannagi R, Izawa M, Koike T *et al.* Carbohydrate-mediated cell adhesion in cancer metastasis and angiogenesis. Cancer Science 2004; 95:377-384.

[18] Ejsing CS, Sampaio JL, Surendranath V *et al.* Global analysis of the yeast lipidome by quantitative shotgun mass spectrometry. Proceedings of the National Academy of Sciences 2009.

[19] Sampaio JL, Gerl MJ, Klose C *et al.* Membrane lipidome of an epithelial cell line. Proceedings of the National Academy of Sciences 2011.

[20] Shaner RL, Allegood JC, Park H *et al.* Quantitative analysis of sphingolipids for lipidomics using triple quadrupole and quadrupole linear ion trap mass spectrometers. Journal of Lipid Research 2009; 50:1692-1707.

[21] Stenman K, Hauksson J, Gröbner G *et al.* Detection of polyunsaturated omega-6 fatty acid in human malignant prostate tissue by 1D and 2D high-resolution magic angle spinning NMR spectroscopy. Magn Reson Mater Phy 2009; 22:327-331.

[22] Katz-Brull R, Seger D, Rivenson-Segal D *et al.* Metabolic markers of breast cancer: enhanced choline metabolism and reduced choline-ether-phospholipid synthesis. Cancer research 2002; 62:1966-1970.

[23] Ruiter GA, Verheij M, Zerp SF, van Blitterswijk WJ. Alkyl-lysophospholipids as anticancer agents and enhancers of radiation-induced apoptosis. International Journal of Radiation Oncology*Biology*Physics 2001; 49:415-419.

[24] Hajra AK. Glycerolipid biosynthesis in peroxisomes (microbodies). Progress in Lipid Research 1995; 34:343-364.

Acknowledgments

I would like to express my sincere gratitudes and great thanks to everyone who has offered me sincere help and solid support during my PhD studies.

Graziano Guella, my tutor, for your insightful guidance, patience on answering all my questions, trust, constant encouragement, and for your support in every aspect of my PhD work, the deepest thanks to you for everything. Andrea Anesi, for always being so helpful and patient in my PhD studies and life. Adriano Sterni, for all your help of my experiment, analysis and especially your kind teaching for my PhD work.

Paolo Macchi, my advisor, for all your guidance and sincere help from starting my PhD in your lab and your valuable feedbacks and corrections to my PhD Work-In-Progress report and manuscript. Laura Vidalino, my supervisor in CIBIO, for all your kind teaching and help of my experiment in your lab and your encouraging talk. Betty Balduin, for all your sincere help and nice talk, which lights up my PhD life in its darkness time.

Urska Vrhovsek, my advisor, for all your help of the academic training and kind conversation in your lab. Pietro Franceschi, for all your advisable guidance, your encouragement and intelligent teaching in many aspects of my PhD studies.

Peter Veranič, Mateja Erdani Kreft and Nataša Resnik, my supervisors and good friend in Institute of Cell Biology, Faculty of Medicine, University of Ljubljana, for all your nice help and collaboration when I stayed in your lab, where I spent one of the most beautiful time during my PhD studies.

Peter Maček, Kristina Sepčič and Matej Skočaj, my supervisors and best friend in Biotechnical Faculty, University of Ljubljana, for all your valuable talk and sincere help when I stayed in your lab, where as well I spent one of my most fantastic time during my PhD work.

My Mama, for your greatest love and support for everything, which is the most valuable encouragement for my PhD and my life. 妈妈，你最伟大的爱给我的博士生涯和我的一生以最有力的支持和鼓励，谢谢你！And Boštjan's Mama, for your love and taking care of me when we stay with you in Slovenia - there is always a "love" in Slovenia - from you. Boštjan je Mama, za tvojo ljubezen in skrb za mene, ko smo ostali z vami v Sloveniji - je vedno "ljubezen" v Sloveniji - od tebe.

感谢我所有的朋友们，中国的，瑞典的，意大利的，你们的支持和关怀是我人生最大最大的财富。特别的感谢送给：瑞典隆德的姐姐唐艳娟唐唐，姐姐许洁喵喵，你们的帮助和关怀是七年来一直照亮和温暖我前行的动力。意大利的同学及好朋友孙薇，这三年的陪伴和互相扶持是我们完成博士的能量。谢谢你们的一直相伴。

Finally, special thanks to Boštjan, my fiancé. Your great love, support and thoughtfulness offer me one of the brightest lands in my PhD and life.